Not a dunce after all? - Dunce isoforms show differential localisation and influence memory in *Drosophila melanogaster* larvae

Inaugural-Dissertation

zur

Erlangung des Doktorgrades

der Mathematisch-Naturwissenschaftlichen Fakultät

der Universität zu Köln

vorgelegt von

Timo Hasselmann

aus Bremen

Köln, 2023

Berichterstatter: Prof. Dr. Henrike Scholz

Prof. Dr.Kei Ito

Tag der mündlichen Prüfung: 26.02.2024

Table of content

Abstract

The ability to learn and to remember is essential for an animal's survival. The mechanisms that lead to memory formation are highly conserved across species. Cyclic adenosine monophosphate (cAMP) is a second messenger that plays an important role in memory formation. Phosphodiesterases (PDEs) hydrolyse cAMP and cyclic guanosine monophosphate, reducing their levels. Dunce (Dnc) is a cAMP-specific PDE in *Drosophila*. *dunce* (*dnc*) is a complex gene that encodes several isoforms (Qiu *et al.*, 1991). In general, Dnc is regarded as a PDE that reduces the overall cAMP concentration, leading to *dnc* mutants with short-term memory (STM) deficits (Aceves-Piña and Quinn, 1979; Davis and Kiger, 1981; Dudai *et al.*, 1976). In this project we will investigate the role of different Dnc isoforms in learning and memory and their localisation at the cellular and subcellular level.

We show in *Drosophila* larvae that Dnc^{PA} and Dnc^{PB} specific mutants display the opposite phenotype to classical *dnc* mutants, increased STM. This demonstrates that the Dnc memory phenotype is isoform-specific. The memory phenotype of a Dnc^{PA}-specific mutant depends on PDE activity in neurons driven by the dnc^{RA} promoter. Of these, expression in a local interneuron projecting to the antennal lobe (AL) is most likely to affect memory formation. Dnc^{PB} is localised in a group of neurons associated with gustatory signals (Melcher and Pankratz, 2005). As gustatory stimuli are used as reinforcers, they are likely to influence memory formation. We also localise other isoforms in the central nervous system. With large differences between the expression patterns of antibodies against the same isoforms, we show that Dnc is a highly interacting and highly modified protein.

In mammals, the subcellular localisation of a PDE isoform has been shown to play an important role in memory formation (Martinez *et al.*, 2023). We show that in *Drosophila* larvae, somatic PDE expression is essential for the memory phenotype in Dnc^{PA}. The fly is able to compensate for increased PDE expression; however, reducing PDE levels in the soma of the correct neurons induces a memory phenotype.

We propose the following mechanism for the influence of Dnc^{PA} on memory formation: The reduced cAMP concentration in the soma of the Hv cluster leads to increased transmission of the reinforcer into the larval AL, thereby enhancing early

memory in the AL. This leads to increased transmission of the signal to the mushroom body, where the memory is formed.

Our findings provide a unique insight into the molecular mechanisms of memory formation. They expand the view of Dnc from a PDE with a specific memory phenotype to a collection of isoforms with their specific localisation, function and memory phenotypes. As PDEs are highly conserved between species, our findings may also provide insight into human memory formation.

Zusammenfassung

Lernen und Gedächtnisbildung sind entscheidend für das Überleben von Tieren. Die Mechanismen der Gedächtnisbildung sind hoch konserviert. Zyklisches Adenosinmonophosphat (cAMP) ist ein Second Messenger, der eine wichtige Rolle bei der Gedächtnisbildung spielt. Phosphodiesterasen (PDEs) hydrolysieren cAMP und zyklisches Guanosinmonophosphat und verringern so dessen Konzentration. Dunce (Dnc) ist eine cAMP-spezifische PDE in *Drosophila*. Das *dunce* (*dnc*)-Gen kodiert für mehrere Isoformen (Qiu *et al.*, 1991). Dnc wird allgemein als PDE angesehen, die die cAMP-Konzentration in der gesamten Fliege reduziert, während *dnc*-Mutanten ein defektes Kurzzeitgedächtnis aufweisen (Aceves-Piña und Quinn, 1979; Davis und Kiger, 1981; Dudai *et al.*, 1976). In diesem Projekt wollen wir verschiedene Dnc-Isoformen hinsichtlich ihrer Rolle bei der Gedächtnisbildung charakterisieren und ihre Lokalisation auf zellulärer und subzellulärer Ebene untersuchen.

Wir zeigen in *Drosophila*-Larven, dass Dnc^{PA}- und Dnc^{PB}-spezifische Mutanten den umgekehrten Phänotyp klassischer *dnc*-Mutanten aufweisen und somit ein verbessertes Kurzzeitgedächtnis zeigen. Dies zeigt, dass *dnc* isoformspezifische Lernphänotypen verursacht. Der Lernphänotyp einer Dnc^{PA}-spezifischen Mutante hängt von der PDE-Aktivität in Neuronen ab, in denen der *dnc*^{RA}-Promotor exprimiert wird. Von diesen Neuronen ist eine lokales Interneuron welches in den Antennallobus (AL) projiziert, am wahrscheinlichsten mit dem Lernphänotyp assoziiert. Dnc^{PB} wird in Neuronen exprimiert, die mit gustatorischen Signalen assoziiert sind (Melcher und Pankratz, 2005). Da wir gustatorische Stimuli als Verstärker in larvalen Lernexperimenten verwenden, könnten diese Neurone einen Einfluss auf die Gedächtnisbildung haben. Wir bestimmen die Lokalisation weiterer Isoformen im larvalen Zentralnervensystem. Die Unterschiede zwischen verschiedenen Antikörpern gegen die gleiche Isoform zeigen, dass Dnc ein stark modifiziertes Protein ist, das mit anderen Proteinen interagiert.

Bei Säugetieren wurde gezeigt, dass die subzelluläre Lokalisation von PDE-Isoformen eine wichtige Rolle bei der Gedächtnisbildung spielt (Martinez *et al.*, 2023). Wir zeigen in *Drosophila*-Larven, dass für Dnc^{PA} die somatische PDE-Expression essentiell für den Gedächtnisphänotyp ist. Die Fliege kann eine erhöhte PDE-Expression kompensieren, aber eine verminderte Expression führt zu einem Gedächtnisphänotyp.

Unsere Erkenntnisse lassen zu folgenden Mechanismus für den Einfluss von Dnc[PA] auf die Gedächtnisbildung zusammenfassen: Die verringerte cAMP-Konzentration im Soma des Hv-Clusters führt zu einer erhöhten Signalübertragung des gustatorischen Verstärkers in den AL der Larve, wodurch das frühe Gedächtnis verstärkt wird. Dies führt zu einer verstärkten Signaltransmission in den Pilzkörper, wo das Gedächtnis gebildet wird.

Unsere Ergebnisse bieten einen einzigartigen Einblick in die molekularen Mechanismen der Gedächtnisbildung. Sie erweitern die Sicht auf Dnc von einer PDE mit einem spezifischen Gedächtnisphänotyp zu einer Gruppe von Isoformen mit spezifischen Lokalisationen und Funktionen. Da PDEs zwischen verschiedenen Spezies stark konserviert sind, können unsere Ergebnisse auch zu einem besseren Verständnis der Gedächtnisbildung beim Menschen beitragen.

1   Introduction

Throughout its life, every animal is exposed to positive stimuli such as food availability and negative stimuli such as danger or pain. It is essential that the animal is able to remember these stimuli and their context in order to avoid painful or dangerous situations in the future or to find food sources. To do this, it has to sort incoming stimuli by importance, remembering important information and forgetting unimportant information.

How does this learning process work? This is a question that has fascinated researchers for decades. Since Ivan Pavlov described classical conditioning in dogs (Pavlov, 1927), multiple different animal models have been used to answer different aspects of this question. Some examples are monkeys (Hikosaka *et al.*, 1995), rats (Mysliveček and Hassmannová, 1979) and mice (Flood and E. Morley, 1997).

Insects have proven to be an accessible and reliable model organism for studying the basic principles of learning and memory that are conserved across species. Ever since Morgan discovered the heritable aspects of eye colour in *Drosophila melanogaster* in 1911 (Morgan, 1911), it has been used as a model for genetic studies. Therefore, when Quinn et al showed that flies learn to associate an external stimulus with a reward (Quinn *et al.*, 1974), there was already a large resource of mutants and genetic methods available to study the molecular basis of learning and memory.

Because *Drosophila melanogaster* has a short generation time, a large number of genetically uniform animals can be used, providing much better data for statistical analysis (Quinn *et al.,* 1974), rather than the small numbers of individuals as used in monkeys.

1.1   The *Drosophila* larva as a model organism for learning and memory

Drosophila lay their eggs directly on food, where the larvae hatch and feed until they are ready to pupate. During this time, they learn to associate olfactory cues with positive or negative reinforcers to increase their chance of survival.

In 1979, Aceves-Piña et al established *Drosophila* larvae as a model system for memory formation for the first time (Aceves-Piña and Quinn, 1979). The disadvantage of using the larva as a model system is its developing nervous system. Larvae of different ages have different numbers of neurons, which may lead to changes in behavioural experiments (Lee *et al.*, 1999; review: Davis, 2023). The

mechanisms underlying learning and memory may differ between larvae with a still developing nervous system and flies with a fully differentiated nervous system (review: Davis, 2023). Larvae have several advantages over adult *Drosophila* as a model for olfactory learning and memory. For example, their central nervous system (CNS) is less complex. It consists of only 10,000 neurons (Truman *et al.*, 1993). This is an order of magnitude smaller than the adult brain, which consists of about 100,000 neurons (Simpson, 2009). Another advantage over the adult is the simplified larval olfactory system. It is described in more detail in the following chapter.

A practical advantage of larvae in learning and memory experiments is the simplicity of larval learning and memory assays. For state-of-the-art associative learning and memory experiments in adult *Drosophila*, flies are trained and tested in a T-maze setup with constant airflow and humidity, and for aversive learning and memory experiments, specially constructed tubes containing an electrifiable grid are required (Tully and Quinn, 1985). Larval learning and memory experiments require only minimal equipment such as agarose, petri dishes and perforated containers for the odorants. Using this setup, several different paradigms can be studied. Larvae can be trained using electric shock as an aversive stimulus. Olfactory stimuli are presented as Conditioned stimuli and the larvae are trained on an agarose plate with two copper electrodes. In the aversive training phases and in the test, an electric shock is delivered through the agarose (Aceves-Piña and Quinn, 1979).

Another aversive stimulus used in larval learning and memory experiments is heat shock. Here, agarose plates in glass Petri dishes are placed on a block heater and heated up to 41°C, which acts as an aversive stimulus (Khurana *et al.*, 2012).

Gustatory unconditioned stimuli (US, also referred to as reinforcer) are widely used in larval learning and memory experiments. For example, 2M NaCl for aversive or 1M fructose for appetitive experiments are mixed in the agarose (Scherer *et al.*, 2003; Widmann *et al.*, 2016). Different NaCl concentrations (Gerber and Hendel, 2006; Widmann *et al.*, 2016), quinine (Apostolopoulou *et al.*, 2014) and caffeine (Apostolopoulou *et al.*, 2016) are other examples of aversive reinforcers (review: Widmann *et al.*, 2018). In a reciprocal aversive learning experiment, larvae are placed on a plate containing the aversive reinforcer and one of the odorants, and after 5 min in the dark they are transferred to the neutral plate containing no NaCl and the other odorant, while in parallel another set of larvae is placed on plates containing the same reinforcer but the opposite odorant. This training is repeated

several times and finally their memory is tested on a NaCl plate with one of the odorants on each side.

Depending on the research question, non-reciprocal paradigms are also used. Variations in the number of repetitions, the retention time between training and test, and a cold shock administered between training and test have been used to decipher memory forms in larvae (Khurana *et al.*, 2009; Widmann *et al.*, 2016). For electric shock associative learning and memory a reciprocal 2-odorant experiment was shown to yield the same result as a 1-odorant non-reciprocal paradigm (Pauls *et al.*, 2010). This shows that although different paradigms used, the results are usually comparable.

Modern optogenetic and thermogenetic tools in the ORNs and the octopaminergic neurons make it possible to induce memory without an odorant or reinforcer (Honda *et al.*, 2016).

1.2   Odorant perception in *Drosophila* larvae

Drosophila larvae have a simple olfactory system capable of discriminating between a large number of odorants (Aceves-Piña and Quinn, 1979; Monte *et al.*, 1989; Si *et al.*, 2019).

The larval chemosensory system consists of three organs: The dorsal organ, the terminal organ, and the ventral organ. The dorsal organ, which contains 21 olfactory receptor neurons (ORNs) and 6 gustatory receptor neurons and is located at the anterior end of the larva, is the olfactory organ, while the terminal and the ventral organ are gustatory (Chu-Wang and Axtell, 1971, 1972a; b; Oppliger *et al.*, 2000; Singh and Singh, 1984; review Stocker, 1994). The 21 ORNs in the dorsal organ are bipolar neurons organized in 7 bundles of 3 neurons each. They project from the dorsal organ via the antennal nerve to the antennal lobe (AL) (Chu-Wang and Axtell, 1971; Python and Stocker, 2002; Ramaekers *et al.*, 2005; Tissot *et al.*, 1997). Larval ORNs mostly express a single olfactory receptor in addition to the ubiquitously expressed Or83b (Larsson *et al.*, 2004; Ramaekers *et al.*, 2005). In *Drosophila* larvae, one ORN projects 1:1:1:1 into the brain (Ramaekers *et al.*, 2005). 21 ORNs project to 21 glomeruli in the lateral AL and then via 21 projection neurons (Berck *et al.*, 2016) to 28 calycal glomeruli in the mushroom body (MB) calyx (Ramaekers *et al.*, 2005). It has been shown that larvae can become habituated to an odorant at the ORN level with prolonged exposure (Larkin *et al.*, 2010).

In contrast, the adult olfactory system consists of 1300 ORNs projecting to 43 glomeruli in the AL (Ramaekers *et al.*, 2005). The signal is transmitted via 150 projection neurons to hundreds of calycal glomeruli in the MB (Ramaekers *et al.*, 2005).

In the larva, Kreher et al were able to map 11 of the receptors to specific neurons, map the region of the AL to which they project, map the different response dynamics of the receptor and identify which receptor responds to which odorant (Kreher *et al.*, 2005). Later, the response dynamics of all 21 ORNs were shown (Si *et al.*, 2019). The higher the odorant concentration, the more ORNs respond, but which ORNs respond at which concentration depends on the odorant (Si *et al.*, 2019).

In both larvae and adults, in addition to this 'vertical' connectivity, there is also 'horizontal' connectivity in the AL (Thum *et al.*, 2011). In the adult fly, GABAergic (GABA = γ-aminobutaric acid) local interneurons modulate the signal by forming inhibitory connections to the glomeruli, thereby modulating the signal from individual odorants (Wilson and Laurent, 2005; review: Jefferis and Hummel, 2006). Cholinergic interneurons modulate the signal by forming excitatory connections to the glomeruli (Shang *et al.*, 2007). In the larva, GABAergic inhibitory interneurons have been reported in the AL (Thum *et al.*, 2011). To date, although there are reports of excitatory cholinergic interneurons in L1 larvae, they have not been detected in L3 larvae, leading to the conclusion that horizontal connectivity in larvae is very different from that in adults (Thum *et al.*, 2011).

1.3   Memory in *Drosophila* larvae

The prediction error theory was formulated for memory formation in *Drosophila*. It was hypothesised that memory is created with the first presentation of the conditioned stimulus and the US, with further repetitions minimising the prediction error by determining the discrepancy between stimulus and prediction (Rescorla and Wagner, 1972; review: Cognigni *et al.*, 2018). During the first trial, memory is induced in a switch-like manner, later only gradual changes in cellular physiology are induced (Springer and Nawrot, 2021).

Memory formation requires both the dopaminergic and the octopaminergic system. (Burke *et al.*, 2012; Liu *et al.*, 2012). Octopamine integrates the energy level of the fly and acts on dopaminergic neurons to inhibit long-term memory (LTM) formation at

low energy levels in the fly (Berger *et al.*, 2023). Dopaminergic neurons (DANs) represent the US.

During repetitions, the strength of input from DANs is changed proportionally to the prediction error based on input from sensory neurons, but also MB output neuron (MBON) feedback (Felsenberg *et al.*, 2017, 2018; Zhao *et al.*, 2021).

Extinction and reversal learning and memory experiments have been established, demonstrating the ability of the fly to re-evaluate its memory. In adult *Drosophila*, it was shown that instead of reducing an aversive memory formed after the omission of the punishment, the fly establishes a competing parallel appetitive memory for the omission of the punishment, resulting in an intermediate learning index (Felsenberg *et al.*, 2018). A similar training protocol can also be used to examine the stability of the memory formed in the larva, thereby unravelling the influence of mutations on different memory forms and on re-evaluation of a stimulus (Mancini *et al.*, 2019).

The time between multiple stimuli or the between the stimuli and the test consolidates the memory acquired by the dorsally paired medial neurons that innervate the MB (Keene *et al.*, 2006; review: Cognigni *et al.*, 2018). This leads to the formation of distinct memory forms within the MB Kenyon cells (Springer and Nawrot, 2021; review: Cognigni *et al.*, 2018).

In *Drosophila*, there are two pathways for memory formation: the protein kinase A (PKA) pathway and the protein kinase C (PKC) pathway (Fig. 1) (review: Margulies *et al.*, 2005). In adult flies, short-term memory (STM), medium-term memory (MTM) and LTM have been shown to be cyclic adenosine monophosphate (cAMP)-dependent and to function via the PKA pathway (Fig. 1) (Chen *et al.*, 2012; Dudai *et al.*, 1976; Margulies *et al.*, 2005; Scheunemann *et al.*, 2012; Tully, Preat, *et al.*, 1994; Tully and Quinn, 1985; Tumkaya *et al.*, 2018; Turrel *et al.*, 2020; Widmer *et al.*, 2018; Yin *et al.*, 1994; Zars *et al.*, 2000). STM and LTM are encoded seperately within the MB, STM in γ-Kenyon cells, LTM in α/β Kenyon cells (Blum *et al.*, 2009). Since STM is first formed and then consolidated into LTM, γ-Kenyon cells are also required for LTM formation (Qin *et al.*, 2012). Anaesthesia-resistant memory (ARM) is formed by another pathway, the PKC pathway (Fig. 1). It is cAMP-independent (Folkers *et al.*, 2006). ARM is encoded separately from STM, MTM and LTM, recruits different neurons of the olfactory pathway and requires different enzymes (Scheunemann *et al.*, 2012). It has also been shown to be independent of protein synthesis (Tully, Preat, *et al.*, 1994). ARM forms memory with multiple temporal profiles that rely on

different sets of KCs (Bouzaiane *et al.*, 2015). In LTM formation, the PKA and PKC pathway both play a role. Suppression of a factor in the Notch pathway inhibits both ARM and LTM, showing that the different forms of memory are not independent from one another (Zhang *et al.*, 2013).

Although there have been far fewer studies of different forms of memory in larvae than in adults, most forms of memory have also been found in *Drosophila* larvae. They form at least three distinct forms of memory, STM, ARM and LTM (review: Thum and Gerber, 2019).
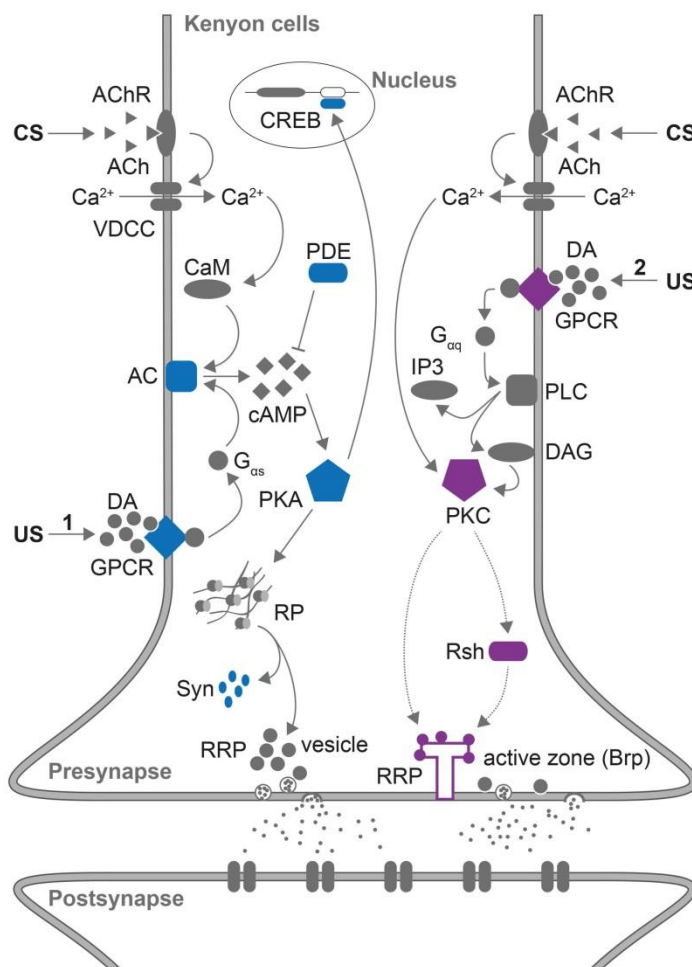
Fig. 1: Memory formation in *Drosophila* larvae
There are two parallel processes of coincidence detection in larvae that lead to two forms of memory.
1: In the PKA pathway leading to STM, coincidence detection leads to a change in cAMP concentration in the Kenyon cell, which activates PKA. Consolidation leads to protein synthesis-dependent LTM.
2: In the PKC pathway leading to ARM, phospholipase C increases intracellular diacylglycerol levels, which activate PKC (Widmann *et al.*, 2016).

Like adults, larvae show different forms of memory that can be observed after different training paradigms. A one-cycle aversive memory paradigm using amyl acetate (AM) and benzaldehyde (BA) as reinforcers leads to aversive STM (Widmann *et al.*, 2016). Larval STM is dependent on the PKA signalling pathway (Fig. 1). ARM can also be detected after a single aversive training cycle (Widmann *et al.*, 2016). ARM is independent of protein synthesis, is PKC-dependent and depends on the function of *radish* and *bruchpilot* (Widmann *et al.*, 2016). *radish* encodes a

functionally unknown protein with multiple phosphorylation sites for PKA and PKC, *bruchpilot* encodes a member of the presynaptic active zone complex (Folkers *et al.*, 2006; Knapek *et al.*, 2011; Widmann *et al.*, 2016).

A previous publication shows *radish* mutants that are defective in MTM (Khurana *et al.*, 2009). However, these experiments only examined the time profiles in which MTM is indistinguishable from ARM. Therefore, anaesthesia-sensitive MTM as in adults has not been defined in larvae (review: Thum and Gerber, 2019).

Protein synthesis-dependent LTM is the third memory form in *Drosophila* larvae. It is formed after a 5-cycle spaced training protocol with a 15 min inter-training interval, or when the energy state of the larva is exceptionally high (Eschment *et al.*, 2020; Widmann *et al.*, 2016). Larvae can retrieve their memory several hours after conditioning (Khurana *et al.*, 2009). It has even been shown that adult *Drosophila* can recall LTM after having been trained as larvae (Tully, Cambiazo, *et al.*, 1994). As in adults, larval *amnesiac* mutants are defective in LTM (Khurana *et al.*, 2009; Turrel *et al.*, 2018).

Current research shows evidence for more memory forms in the adult fly than in the larva. Whether this is due to the simplified CNS in larvae compared to adult flies, or because this question has been more thoroughly investigated in the adult fly, remains to be seen in the future.

In summary, memory is formed after the initial presentation of the stimulus and is refined by repetition. Consolidation leads to different memory forms. Although more forms of memory have been found in adult *Drosophila*, in larvae there is conclusive evidence for STM, ARM and LTM. STM depends on cAMP concentration, LTM depends on protein synthesis and ARM depends on the function of *radish* and *bruchpilot*.

1.4 Compartmentalised cAMP and its role in learning and memory

cAMP is an important second messenger in the vertebrates and invertebrates, playing a role in the PKA- pathway of learning and memory leading to STM and LTM, but also in many other physiological processes in the animal, such as signalling in mammalian mitochondria or in the heart (reviews: Fertig and Baillie, 2018; Valsecchi *et al.*, 2013). Originally described in 1956 and awarded a Nobel Prize in 1971 to E. Sutherland (Sutherland, 1972), cAMP is localized to specific intracellular spaces and can elicit multiple receptor-specific responses within a cell (Hayes *et al.*, 1980). This

subcellular compartmentalisation is regulated by compartmentalised adenylate cyclase isoforms (Conti *et al.*, 2007) and protein kinases anchored by A-kinase anchoring proteins (AKAPs) (Michel and Scott, 2002; Sarkar *et al.*, 1984). cAMP is a small molecule that can equilibrate within the cell in milliseconds (Conti *et al.*, 2002). Therefore, compartmentalised phosphodiesterases (PDEs) are required to locally down-regulate the local cAMP concentration (Hayes and Brunton, 1982; Martinez *et al.*, 2023; Mongillo *et al.*, 2004; Zaccolo and Pozzan, 2002).

1.5 Phosphodiesterases

PDEs play a critical role in maintaining cAMP and cyclic guanosine monophosphate (cGMP) homeostasis and compartmentalisation not only in neurons but in many different cell types. In the mammalian neuron, the subcellular localization of PDE4D5 has been shown to play a crucial role in learning and memory (Martinez *et al.*, 2023). It was shown that nuclear PDE must be exported to facilitate LTM formation (Martinez *et al.*, 2023).

In mammals, there are several families of PDEs, some of which specifically hydrolyse cAMP (PDE4, PDE7, PDE8), specifically hydrolyse cGMP (PDE5, PDE6, PDE9) or hydrolyse both cAMP and cGMP (PDE1, PDE2, PDE3, PDE10, PDE11) (review: Houslay, 2009).

PDE4 is highly conserved, with homologues in mammals, *Drosophila* (Dudai *et al.*, 1976), *Aplysia* (Park *et al.*, 2005) and many other species. In mammals, the genes for PDE4A, PDE4B, PDE4C and PDE4D encode more than 20 different isoforms (review: Houslay, 2009). These isoforms have been shown to be important for the subcellular localisation of cAMP (Baillie and Houslay, 2005; Martinez *et al.*, 2023). Through this subcellular localisation, PDEs have unique functions, such as PDE4D5, which desensitises the β_2-adrenergic receptor in human kidney cells, or PDE4D4, which localises cAMP to the cell-cell contact sites in pulmonary microvascular endothelial cells to ensure the integrity of the endothelial barrier in the lung (Creighton *et al.*, 2008; Lynch *et al.*, 2005).

The human PDE4 isoforms all contain a catalytic domain, which hydrolyses cAMP to AMP, and up to two upstream conserved regions (UCRs) (Fig. 2) (Bolger *et al.*, 1993). The catalytic domain has been shown to be conserved between mammals, *Drosophila* and yeast (Charbonneau *et al.*, 1986).

12

The N-terminal region is important for the subcellular localisation of the PDE (review: Houslay, 2009). It interacts with scaffolding proteins that regulate subcellular localisation. In mammals, PDE4D3 has been shown to interact via the first 15 residues with muscle-selective AKAP (Dodge *et al.*, 2001). Together with PKA, they form a macromolecular unit localised to perinuclear regions in cardiomyocytes (Dodge *et al.*, 2001). There they regulate the contractile force of the heart and are tightly regulated by phosphorylation (Dodge *et al.*, 2001).

PDE4D3 also forms a complex with AKAP450 and PKA (Taskén *et al.*, 2001). Together with PKA, they form a signalling unit in mammalian T-lymphocytes that targets the centrosome and thereby regulates cytoskeletal architecture (Ong *et al.*, 2018; Taskén *et al.*, 2001). In Sertoli cells, it is important for maturation and spermatogenesis (Schimenti *et al.*, 2013).

PDE4D5 interacts with the scaffolding protein RACK1 via its N-terminal sequence, thereby forming a complex with integrins and other proteins (Liliental and Chang, 1998; Yarwood *et al.*, 1999). PDE4D5, normally localised in the nucleus, is exported from the nucleus upon activation of the β_2-adrenergic receptor by forming a complex with it and with arrestin3 (Martinez *et al.*, 2023). This export plays a role in LTM formation in mammals (Martinez *et al.*, 2023). These examples demonstrate the importance of different PDEs and their interaction with scaffolding proteins for the subcellular regulation of cAMP.
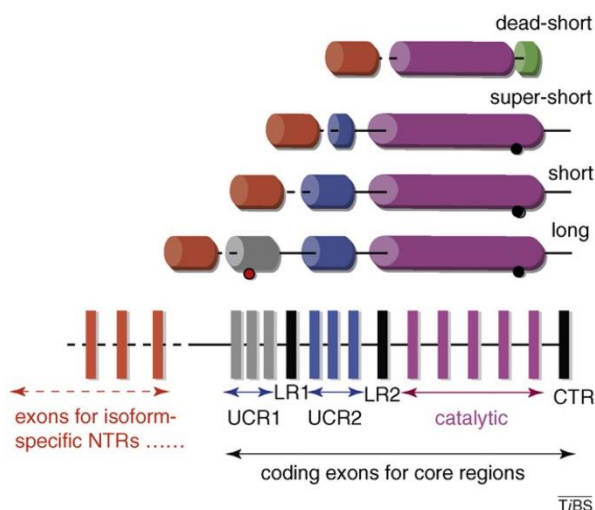
Fig. 2: PDE4 isoforms
Depending on how many UCRs are transcribed, PDE4 can be classified into dead-short isoforms with no UCRs and a truncated PDE, super-short isoforms with no UCR1 and a truncated UCR2, short isoforms with no UCR1 but a UCR2 and long isoforms with UCR1 and UCR2. The catalytic domain is necessary for PDE function, the UCRs mediate oligomerisation and have regulatory functions, the N-terminal region is important for subcellular localisation. (Houslay, 2009, modified)

Depending on how many UCRs are transcribed, PDE isoforms can be subdevided into long isoforms containing both UCRs, short isoforms lacking the UCR1, super-short isoforms lacking UCR1 and having a truncated UCR2, and dead-short isoforms

lacking UCR1 and UCR2 and having an inactive, truncated catalytic subunit (Fig. 2) (Bolger *et al.*, 1993; Houslay, 2001; Mackenzie *et al.*, 2008; Sullivan *et al.*, 1998). The UCRs form a regulatory module that faciliates the phosphorylation of the catalytic subunit by ERK2 and MK2, thereby activating the PDE (Houslay *et al.*, 2017; MacKenzie *et al.*, 2000). The UCRs also mediate homo- and hetero-oligomerisation of PDE4s by interacting with each other (Richter and Conti, 2002; Xie *et al.*, 2014). Short isoforms form monomers, while long isoforms form homo- and heteromultimers (Richter and Conti, 2002; Xie *et al.*, 2014). An interface at the catalytic domain is also involved in oligomerisation (Bolger *et al.*, 2015). This oligomerisation is essential for the regulation of the PDE, but not for the catalytic activity itself (Richter and Conti, 2004; Xie *et al.*, 2014).

1.6   The *Drosophila* phosphodieaterase Dunce

The *Drosophila* genome encodes 6 PDEs: PDE1, Dunce (Dnc), PDE6, PDE8, PDE9 and PDE11 (Day *et al.*, 2005). Of these, two PDEs, PDE6 and PDE9, are cGMP specific (Day *et al.*, 2005). PDE1 and PDE11 are dual-specificity enzymes, hydrolysing both cAMP and cGMP (Day *et al.*, 2005). PDE8 and Dnc, the *Drosophila* PDE4D homologue, are the only *Drosophila* PDEs that are specific for cAMP (Bolger *et al.*, 1993; Day *et al.*, 2005). PDE8, a homologue of human PDE8A, is associated with resistance to cellular stress (Brown *et al.*, 2013). Dnc shares structural properties and subunits with mammalian PDE4D (Bolger *et al.*, 1993).

The *dunce* (*dnc*) gene spans a genomic region of 167.3kb (Khoroshko *et al.*, 2019). Within this region, *dnc* encodes multiple exons with introns large enough to contain other genes (Chen *et al.*, 1987; Furia *et al.*, 1990). In 1991, *dnc* was first shown to encode multiple gene products through multiple transcription start sites (tss) and alternative splicing (Qiu *et al.*, 1991). Six groups of *dnc* transcripts from three different tss were proposed (Qiu *et al.*, 1991). This was later refined to only five distinct groups (Qiu and Davis, 1993). More recent publications confirm at least eight different Dnc transcripts, a database search suggests that there are 17 (FlyBase, 2023; Ruppert, Franz *et al.*, 2017). The different isoforms are associated with different phenotypes and functions (Qiu and Davis, 1993; Ruppert, Franz *et al.*, 2017).

dnc mutants show increased cAMP- levels and decreased cAMP hydrolysis (Davis and Kiger, 1981). There are different *dnc* mutants with stronger and weaker effects

on the cAMP hydrolysis. dnc^1, the mutant established by Aceves-Piña et al. in 1979, shows a 27% reduction in total cAMP hydrolysis, whereas dnc^{M14} shows a 69% reduction (Davis and Kiger, 1981). dnc^1 has a point mutation within the dnc gene that leads to a significant down-regulation of PDE-activity (Byers *et al.*, 1981; Davis and Kiger, 1981; Dudai *et al.*, 1976). However, the exact location of the mutation to date has not been characterized.
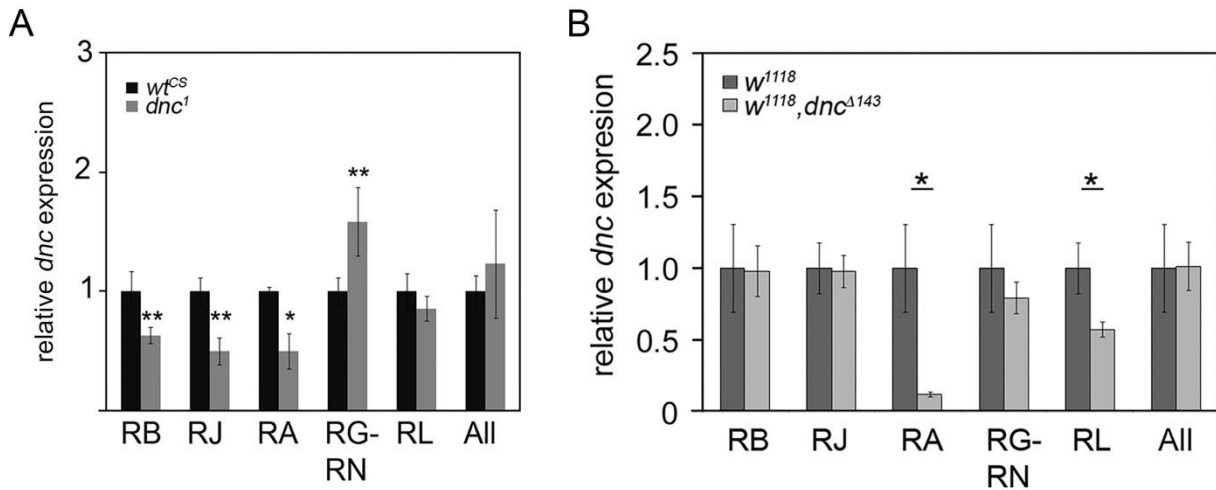
Fig. 3: Expression of *dnc* isoforms in *dnc^1* and *dnc^{Δ143}*
A: In a quantitative polymerase chain reaction (qPCR) analysis, the Dnc mutant dnc^1 showed a significantly reduced expression of dnc^{RB}, dnc^{RJ} and dnc^{RA} and a significantly increased transcription of dnc^{RG}/dnc^{RN}. **B:** The isoform-specific mutant $dnc^{Δ143}$ showed a significantly reduced expression of dnc^{RA} and dnc^{RL} (Ruppert, Franz *et al.*, 2017).

The mutation in dnc^1 has different effects on the expression of dnc isoforms. It significantly down-regulates dnc^{RB}, dnc^{RJ}, and dnc^{RA} while up-regulating dnc^{RG-RN} (Fig. 3) (Ruppert, Franz *et al.*, 2017). For the expression of dnc^{RL}, no significant effect was measured (Ruppert, Franz *et al.*, 2017). $dnc^{Δ143}$, on the other hand, is a newer isoform-specific mutant with a deletion in the first exon of the dnc^{RA} transcript, resulting in significantly lower expression of dnc^{RA} and dnc^{RL} than its control w^{1118} (Fig. 3) (Ruppert, Franz *et al.*, 2017).

1.7   Dunce in associative learning and memory

The dnc gene was originally discovered via its behavioural phenotype. dnc^1 flies were shown to perform significantly worse than their control *CantonS* (*CS)* in both aversive and appetitive olfactory learning and memory experiments in adult *Drosophila* (Dudai *et al.*, 1976; Tempel *et al.*, 1983). Although dnc^1 mutants can remember an

association in the first few seconds after training, they perform worse than the control after a few minutes (Dudai, 1983). Larvae also show impaired memory in an aversive paradigm (Aceves-Piña and Quinn, 1979; Khurana *et al.*, 2012). With impaired cAMP regulation, the Dnc PDE mutant *dnc[1]* was originally considered to be the typical mutant with a primarily defective STM formation (Tully and Gold, 1993). The *dnc[1]* learning and memory phenotype in adult flies can be significantly improved by expressing the Dnc PDE domain or its rat homologue in *dnc[1]* and activating this expression 2 and 4 h before training (Dauwalder and Davis, 1995).

The debate as to whether the *dnc[1]* learning phenotype is due to acquisition or defective STM (Tully and Gold, 1993) has been settled with a "both". Part of the adult *dnc[1]* learning and memory defect is due to the effects of electric shock on odorant perception initiated by changes in neuronal morphology (Préat, 1998). However, a mutation in the Dnc PDE in the MB, a structure in the *Drosophila* brain not associated with memory acquisition but with memory itself, is sufficient to disrupt learning (Préat, 1998; Walkinshaw *et al.*, 2015). Dnc expression in specific sets of Kenyon cells is essential for ARM formation (Bouzaiane *et al.*, 2015; Scheunemann *et al.*, 2012). Dnc also plays a role in the regulation of olfactory aversive LTM. A pair of serotonergic projection neurons that project to the MB peduncle has been identified as a checkpoint for LTM formation in adult flies (Scheunemann *et al.*, 2018). There, Dnc activity provides the switch between ARM, which is formed when Dnc is active in this pair of neurons, and protein synthesis-dependent LTM, which is formed when Dnc is inhibited in this pair of neurons (Scheunemann *et al.*, 2018). In larvae, STM and ARM are formed in parallel after a single aversive training cycle, with *dnc[1]* showing ARM which is not significantly different from its control *CS* (Widmann *et al.*, 2016).

dnc plays a role in ARM in adults but not in larvae (Bouzaiane *et al.*, 2015; Scheunemann *et al.*, 2012; Widmann *et al.*, 2016). On the one hand, this could be due to the simplified CNS in larvae and therefore effects of *dnc* outside the MB Kenyon cell regulating excitatory or inhibitory projection neurons (Lee, 2015; Scheunemann *et al.*, 2018), which have not yet been identified in the larvae. On the other hand, it could be that the adult fly is a more common model system and therefore has been studied in more experiments than the larva, and the memory phenotype of dnc mutants will be further investigated in the future. However, the findings in both adults and larvae show that Dnc plays a crucial role in regulating the type of memory that is formed after a stimulus.

rut^1, a mutant with defective *rutabaga* is an adenylate cyclase mutant that has the opposite effect to *dnc* mutants and therefore has elevated total cAMP levels (Livingstone *et al.*, 1984). The memory phenotype of the Dnc mutant *dnc^{M11}* cannot be restored to control levels by reducing cAMP-levels using a double mutant with the adenylate cyclase mutant *rutabaga*. The different cellular and subcellular localisation of cAMP may be one of the reasons why *rut^1*, cannot rescue the learning and memory phenotype of Dnc mutants (Ueda and Wu, 2012). *dnc* and *rut* affect different forms of memory (Scheunemann *et al.*, 2012). Both mutants disrupt STM, *dnc^1* shows defective ARM, whereas *rut^1* shows defective anaesthesia-sensitive MTM in adult flies (Scheunemann *et al.*, 2012).

In summary, Dnc has an important function in learning and memory. Dnc mutants are defective in memory acquisition and in STM, but total cAMP-levels are not sufficient to restore the memory phenotype of Dnc mutants to a control memory phenotype.

1.8   The *dnc^{Δ143}* mutants learn quicker

dnc^1 is still used in many current studies (Khurana *et al.*, 2012; Scheunemann *et al.*, 2018; Widmann *et al.*, 2016; Zhao *et al.*, 2020). As mentioned above, this mutant affects the transcription of multiple Dnc isoforms. *dnc^{Δ143}* is an isoform-specific mutant with a deletion in the promoter region and the first exon of the *dnc^{RA}* transcript, resulting in significantly lower expression of *dnc^{RA}* and *dnc^{RL}* than the control *w^{1118}* (Fig. 3) (Ruppert, Franz *et al.*, 2017).

To analyse whether *dnc^{RA}* affects memory performance, M. Gompert performed olfactory aversive learning and memory experiments in *Drosophila* larvae using AM and ethyl acetate (EA) as odorants and 2M NaCl as reinforcer (Gompert, 2019). In a one-cycle experiment, *CS* shows no significant memory and therefore no difference to *dnc^1* can be detected (Fig. 4 A). *w^{1118}* also shows no significant memory, leading to the conclusion that wild-type *Drosophila* larvae trained with this paradigm do not show significant memory after one training cycle. *dnc^{Δ143}* shows significant memory and thus learns significantly better than its control *w^{1118}* (Fig. 4 A).
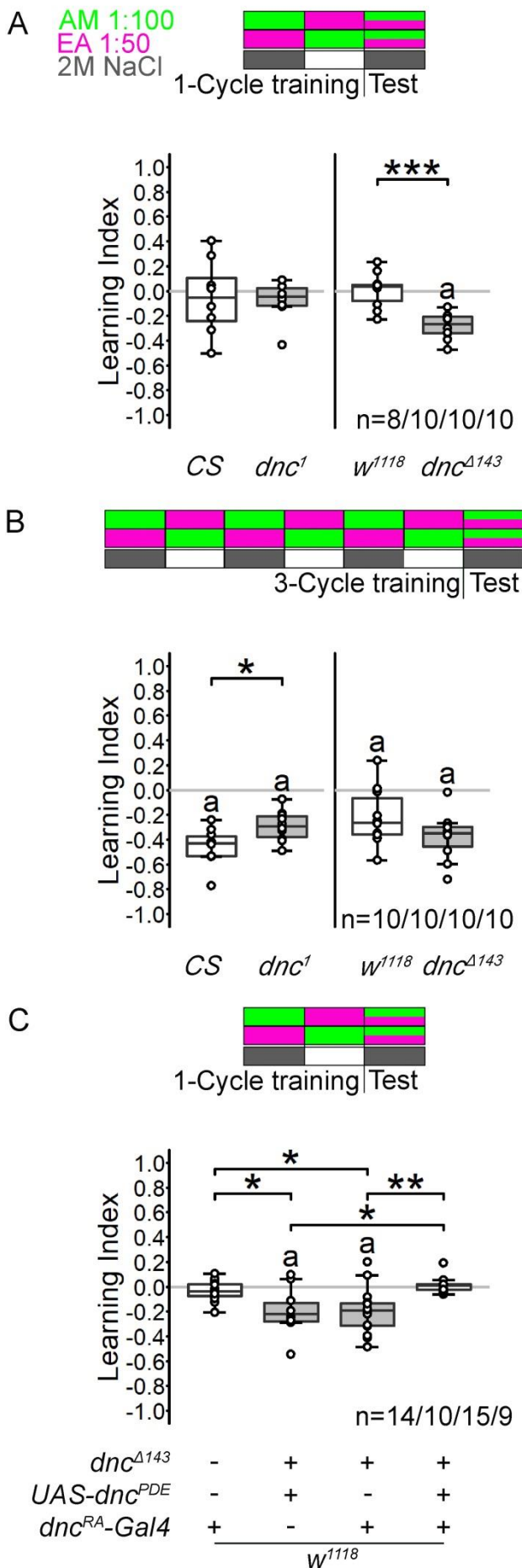
After three training cycles, *CS* shows significant memory. *dnc[1]* performs significantly worse than its control *CS* (Fig. 4 B). These results confirm the published phenotype (Aceves-Piña and Quinn, 1979; Khurana *et al.*, 2009; Widmann *et al.*, 2016). *w[1118]* and *dnc[Δ143]* both show memory, they are not significantly different from each other (Fig. 4 B). This shows that either *dnc[RA]* or *dnc[RL]* has an effect on memory performance in *Drosophila* larvae.

Fig. 4: Dnc[PA] is a negative regulator of memory after one training cycle.
A: After one training cycle, *dnc[Δ143]* larvae learn the association of odorants with 2M NaCl. *dnc[1]* and the respective controls *w[1118]* or *CS* do not form significant memory. **B**: After three training cycles, *dnc[1]* forms significantly less memory than *CS* while *dnc[Δ143]* does not show significantly improved memory compared to its control *w[1118]*. **C**: Expression of the PDE domain of Dnc under the control of the *dnc[RA]*-Gal4 driver reduces the learning of *dnc[Δ143]* to control levels. Significant differences from random choice were determined by one-sample t-test ($P < 0.05$) and are indicated by 'a'. Differences between two groups were analysed by Student's t-test, differences between more than two groups were analysed by ANOVA with Tukey's post-hoc-test with *: $P < 0.05$, **: $P < 0.01$ and *** $P < 0.001$. Experiments shown in this figure were conducted by Magdalena Gompert (Bachelor thesis: Gompert, 2019).

18

To investigate whether PDE activity in dnc^{RA}-positive cells is required to suppress memory in flies, the Dnc PDE domain, a domain common to all Dnc isoforms that encodes the catalytic subunit, was reintroduced into $dnc^{\Delta143}$ mutants using the dnc^{RA}-Gal4 driver. Expression is sufficient to reduce the enhanced memory phenotype of $dnc^{\Delta143}$ mutants to control levels. This shows that PDE activity is required in dnc^{RA}-positive cells to inhibit the enhanced memory phenotype, providing evidence that the enhanced memory phenotype is due to reduced expression of dnc^{RA}. These findings may reveal the neurons that are required to suppress premature memory formation.

1.9   The larval neuromuscular junction as a model of synaptic plasticity

Synaptic plasticity is the basis of memory formation (Castellucci *et al.*, 1970; Maren, 2005; review: Milner *et al.*, 1998). Because the Drosophila larval neuromuscular junction (NMJ) is homologous to synapses in the vertebrate brain and is easily accessible and distinguishable, it is the perfect model system to study synaptic plasticity and thus a model to study synaptic transmission not only to muscle but also in the CNS (Jan and Jan, 1976; review: Menon *et al.*, 2013).

For the larval memory experiments, the readout is based on the larva's ability to enervate its muscles and to move in a controlled manner. Changes in muscle enervation affect the performance. They can be observed directly at the NMJ.

In each of the abdominal hemisegments A2 to A7, the larval ventral nerve cord (VNC) is connected to 30 muscle fibres of the larval body wall via 32 individually identifiable motor neurons (Fig. 5) (Hertweck, 1931; Landgraf *et al.*, 1997; Nicholson and Keshishian, 2006; Schmid *et al.*, 1999). They have a distinct morphology and their muscle targets are well defined (review: Menon *et al.*, 2013).

Intersegmental motor neurons innervate muscles via three classes of boutons: Type I, Type II and Type III. The classes are defined by their size and their neurotransmitters.

Type I boutons are glutamatergic (Hoang and Chiba, 2001; Johansen *et al.*, 1989). They are divided into two classes with Type Ib being 3-6µm and Type Is being 2-4µm (Hoang and Chiba, 2001). Type II boutons are 1-2µm and octopaminergic (Hoang and Chiba, 2001; Johansen *et al.*, 1989; Monastirioti *et al.*, 1995). Type III boutons are 2-3µm and contain glutamate and insulin (Gorczyca *et al.*, 1993; Hoang and Chiba, 2001).

NMJ morphology is strongly influenced by cAMP levels. It has been shown that Dnc mutants have a significant increase in the concentration of cAMP (Davis and Kiger, 1981). At the NMJ, Dnc mutants show an increased number of varicosities and increased branching (Corfas and Dudai, 1991; Zhong *et al.*, 1992). They have increased morphological and physiological variability between boutons and within a bouton (Renger *et al.*, 2000). Dnc overexpression reduces cAMP in the larval CNS by 60%, resulting in a significantly reduced total number of varicosities (Cheung *et al.*, 1999).
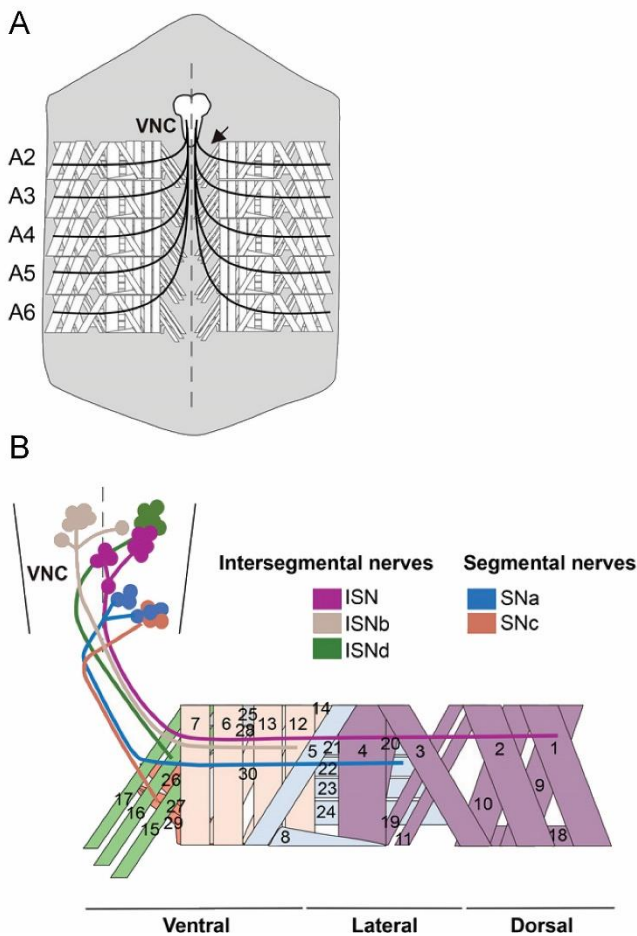
Fig. 5: The NMJ in the 3rd instar *Drosophila* larva
A: The motor neurons of the abdominal region of the VNC project to the muscles in the body wall by about 30 motor neurons per segment. Only segments A2-A6 are shown. **B:** Body wall of each of the repetitive abdominal hemisegments. ISN stands for intersegmental nerve, SN for segmental nerve. The muscles innervated by each nerve are shown in a lighter colour than the nerve. The dots represent individual cell bodies, with axons enervating the respective muscle cells.
Many studies examine segment A4 NMJ 6/7. It is enervated by two parallel motor neurons, ISNb-Is and ISNb-Ib, via Is and Ib boutons (Pérez-Moreno and O'Kane, 2019).

It has been shown that varicosity formation is regulated by cAMP via two factors: Fasciclin II (FasII) is localised in the pre- and postsynaptic membrane and is required for synapse stabilisation (Schuster *et al.*, 1996a). Elevated cytosolic cAMP -levels down-regulate FasII, leading to synaptic sprouting (Schuster *et al.*, 1996b). FasII needs to maintain a pre-/postsynaptic symmetry and interacts with Appl via the Appl-binding protein dX11 (Ashley *et al.*, 2005). To fill the newly formed synapses with release machinery, cytoplasmatic cAMP increases dCREB2a (CREB = cAMP-

response element-binding protein) activity in the nucleus, thereby promoting the transcription of the release machinery (Davis *et al.*, 1996).

1.10 Localisation of Dunce at the cellular and subcellular level

Using a putative anti-Dnc antibody, it has been shown that Dnc is concentrated in the MB (Nighorn *et al.*, 1991). However, the specificity of this antibody is controversial as it was only tested on extracts of bacteria transformed with a polypeptide.

In the MB, Dnc has been shown to be essential for cAMP- compartmentalisation (Gervasi *et al.*, 2010). In wild-type flies, Dnc compartmentalises dopamine-induced PKA activation to the α-lobe of the MB, whereas *dnc¹* mutants do not show this localisation (Gervasi *et al.*, 2010). *dnc* plays a role in the AL in GABAergic local neurons, in the MB in α,β and γ Kenyon cells and in a number of serotonergic projection neurons (Scheunemann *et al.*, 2012, 2018; Walkinshaw *et al.*, 2015). *rut* has also been shown to be important in α,β and γ Kenyon cells (Scheunemann *et al.*, 2012).

At the subcellular level, it has been shown at the *Drosophila* larval NMJ that in neurons, the cell body, axon and bouton form three independent cAMP signalling compartments (Maiellaro *et al.*, 2016). Dnc overexpression affects cAMP-concentration mainly in the presynaptic bouton (Cheung *et al.*, 1999). In wild-type larvae, elevated cAMP levels in individual boutons are unable to travel further than the adjacent bouton (Maiellaro *et al.*, 2016). The activity and specific localisation of PDEs is required to maintain these signalling compartments and prevent the signal from spreading to other compartments (Maiellaro *et al.*, 2016). The reduced efficiency of the cAMP degradation in *dnc¹* leads to the spread of localised cAMP signals (Maiellaro *et al.*, 2016).

The different isoforms are proposed to influence subcellular localisation (Gervasi *et al.*, 2010). Although this has not yet been shown in *Drosophila* neurons, it has been shown that the different Dnc isoforms localise differently within epithelial cells. In large epithelial follicle cells of the ovary, Dnc^PG is expressed in the nucleus, whereas Dnc^PA and Dnc^PL are mainly expressed in the cytoplasm (Ruppert, Franz *et al.*, 2017). Dnc also affects neuronal development. While the number of axons increases over time after eclosion in the wild type, the number of axons decreases in *dnc* mutants (Balling *et al.*, 1987).

The increased cAMP concentration in *dnc* mutants leads to altered electrophysiology in neurons (Bhattacharya *et al.*, 1999; Delgado *et al.*, 1998; Ganguly and Lee, 2013). Ca^{2+} channel current is increased and cAMP-regulated K^+ channels are decreased in *dnc^1* (Bhattacharya *et al.*, 1999; Delgado *et al.*, 1998). Inhibitory GABAergic postsynaptic currents are also reduced in *dnc^1* (Ganguly and Lee, 2013).

In a Dnc knockdown line, postsynaptic cAMP was shown to downregulate the glutamate receptor GluRIIA and upregulate GluRIIB (Zhao *et al.*, 2020).

dnc^1 shows altered synaptic plasticity in both sensory and motor neurons, with increased branching in motor neurons due to elevated cAMP levels (Corfas and Dudai, 1991; Vonhoff and Keshishian, 2017; Zhong *et al.*, 1992; Zhong and Wu, 1991). Alterations in synaptic transmission and long-term facilitation at cholinergic synapses in the CNS have also been shown in cultured embryonic neurons of *dnc* mutants (Lee and O'Dowd, 2000). The Ca^{2+} homeostasis is also disturbed. Elevated cAMP levels upregulate Dihydropyridine-sensitive Ca^{2+} channels via PKA (Bhattacharya *et al.*, 1999), resulting in a higher peak Ca^{2+} concentration and a shorter decay time (Alshuaib *et al.*, 2004).

In summary, within the CNS, Dnc is particularly important in the MB. Within the neuron it is important for cAMP compartmentalisation. In Dnc mutants, subcellular localisation of cAMP is disturbed and neuronal development is altered.

1.11 Other phenotypes of Dunce mutants

cAMP and thus the Dnc PDE play a role in several other processes in the fly. One example is habituation. Short-term habituation has been shown to be caused by central synaptic mechanisms and not by adaptation of sensory neurons (Larkin *et al.*, 2010). *dnc^1* habituates more slowly than wild-type flies in experiments examining the habituation of the jump reflex to an odorant stimulus (Asztalos *et al.*, 2007). Habituation of the proboscis extension reflex is also impaired in *dnc^1* (Duerr and Quinn, 1982). Other reflexes in other *dnc* mutants show a different picture. The escape circuit of *dnc^{M14}* through the giant fibre response shows an improved habituation phenotype (Engel and Wu, 1996), as does *dnc^2*, which shows improved habituation of the landing response (Rees and Spatz, 1989).

In operant visual conditioning experiments, *dnc^1* flies show a reduced ability to learn, similar to what has been shown in associative olfactory conditioning (Gong *et al.*, 1998). With a reduced ability to focus on specific visual figures, *dnc^1* also shows

deficits in visual attention (Wu *et al.*, 2000). *dnc*[1] shows a defect in responding to novel visual stimuli (van Swinderen, 2007).

Mutations in the *dnc* gene also affect female fertility and male courtship behaviour (Gailey *et al.*, 1985). This effect is observed in *dnc*[M14], a mutant in which homozygotes are female sterile (Davis and Kiger, 1981). *dnc* is required in the germline to control oocyte growth (Swan *et al.*, 2001).

dnc mutants also show an abnormally shortened circadian period (Levine *et al.*, 1994). In larvae, *dnc*[1] mutants show faster locomotion than their control *CS* (Aleman-Meza *et al.*, 2015).

The cAMP pathway also plays a role in odorant perception (Martín *et al.*, 2001). Dnc can be localised in *Drosophila* antennae, and *dnc*[1] mutants show a significantly reduced sensitivity to some odorants such as EA, while the sensitivity to BA is increased (Martín *et al.*, 2001). *dnc*[1] mutants also fail to adapt to odorant exposure by being unable to change the volume of olfactory glomeruli (Devaud *et al.*, 2001).

Apart from its role in learning and memory, the cAMP-CREB signalling pathway also plays an important role in addiction (review: Blendy and Maldonado, 1998). For ethanol, initial alcohol sensitivity does not differ from the control, but tolerance in re-exposure is reduced by 43% (Ruppert, Franz *et al.*, 2017). This lack of ethanol tolerance was further restricted to the Dnc[PA] isoform (Ruppert, Franz *et al.*, 2017). For nicotine, a highly addictive acetylcholine receptor agonist with a high efficacy on nicotinergic acetylcholine receptors in mammals and in *Drosophila* (Corrigall and Coen, 1989; Mulle *et al.*, 1991; review: Gundelfinger and Hess, 1992), *dnc*[1] was shown to be more responsive than its control, both at the level of fly behaviour and endogenous cAMP levels (Hou *et al.*, 2004).

In summary, Dnc is a PDE that is not only important for associative learning and memory, but also for many other phenotypes. Prominent examples include habituation, reproduction and addiction.

1.12 Objective

dnc^1 is the classical mutant associated with a function in STM (Dudai *et al.*, 1976). However, recent publications have increasingly pointed to specific roles for different isoforms. The Dnc PDE has been shown to play a role in intracellular cAMP dynamics, and different isoforms have been suggested to play a role (Gervasi *et al.*, 2010; Maiellaro *et al.*, 2016). It was shown that the Dnc isoforms localise differently in the cell (Ruppert, Franz *et al.*, 2017). M. Gompert provided first evidence for an isoform-specific memory phenotype (Gompert, 2019).

In this work, we aimed to identify which Dnc isoforms contribute to the regulation of learning and memory and in what way.

The following main questions were addressed:

1.   What are the functions of different Dnc isoforms in learning and memory?

2.   In which neurons of the larval CNS are the different isoforms expressed?

3.   Where at the subcellular level are the different Dnc isoforms expressed?

For the first question, we investigated the impact of the Dnc^{PA} and Dnc^{PB} on learning and memory by characterising the memory phenotype of several Dnc mutants. We examined dnc^1, the mutant that affects the expression of multiple Dnc isoforms (Ruppert, Franz *et al.*, 2017), the Dnc^{PA}-specific mutant $dnc^{\Delta143}$ (Ruppert, Franz *et al.*, 2017), and dnc^{EP1395}, a mutant that we show to be Dnc^{PB}-specific. We confirmed the phenotype of $dnc^{\Delta143}$ using a dnc^{RA} knockdown. To dissect the affected forms of memory, we used different learning and memory paradigms and reintroduced different isoforms.

To analyse in which neurons in the larval CNS the different Dnc isoforms are expressed, we used a dnc^{RA} isoform-specific promoter-Gal4 line to study the localisation of Dnc^{PA}. We also designed and tested an antibody against most of the isoforms and putative antibodies against Dnc^{PB}, Dnc^{PJ}, Dnc^{PG} and Dnc^{PF}.

Finally, to investigate the subcellular localisation of Dnc^{PA} and the influence of the subunits on localisation, we analysed their structure using AlphaFold (Jumper *et al.*, 2021) and showed their differential localisation within the neuron at the NMJ. We also investigated the localisation of Dnc^{PG}, an isoform containing a nuclear localisation sequence, at the NMJ (Ruppert, Franz *et al.*, 2017). To investigate the localisation of memory formation, we expressed differentially tagged Dnc^{PA} transgenes and Dnc^{PG} in $dnc^{\Delta143}$ mutants. To investigate the subcellular localisation of Dnc^{PB}, Dnc^{PJ}, Dnc^{PG} and Dnc^{PF}, we also used the putative isoform-specific antibodies.

2 STAR☆Methods

2.1 Resource availability

2.1.1 Lead contact
Further information and requests for resources and reagents should be addressed to and will be fulfilled by the supervisor, Prof. Dr. Henrike Scholz (henrike.scholz@uni-koeln.de).

2.1.2 Materials availability
All materials produced will be made available upon request.

2.2 Data availability
All raw data will be made available upon request.

2.3 Experimental model and subject details
Drosophila melanogaster was used for all experiments. The transgenic lines used are listed in the key resources table (Table 1). Flies were maintained on a standard cornmeal-based food at 25°C and 60% relative humidity on a 12 h light/dark cycle. For behavioural experiments, flies were reared under density control, i.e. 30 virgins were crossed with 15 males. All experiments except the western blots were performed on L3 larvae, the behavioural experiments on foraging L3 larvae and the immunohistochemistry on wandering L3 larvae.

2.4 Method details

2.4.1 Larval learning and memory
The learning and memory assays performed were associative aversive olfactory memory assays on foraging L3 *Drosophila* larvae. The reinforcer used was 2M NaCl. BA (pure), EA (1:50) and AM (1:100) were used as odorants. To control for the influence of the mutation on odorant perception and on signal strength, a preference and a balance test for the two odorants used in the assay were performed as a prerequisite for the learning and memory assays.

In the preference test, an odorant cup containing an odorant was placed on one side of the 2.5% agarose plate and an odorant cup containing paraffin was placed on the opposite side. 20 larvae were collected, washed in water and placed in the neutral zone, a 1 cm wide area in the centre of the plate. The plate was covered with a perforated lid and left in the dark for 5 min. The larvae on each side and in the neutral

zone were then counted and the preference index was calculated. This test was performed on agarose plates without NaCl and on agarose plates containing 2M NaCl, for both odorants and for each genotype. In the balance test, two different odorants were placed on opposite sides. The concentrations of the odorants were chosen so that the larvae perceive the odorant and both odorants are equally attractive in a choice situation. Potential changes in the attractiveness of the odorants due to the reinforcer during the training are also controlled for by the balance test.

The associative aversive larval olfactory learning and memory assays were conducted according to the reciprocal aversive learning paradigm of Widmann et al with one or three training cycles (Widmann *et al.*, 2016). Two groups of approxymately 20 larvae were collected. They were first trained on a 2M NaCl agarose plate for 5 min, one group with odorant A, the other group in parallel with odorant B. Then, they were trained on a neutral plate with the other odorant for 5 min. The training cycles were repeated up to two times for a three-cycle learning experiment. Tests were performed for 5 min in the presence of 2M NaCl with both odorants. Training and testing were performed in the dark. Changes in the learning paradigm are shown in the scheme in Figure 9.

2.4.2 Antibody design

The isoform-specific antibodies have been designed against polypeptides encoded by exons unique to one or two isoforms of *dnc*. They are mouse antibodies ordered from Abmart in 2019. The antibodies were developed using the PETAL™ method (Wang *et al.*, 2020). It takes advantage of the multispecifity of antibodies and uses a microarray of 62,208 proteome epitope tag antibody library (PETAL™) (Wang *et al.*, 2020). The sequences of the polypeptides against which the antibodies were designed are shown in Table 2 in the Supplementary Appendix.

The anti-Dnc[all] antibody serum was raised against two polypeptides. The peptides are encoded by an exon common to all Dnc isoforms except Dnc[PL]. The sequences of the polypeptides against which the antibody was raised are shown in the Supplementary Appendix (Table 2). Immunisation was performed by Eurogentec following the AL-DOUB-LX programme by Eurogentec in 2010, where two different peptides each were used in the same rabbit; this procedure was performed on two animals. The antibody serum of the second bleed of both animals was mixed and affinity purified by Eurogentec.

26

2.4.3 Immunohistochemistry

To label the larval CNS, wandering 3rd instar larvae were dissected in ice-cold phosphate-buffered saline (PBS). They were fixated for 20 min in 3.7% formaldehyde in PBS. After three rinses and three 20-min washes with PBS containing 0.3% Triton (0.3% PBT), the CNS were blocked with 5% FCS (0.3% PBT with 5% fetal bovine serum (FCS)) for 2 h and then incubated with the primary antibody in 5% FCS on a shaker at 4°C for two nights. Before application of the secondary antibody, the CNS were rinsed three times and washed three times for 20 min with 0.3% PBT. They were incubated with the secondary antibody in 0.3% PBT at 4°C overnight and the CNS were again rinsed three times and washed three times for 20 min with 0.3% PBT. Finally, the samples were incubated in 50% glycerol in PBS for 30 min and then mounted on a microscope slide in VectaShield® with spacers or in VectaShield® containing 1.5µg/ml 4′,6-diamidino-2-phenylindole (DAPI) with spacers. Confocal images were captured using either an Olympus Fluoview FV1000 or a Leica SP8 with 20x air, 40x or 63x glycerol immersion objectives. The resulting image stacks were analysed using Fiji Image-J and processed in Photoshop. To identify brain regions, we used larvalbrain.org (Thum *et al.*, 2021).

For analysis of the NMJ, the wandering L3 larvae were placed on ice and the body wall was dissected in ice-cold PBS, the CNS was not removed. Multiple genotypes were pinned to the dissection plate and not removed until the mounting to ensure equal treatment. Samples were fixated in 3.7% formaldehyde/PBS solution three times for 30 sec and once for 15 min. After three rinses and three washes for 20 min in PBS with 0.1% Triton (0.1% PBT), the body walls were blocked in 5% FCS (0.1% PBT with 5% FCS) for 30 min and then incubated with the primary antibody in 5% FCS at 4°C overnight. Before application of the secondary antibody, the body walls were rinsed three times and washed three times with 0.1% PBT for 20 min. They were incubated with the secondary antibody in 0.1% PBT for 2 h at room temperature and the body walls were rinsed three times and washed three times for 20 min with 0.1% PBT. Finally, they were incubated in 50% glycerol in PBS for 30 min and then mounted on a slide in VectaShield®. Segment A4 NMJ 6/7 was scanned using a Leica SP8 with a 63x glycerol immersion objective. The resulting image stacks were analysed using Fiji Image-J, they were rotated and organised using Photoshop.

2.4.4 Western blots

Heads from 500 adult *Drosophila* were used for the Western blots. Flies were frozen at -80°C for 20 min and heads were removed using liquid nitrogen and two metal sieves. Fly heads were homogenised in 200µl RIPA lysis buffer supplemented with cOmplete™ protease inhibitor. They were then incubated on ice for 30 min and centrifuged at 14000 rpm for 20 min at 4°C. The proteins in the supernatant were stored on ice and their concentration was measured using a Bradford assay. Samples were prepared in 4x Laemmli buffer with 5% β-mercaptoethanol and then denatured at 100°C for 10 min. They were run on a 9% sodium dodecyl sulfonate-polyacrylamide gel electrophoresis (SDS-PAGE) gel and transferred to a 0.45µm nitrocellulose membrane at 100V for one hour. The membrane was stained with Ponceau S to ensure that the transfer worked and washed with H_2O. It was blocked with 5% milk in Tris-buffered saline with Tween (TBST) buffer and primary antibodies were incubated overnight at 4°C. The membrane was washed three times with TBST for 10 min and incubated with the secondary antibody for 2 h at RT. The membrane was stripped for reprobing using mild stripping buffer (15g glycine, 1g SDS and 10ml Tween in 1l H_2O). Detection was performed using a home-made ECL kit, consisting of two components. Component A and B were mixed and incubated on the membrane for 10 min. The film was developed for 10-40 min. The films were then digitalised on an office scanner/photocopier.

2.4.5 Quantitative PCR

For the qPCR, 90 larval CNS were dissected and collected in TRIzol on ice within one hour. Total RNA was extracted by thiocyanate-phenol-chloroform extraction using TRIzol according to the manufacturer's standard protocol for tissues scaled down to 400 µl (ThermoFisher, 2016). The incubation with chloroform was reduced to 15 s. The optional precipitation step and the washing step were added. A second washing step was added by incubating the pellet with 1ml 70% ethanol and centrifuging at 7500 g at 4 °C. cDNA was synthesised using Superscript II Reverse Transcriptase according to the manufacturer's standard protocol (Life Technologies Corporation, 2010). RNA was removed by incubation with RNase at 37 °C for 30 min. The cDNA concentration was adjusted to 100ng/µl prior to qPCR. We used Eurogentech's MESA blue qPCR master mix according to the manufacturer's standard protocol in an iCycler iQ5 Multicolor Real-Time PCR Detection System. The

optimal reference gene, actin, was identified using the NormFinder Excel plug-in. The sequences of the primers used are shown in the Supplementary Appendix (Table 3).

2.4.6 Predictive models for Dnc proteins

AlphaFold2 was used to analyse the structure of green fluorescent protein (GFP) tagged Dnc^{PA} proteins (Jumper *et al.*, 2021). We followed the pipeline and parameters published in the AlphaFold Google Colaboratory notebook with default settings except for a disabled relaxation step (AlphaFold Google Colaboratory, 2022). The resulting model was analysed and rotated using PyMOL and organised using Photoshop CS5.

2.5 Quantification and statistical analysis

2.5.1 Larval learning and memory assays

To calculate the results of the preference and balance test, the preference index (PI) was calculated as follows:

$$PI = \frac{Number\ of\ larvae\ (odorant\ A) - Number\ of\ larvae\ (odorant\ B)}{Total\ number\ of\ larvae}$$

For the reciprocally trained larvae in the learning and memory assay, a preference index was calculated for both of the reciprocal experiments. In this case, the odorant reinforced with the negative gustatory stimulus was used as odorant A, the non-reinforced odorant as odorant B. From the preference indices of the reciprocal experiments, the learning index (LI) was calculated:

$$LI = \frac{PI_{Aversive\ odorant\ A} - PI_{Aversive\ odorant\ B}}{2}$$

Thus, with the exception of a different naming of the indices, our analysis follows the protocol used by Widmann et al (2016). In R, we used a one-sample t-test to determine whether larvae showed a difference from random choice. To determine differences between genotypes, for experiments with two genotypes, we performed a Student's t-test between the two genotypes and an ANOVA with Tukey's honest significant difference test for experiments with more than two genotypes. Therefore, we used stats and rstatix packages of R. Plots were generated in R using functions from ggplot2, ggpubr and ggthemes.

2.5.2 Immunohistochemistry

To analyse the structures recognised by the anti-Dnc[all] antibody or the Anti-GFP antibody in *dnc[RA]-Gal4* –driven neurons (Fig. 10, 18), multiple CNS were analysed. The number of CNS or hemispheres analysed is indicated in the respective figures. The results were summarised in a cartoon created using Photoshop. One brain hemisphere and one side of the VNC were considered as one repetition. The number of neurons observed in a cluster is documented in Excel. Across all brain sides, an average and a standard deviation are calculated. A Student's t-test was used to compare the number of neurons between mutants and their control genotype.

To analyse the morphology of neurons at the NMJ the number of branches and the total number of boutons were counted. The anti-horseradish peroxidase (HRP) antibody was used to visualize branches and boutons. Anova with Tukey's honest significant difference test was used for comparison between different genotypes using the stats and rstatix packages in R. Plots were generated in R using ggplot2, ggpubr and ggthemes.

2.5.3 Western blots

The distance travelled by the ladder and bands was measured in Photoshop. Following the molecular weight calculation protocol published on the Bio-Rad website (Bio-Rad Laboratories Inc, 2023), we used Excel to calculate the R_f value for each band. The R_f value is calculated as follows:

$$R_f = \frac{Distance\ to\ the\ band}{Distance\ to\ the\ dye\ front}$$

We used the function linear fit on wolframalpha.com (Wolfram|Alpha, 2023) to the logarithm of the molecular weight as a function of R_f of the ladder bands. Using the resulting equation and the R_f values of the unknown bands we determined the logarithm of the molecular weight of the bands in the protein under investigation.

For Figure 15 C, D, we calculated the molecular weight on 3 blots using the above method and used Excel to calculate the average molecular weight and standard deviation for each band. For the quantitative analysis, the bands of the studied antibody and the same band incubated with β-actin were analysed in Image-J according to the protocol in the Electrophoretic Gel Analysis section of the ImageJ website (ImageJ, 2023). Briefly, this protocol marks the lanes analysed and generates a plot of the lane profile. The boundaries of the peaks were determined using a line drawing tool and the area in the plot was measured. The results were

then loaded into Excel and then normalised to the β-actin results. The % change compared to a control was calculated in Excel. This was repeated for all 3 blots of the same genotype and finally the mean and the standard deviation of the change was calculated in Excel.

2.5.4 Quantititive PCR

The qPCR was analysed in Excel using the Pfaffl method (Pfaffl, 2001). Three replicates were performed on the same plate. A Student's t-test was used in Excel to analyse whether the difference between the groups was significant. R and its packages ggplot2, ggpubr and ggthemes were used to generate a bar plot.

2.6   Key Resources Table

Table 1: Key resource table

Reagent or resource	Source	identifier
Fly strains		
w^{1118}	Hazelrigg *et al.*, 1984	BDSC No. 6326
CantonS		BDSC No. 64349
$w^{1118}, dnc^{\Delta143}$	Ruppert, Franz *et al.*, 2017	N/A
dnc^1	Dudai *et al.*, 1976	BDSC No. 6020
$w^{1118}, dnc^{\Delta143};;dnc^{RA}$-Gal4	Manuela Ruppert	N/A
$w^{1118}, dnc^{\Delta143};UAS\text{-}dnc^{PDE}$	Manuela Ruppert	N/A
UASmCD8::GFP;UASmCD8:: GFP;UASmCD8::GFP	Lee and Luo, 1999	N/A
$w^{1118};UAS\text{-}tau::GFP$	Brand, 1995	N/A
DV-Glut-Gal4/CyO;TM2/TM6bb	Daniels *et al.*, 2004	N/A
$w^{1118};UAS\text{-}dnc^{RA}::eGFP$	Ruppert, Franz *et al.*, 2017	N/A
$w^{1118};UAS\text{-}GFP\text{-}dnc^{RA}$	Li Ming Gooi	N/A
$w^{1118};UAS\text{-}dnc^{RG}::eGFP$	Li Ming Gooi	N/A
$dnc^1;;UAS\text{-}dnc^{PDE}$	Henrike Scholz	N/A
$dnc^1;; dnc^{RA}$-Gal4	Manuela Ruppert	N/A
$w^{1118}, dnc^{\Delta143}; UAS\text{-}dnc^{RA}::eGFP$	Manuela Ruppert	N/A
$w^{1118}, dnc^{\Delta143};UAS\text{-}GFP\text{-}dnc^{RA}$	Manuela Ruppert	N/A
$w^{1118}, dnc^{\Delta143};UAS\text{-}dnc^{RG}::eGFP$	Manuela Ruppert	N/A
$w^{1118};;dnc^{RA}$-Gal4	Ruppert, Franz *et al.*, 2017	N/A
dnc^{EP1395}	Rørth, 1996	BDSC 11068
Appl-Gal4	Torroja *et al.*, 1996	BDSC 32040
$y^1, dnc^{M14}cv^1v^1f^1$/FM7a	Mohler, 1977	BDSC 4714
$w^{1118},HugS3$-Gal4	Melcher and Pankratz, 2005	BDSC 58769
$w^{1118};TH$-Gal4	Friggi-Grelin *et al.*, 2003	BDSC 8848
$UAS\text{-}dnc^{RNAi}$	Fenckova *et al.*, 2019	VDRC 107967

Reagent or resource	Source	identifier
Antibodies		
Anti-GFP mouse (1:200, Western blot: 1:500)	Invitrogen	A-11120
Anti-GFP rabbit (1:1000)	Rockland Immunochemicals	600-401-215
Anti-nc82 mouse (1:20)	Schroll *et al.*, 2006	AB_2314866
Anti-FasII mouse (1:50)	Hummel *et al.*, 2000	AB_528235
Anti-discs large (DLG) mouse (1:1000)	Parnas *et al.*, 2001	AB_528203
Anti-ChAT mouse (1:100)	Takagawa and Salvaterra, 1996	AB_528122
Anti-Lamin mouse (1:100)	Riemer *et al.*, 1995	AB_528336
Cy3-conjugated anti-HRP goat (1:500)	Jackson Immuno-Research Ltd	123-165-021
Anti-n-Cathenin (n-Cath) rat (1:2000)	Iwai *et al.*, 1997	AB_528121
Anti-tyrosine hydroxylase (TH) rabbit (1:500)	Chemicon Millipore	AB152
Anti- hydroxyltryptamine (5HT) rat (1:100)	EMD Millipore	MAB352
Anti-tyramine β-hydroxylase (TβH) rabbit (1:500)	Cibik, 2007	N/A
Anti-Dnc[all] rabbit (1:500, Western blot: 1:5000)	Eurogentec	N/A
Anti-Dnc[PB]-C6 (1:1000)	Abmart	N/A
Anti-Dnc[PB]-C10 (1:500)	Abmart	N/A
Anti-Dnc[PJ]-C1 (1:500)	Abmart	N/A
Anti-Dnc[PJ]-C4 (1:500)	Abmart	N/A
Anti-Dnc[PJ]-C8 (1:500)	Abmart	N/A
Anti-Dnc[PJ]-C10 (1:500)	Abmart	N/A
Anti-Dnc[PJ]-C11 (1:500)	Abmart	N/A
Anti-Dnc[PG]-C1 (1:1000)	Abmart	N/A
Anti-Dnc[PG]-C4 (1:500)	Abmart	N/A
Anti-Dnc[PG]-C5 (1:500)	Abmart	N/A
Anti-Dnc[PF]-C2 (1:500)	Abmart	N/A
Anti-β-Actin mouse (Western blot: 1:2000)	Abcam	mAbcam 8224
Anti-rabbit AF488 (1:500)	Invitrogen	A10522
Anti-rabbit Cy3 (1:500)	Jackson Immuno Research Ltd	111-065-008
Anti-mouse AF488 (1:500)	Invitrogen	A1101
Anti-mouse AF633 (1:500)	Invitrogen	A-21050
Anti-mouse Cy3 (1:500)	Jackson ImmunoResearch	115-165-146
HRP-conjugated anti-rabbit (Western blot: 1:80000)	Jackson ImmunoResearch	211-032-171
HRP-conjugated anti-mouse (Western blot: 1:3000)	GE Healthcare	RPN4201

Reagent or resource	Source	identifier
Odorants		
EA (1:50)	Sigma-Aldrich	58958
AM (1:100)	Emplura	8.18700
BA (pure)	Sigma-Aldrich	12010
Paraffine oil	Sigma-Aldrich	18512-1L
Key reagents		
TRIzol	Invitrogen	12044977
DNase	Roche	04716728001
RNase	Roche	11119915001
MESA Blue qPCR Mastermix Plus for Cyber	Eurogentech	RT-SY2X-03+WOUB
FCS	Sigma-Aldrich	F0804
Superscript II	Invitrogen	18064022
cOmplete™ EDTA-free protease inhibitor	Roche	11836170001
RIPA lysis buffer	150 mM NaCl, 50 mM Tris (pH 8.0), 5 mM EDTA, 1 mM EGTA, 1 % NP-40, 0.5 % Na-Deoxycholate, 0.1% SDS, ddH2O	
TBST	100 mM Tris Cl, 150 mM NaCl, 0.1 % Tween©20, pH 7.5	
Laemmli buffer	BioRad	#1610737
ECL component A	1ml Tris/HCl pH 8.5, 44µl PCA + 100µl luminol	N/A
ECL component B	10ml Tris/HCl pH 8.5 + 7µl H_2O_2	N/A
Critical equipment		
Confocal microscope	Olympus	Fluoview FV 1000
Confocal microscope	Leica	SP8
qPCR	BioRad	IQ™5
Software		
AlphaFold2	Jumper *et al.*, 2021	2.3.2
PyMOL	Schroedinger LLC, DeLano, 2021	2022.12.0
ggplot2	Wickham, 2016	v.3.3.3
ggpubr	Kassambara, 2023a	v. 0.6.0
rstatix	Kassambara, 2023b	v. 0.7.2
ggthemes	Arnold *et al.*, 2021	v. 7.1.1
R	R Core Team, 2021	v. 4.0.5
RStudio	Prosit Software	v. 2022.12.0+353
Fiji ImageJ	Schindelin *et al.*, 2012	v. 1.53c
NormFinder for Excel	Andersen *et al.*, 2004	v. 20
Photoshop CS5	Adobe	v. 12.0
Excel	Microsoft	v. 14.0.4760.1000
Bio-Rad iQ5	Bio-Rad Laboratories Inc	v. 2.1.94.617

3   Results

3.1   Dnc^{PA} is a negative regulator of short-term memory in the *Drosophila* larvae.

3.1.1   The learning and memory phenotype of *dnc*^{Δ143} is reproducible with another odorant pair.

Previously it was shown that *dnc*^{Δ143} mutants show improved memory after a single training cycle in an aversive paradigm using AM and EA as odorants and 2M NaCl as a reinforcer (Fig. 3) (Gompert, 2019). To address whether the improved memory phenotype of *dnc*^{Δ143} is odorant-independent we tested learning and memory of *dnc*^{Δ143} after one and three training cycles using AM and BA as conditioned stimuli and 2M NaCl as reinforcer (Fig. 6). In addition to that, *dnc*^{1} was analysed with its respective control for comparison (Fig 6).
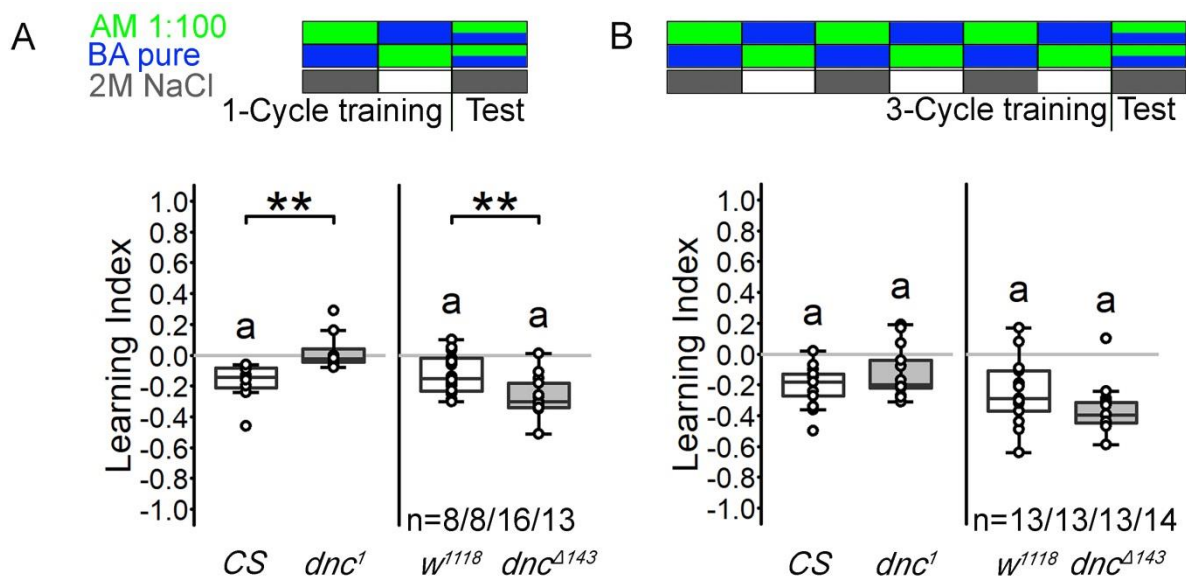
Fig. 6: The improved learning and memory abilities of *dnc*^{Δ143} can also be observed using BA and AM as conditioned stimuli.
A: After one cycle of training using BA and AM as odorants, *dnc*^{1} shows a significantly reduced learning and memory performance compared to its control *CS*. *dnc*^{Δ143} shows a significantly improved aversive olfactory learning and memory compared to its control *w*^{1118}. **B**: After three cycles of training, all tested genotypes learn the association between the odorant and the aversive reinforcer. Although no significant differences can be seen, *dnc*^{1} still shows a slightly worse performance than its control while *dnc*^{Δ143} shows a slight better performance. Significant differences from random choice were determined using one sample t-test ($p < 0.05$) and labelled with the letter "a". Differences between two groups were analysed using Student's t-test with *: $p < 0.05$, **: $p < 0.01$ and *** $p < 0.001$.

After one training cycle, *CS* showed significant memory. *dnc¹* showed significantly less memory. *w¹¹¹⁸* also showed significant memory after a single training cycle. *dnc^{Δ143}* shows significantly improved memory (Fig. 6 A). After three training cycles all genotypes tested show significant memory. *CS* control larvae show similar levels of memory as *dnc¹* mutants.

Consistent with previous findings, *dnc¹* mutants show reduced learning and memory after one training cycle (Widmann *et al.*, 2016). Our findings with AM/EA show a different result, with *dnc¹* memory after one training cycle not being significantly different from the control, but showing significantly worse memory performance after three training cycles (Fig.4 A, B). In addition to that, the observed memory of the control after one training cycle of *CS* differed from our previous findings with AM and EA. This suggests that the differences in learning between the two experiments may be odorant specific.

For *dnc^{Δ143}* we observe the same improved level of learning and memory after one training cycle for both pairs of odorants (AM/BA and AM/EA). Thus, regardless of the conditioned odorants, *dnc^{Δ143}* learns better than its respective control after one training cycle.

3.1.2 The *dnc¹* learning and memory defect does not depend on phosphodiesterase activity in *dnc^{RA}*-positive neurons.

The *dnc¹* mutation has an influence on the expression of serveral *dnc*-isoforms, including a significant reduction in *dnc^{RA}* (Fig. 3) (Ruppert, Franz *et al.*, 2017). To determine whether PDE-activty in neurons that normally require *dnc^{RA}* to suppress memory is responsible for the defective STM in *dnc¹*, we introduced the Dnc PDE-domain under the control of the dnc^{RA} promoter into *dnc¹* and analysed learning and memory after three training cycles. If the reduced expression of *dnc^{RA}* was the reason for the memory defect in *dnc¹*, we would expect this reintroduction to restore the memory phenotype to wild-type levels.

As a control, we used *CS* larvae. They show significant memory after three training cycles (Fig. 7).

We examined the effect of the *UAS-dnc^{PDE}* transgene alone and the *dnc^{RA}* promoter-Gal4 alone by crossing them into *dnc¹* and testing heterogeneous larvae that have been crossed with *dnc¹*. They show similar memory impairements as *dnc¹* mutants.

The expression of the PDE activity under the control of the Dnc^{RA}-Gal4 driver in dnc^1 mutants did not improve the learning and memory defects (Fig. 7). These results suggest that the the impaired memory phenotype of dnc^1 is not caused by the defective regulation of cAMP levels in the in dnc^{RA}-positive cells.
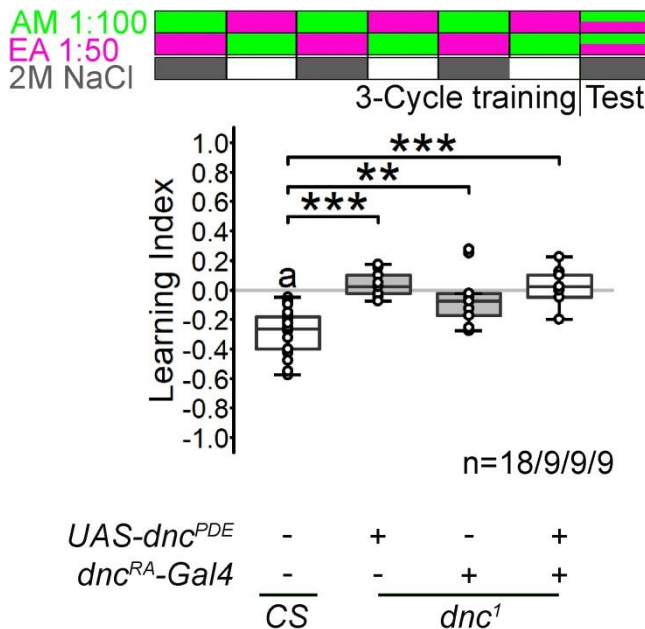

Fig. 7: Reduced Dnc expression in dnc^{RA}-positive cells is not the cause of the dnc^1 memory defects. Expression of the Dnc PDE domain under the control of the dnc^{RA}-Gal4 promoter in dnc^1 did not change learning and memory performance in a three-cycle olfactory learning and memory assay. The letter 'a' indicates significant differences from random choice as determined using one sample t-test ($p < 0.05$). Differences between groups were analysed using ANOVA with Tukey's post-hoc-test with *: $p < 0.05$, **: $p < 0.01$ and *** $p < 0.001$. Experiments shown in this figure were conducted by Victoria Brüning (Bachelor thesis: Brüning, 2022),

3.1.3 Dnc^{PA} is required to suppress learning and memory in a distinct set of cells.

$dnc^{Δ143}$ learns and remembers better after one training cycle than controls. The improved learning can be restored to normal non-learning by introducing of PDE activity in dnc^{RA}-positive cells (Fig. 4). To prove that a reduction in Dnc expression is sufficient for the Dnc phenotype, we wanted to reduce Dnc expression under the control of the dnc^{RA}-Gal4 driver using the UAS-dnc^{RNAi} construct. Previously, this construct, expressed under the control of $elav$-Gal4, a driver line that is expressed post-mitotically in all neurons of in the nervous system (Robinow and White, 1988), was shown to be defective in habituation (Fenckova et $al.$, 2019). As controls, we used the UAS-dnc^{RNAi} line without promoter and the dnc^{RA}-Gal4 line without construct, expressed in a w^{1118} background. Both controls show significant memory (Fig. 8). As an experimental group we crossed these two genotypes for a Dnc knockdown in dnc^{RA}-positive cells. It shows a significantly improved memory phenotype compared to its controls (Fig. 8). This shows that PDE-activity in dnc^{RA}-positive cells is the reason for the improved learning and memory phenotype of

$dnc^{\Delta143}$. Reduced expression leads to an improved learning performance (Fig. 8), whereas reintroduction leads to a reduction to control levels (Fig. 4 C).
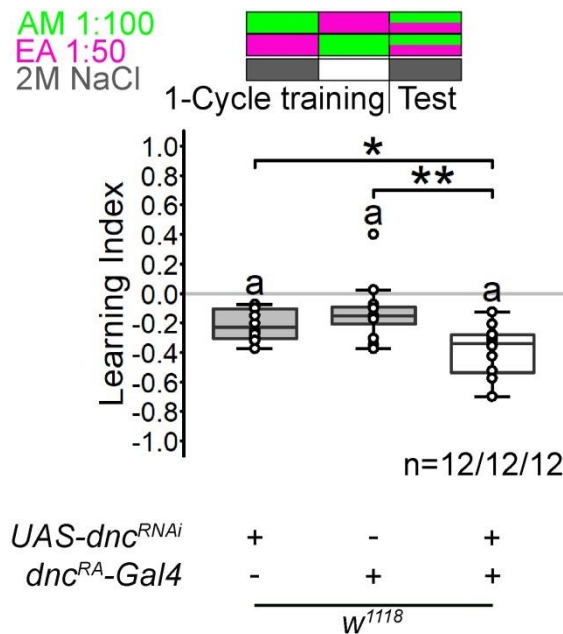

Fig. 8 Dnc knockdown in dnc^{RA}-positive cells improves memory
Knockdown of dnc in dnc^{RA}-positive cells significantly improves memory performance after one training cycle. The letter "a" indicates significant differences from random choice as determined using one sample t-test ($p < 0.05$). Differences between groups were analysed using ANOVA with Tukey's post-hoc-test with * $p < 0.05$, ** $p < 0.01$ and *** $p < 0.001$. Experiments shown in this figure were conducted by Evelin Fahle.

3.1.4 The $dnc^{\Delta143}$ mutant forms a stable yet flexible memory.

To further investigate the stability of the memory formed by $dnc^{\Delta143}$, we performed a series of learning and memory experiments on w^{1118} (Fig. 9 A) and the isoform-specific mutant $dnc^{\Delta143}$ (Fig. 9 B) in larvae. As a control, we trained all animals once and tested their learning and memory abilities (Fig. 9 C). Next, we performed a decay experiment to show the effect of longer retention time (Fig. 9 C). Although it has been shown that after three training cycles, longer retention time leads to worse memory performance (Khurana *et al.*, 2009; Widmann *et al.*, 2016), for consolidated memory phases, rest periods play an important role in memory formation (Isabel *et al.*, 2004). In an extinction experiment, the previously formed aversive memory is added by an appetitive memory of the presence of "no punishment" (Felsenberg *et al.*, 2017, 2018). These possible influences of retention time make it important to control the extinction and reversal learning experiment with a decay experiment with a retention time equal to the training cycles.
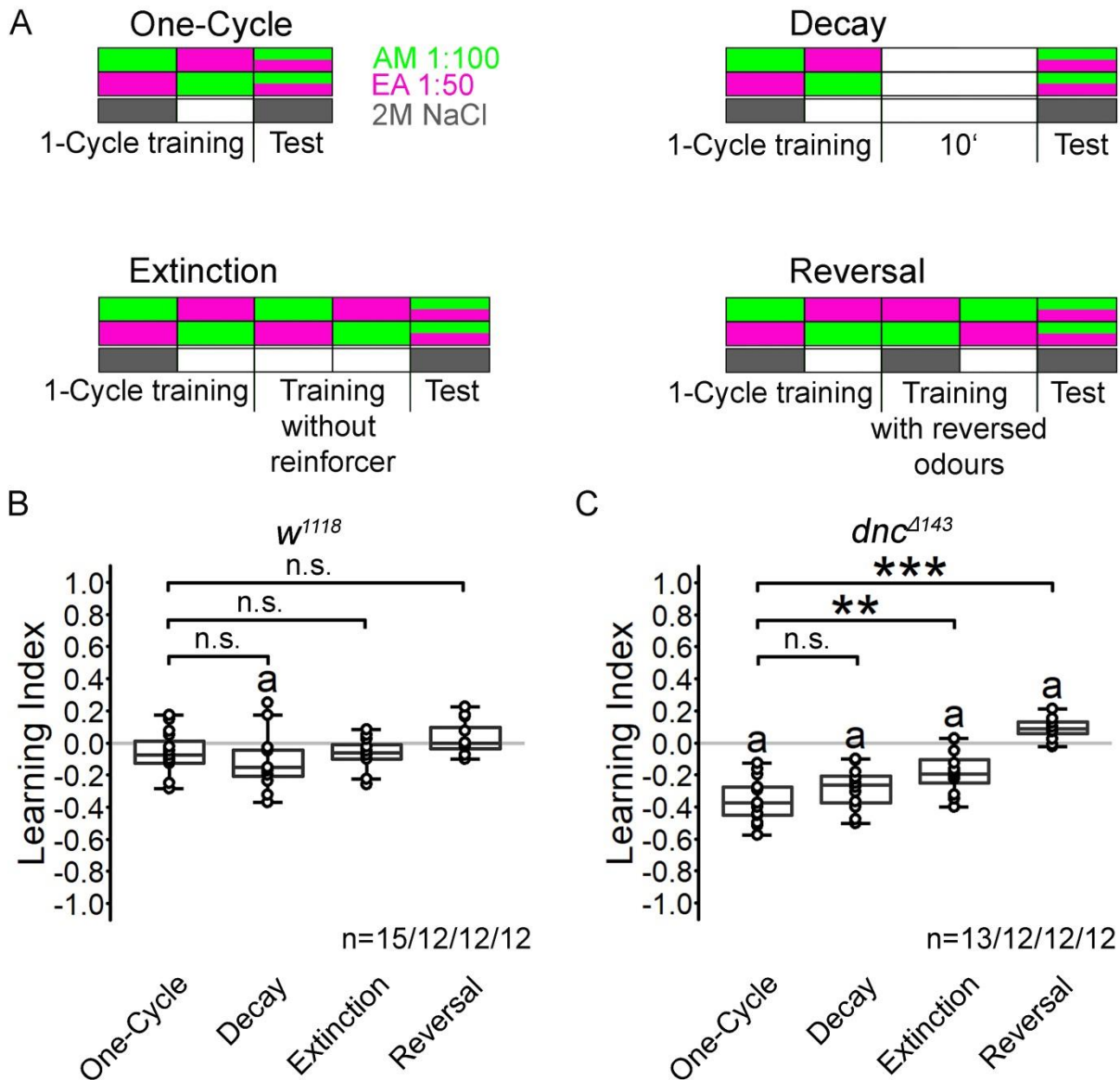
Fig. 9: Stability of memory after one training cycle in *dnc^Δ143* mutants
A: Schematic of the protocols of the different learning and memory experiments. To test for memory decay, larvae were trained and then placed on a neutral plate without odorants for 10 min. To test for memory extinction, after training the larvae were presented with both odorants on neutral plates for 5 min each. To test memory reversal, they were presented both odorants in reverse order on a 2M NaCl and a pure agarose plate for 5 min each, before being tested. **B**: *w^1118* larvae do not learn after one training cycle. After 10 min of retention, *w^1118* shows an emerging memory, however this is not significantly different from the control. No significant memory was observed when the odorants were presented during the retention period. After one cycle of learning followed by a cycle with reversed odorants, *w^1118* larvae neither memorise the previously presented odorants nor learn a new association. **C**: *dnc^Δ143* larvae show a significant aversive olfactory memory after one training cycle. After 10 min retention time *dnc^Δ143* larvae still show significant memory. Presentation of the odorants during the retention period does not significantly inhibit memory. After one cycle of learning followed by one cycle of reversely reinforced odorants, *dnc^Δ143* immediately memorises the new association. a: Significant differences from random choice determined by one sample t-test ($p < 0.05$), *: $p < 0.05$ from one-cycle

38

learning in an ANOVA with Tukey's post-hoc test, **: $p < 0.01$, ***: $p < 0.001$. Experiments shown in this figure were conducted by Marcel Verbrüggen

w^{1118} did not form significant memory after one training cycle. Surprisingly, it was able to form a significant memory after 10 min of retention time, although this memory was not significantly different from the one-cycle experiment. It did not form significant memory in the extinction and reversal experiment (Fig. 9 A). In contrast to w^{1118}, $dnc^{\Delta143}$ showed significant memory after one training cycle (Fig. 9 B), as shown in Figure 4 A. It was also able to show significant memory in the decay assay, which was not significantly different from the one-cycle experiment. Thus, memory after one training cycle lasts for at least 10 min, and in larvae, STM is significantly reduced after 20 min (Khurana *et al.*, 2009; Widmann *et al.*, 2016).We do not observe a significant reduction after 10 min. In her bachelor thesis, M. Gompert showed that $dnc^{\Delta143}$ larvae do not show a significant memory after 30 min, which is not significantly different from immediately after training (Gompert, 2019). This shows that STM is the main memory form which is improved $dnc^{\Delta143}$.

In the extinction experiment $dnc^{\Delta143}$ forms a significant memory, although significantly reduced when compared to animals tested directly after training.

In the reversal experiment larvae were able to associate the punishment with the odorant that was reinforced in the second training session (Fig. 9 B), demonstrating the flexibility of the memory and the ability of the larvae to learn new information.

In summary, $dnc^{\Delta143}$ mutants, in contrast to the controls, are able to form a stable association with an odorant more quickly and are more flexible in learning new odorant information.

3.1.5 Dnc^{PA} is expressed in a set of neurons that project to the antennal lobe.

To find out exactly which cells are responsible for the enhanced learning and memory phenotype, we analysed the expression of the dnc^{RA}-*Gal4* driver using the *UASmCD8::GFP* transgene. We detected 20 different clusters per side in the larval CNS excluding SStrhl (Fig. 10 A and B). In the VNC 13 clusters were detected (Fig. 10 A, B).
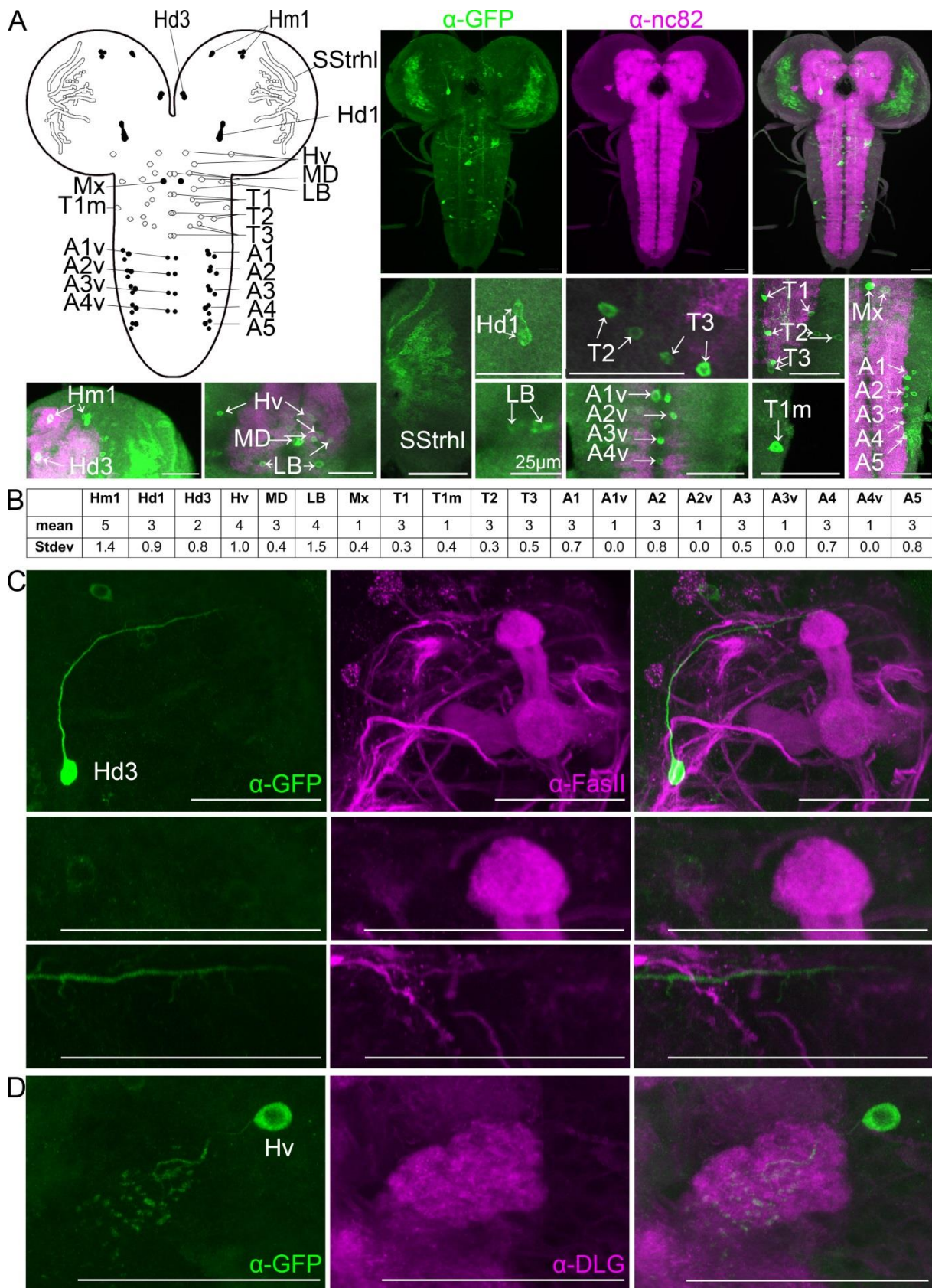
Fig. 10: *dnc^RA-Gal4* drives transgene expression of a set of neurons projecting to the AL.

A: The cartoon summarises the expression domain of the *dnc^RA-Gal4* driver. The *dnc^RA –Gal4* line drives transgene expression in multiple cells in the larval CNS. The

neuropil is labelled with the anti-nc82 antibody (in magenta) and the Gal4 expression domain of the *dnc^{RA}–Gal4* driver is visualised with the *UAS-mCD8::GFP* transgene (in green). The table in **B** summarises the analysis of the expression domain over six brains. **C:** The Hd3-cluster does not enervate the MB. FasII expression (in magenta), is used as a marker for the MB. **D:** The Hv neuron innervates the AL. The AL is labelled with anti- Discs large (DLG). Brains were scanned at 20x and 40x magnification with 1µm optical sections or 63 x magnification with 0.33µm optical sections respectively. Scale bars are 50µm unless stated otherwise. Experiments were conducted by by M.Müller (Müller, 2021).

In the larval brain, 7 clusters targeted by the *dnc^{RA}-Gal4* driver were detected (Fig. 10 A, B). One cluster, SStrhl, consists of a large number of cells and is located close to the optical lobe in the larval brain, also known as the larval optical neuropil. This neuropil has been shown to mediate light avoidance and circadian rhythm in larvae (Keene *et al.,* 2011). Light avoidance is a cue that does not play a role in our olfactory learning and memory experiment, as the training and the choice experiment are performed in the dark. In addition, SStrhl neurons are not projection neurons, their morphology identifies them as glial cells (Hartenstein, 2011). For this reason, we have not included them in the table in Figure 10 B.

The Hm1 cluster consists of 5 +/- 1 projection neurons. It is located close to the superior protocerebrum and projects into it (Fig. 10 A, B). The projections of the Hm1 cluster do not come close to the MB or the AL.

The Hd1 cluster consists of 3 +/- 1 neurons. It is located dorsal to the deuterocerebrum. (Fig. 10 A, B)

The MD cluster consists of 3 neurons, the LB cluster of 4 +/- 1 neurons and the Mx cluster of 1 neuron. They are located in the subesophageal zone. (Fig. 10 A, B)

The Hd3 cluster is in close proximity to the MB but does not project into it (Fig. 10 C). The Hv cluster projects into the AL (Fig. 10 D).

In summary, the *dnc^{RA}-Gal4* line specifically drives expression in several clusters throughout the larval CNS, some of which may have an impact on larval learning and memory, and one of which projects into the AL.

3.1.6 The GFP tag affects the conformation of Dnc^{PA}.

The GFP tag could affect the conformation of the Dnc^{PA}. Depending on the position of the tag in the protein, this change in conformation could influence the subcellular localisation or functionality of the PDE.

To investigate whether the tag of the UAS-Dnc^{PA} transgene affects conformation, we analysed the 3-D structure of N- and C- terminally tagged Dnc using AlphaFold2 (Jumper *et al.*, 2021).

In the Dnc isoforms, three domains are important for the function and interaction of Dnc: The UCR1 region, the UCR2 region and the catalytic domain (Bolger *et al.*, 1993).

Figure 11 A shows the untagged configuration of Dnc^{PA} with the functional domains highlighted in different colours, Figures 11 B and C show the same for N- and C-terminally tagged Dnc^{PA}.

Figure 11 A' shows the untagged configuration of the catalytic domain of Dnc^{PA} (Bolger *et al.*, 1993; Jin *et al.*, 1992). The alignment with the catalytic domain of N- and C-terminally tagged Dnc^{PA} shows that the GFP tag on either side does not induce structural changes in the catalytic domain (Fig. 11 B', C').

In the UCR1-region (Bolger *et al.*, 1993), the main α-helix of the UCR1 is unchanged from the untagged Dnc^{PA} (Fig. 11 A'', B'', C''). The side chains, which can also be predicted with high accuracy by AlphaFold (Jumper *et al.*, 2021), are one of the things that differ, slightly in GFP::Dnc^{PA} (Fig. 11 B''), more so in Dnc^{PA}::GFP (Fig. 11 C''). In addition, two structural domains do not form at all in Dnc^{PA}::GFP (Fig. 11 C'').

The UCR2-region (Bolger *et al.*, 1993) is almost unchanged in Dnc^{PA} with the N-terminal GFP tag (Fig. 11 B'''), but the orientation of the helices to each other is strongly altered in Dnc^{PA} with the C-terminal GFP tag (Fig. 11 C''').

In conclusion, the simulation of the structure of the different Dnc^{PA} transgenes shows that the GFP tag has an effect on the UCR-regions, but not on the PDE-domain. The N-terminally tagged GFP::Dnc^{PA} is structurally very similar to the untagged Dnc PDE. To evaluate whether the transgene reflects the endogenous expression domain of Dnc^{PA}, we need to consider the importance of interactions via the UCRs (Richter and Conti, 2004, 2002; Xie *et al.*, 2014), the importance of the N-terminus for subcellular localisation (review: Houslay, 2009) and the importance of the UCRs for multimerisation (Bolger *et al.*, 2015). Of the two tagged transgenes, the C-terminally tagged Dnc^{PA} probably best reflects the endogenous expression.
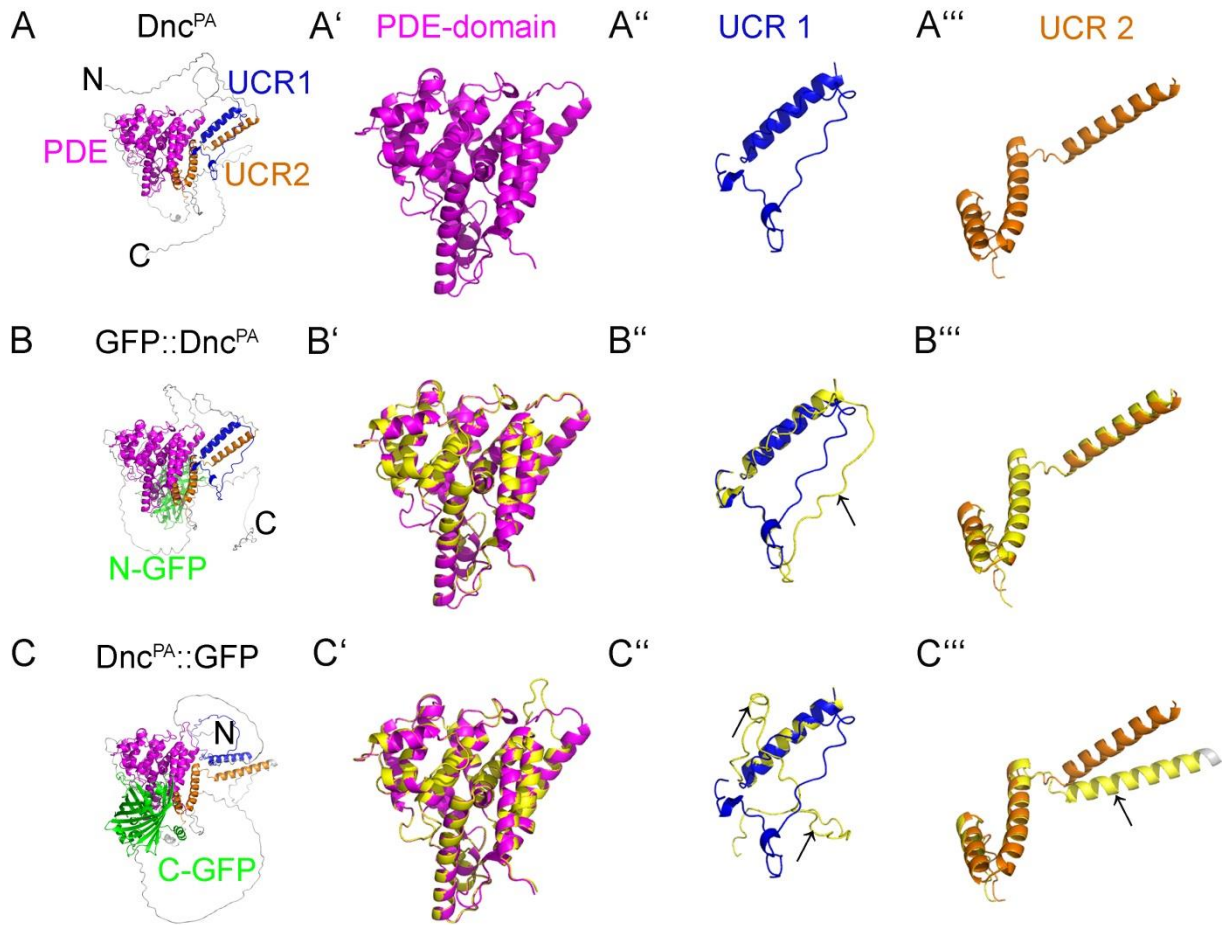
Fig. 11: The position of the GFP tag influences the structure of the UCRs but not of the catalytic domain GFP-tagged Dnc^PA transgenes.

Predicted models of **A**: Dnc^PA **B:** Dnc^PA with N-terminal GFP tag **C:** Dnc^PA with C-terminal GFP-Tag. **A'-C':** The PDE-domain is perfectly aligned in the differently tagged Dnc^PA transgenes. PDE domain of **A':** Dnc^PA (magenta) **B':** GFP::Dnc^PA (yellow) aligned with Dnc^PA (magenta) **C':** Dnc^PA::GFP (yellow) aligned with Dnc^PA (magenta) **A''-C'':** The UCR1-domain of GFP::Dnc^PA differs from the untagged UCR1 only in one side chain, the UCR1 domain of Dnc^PA::GFP also differs in one side chain and does not form two small structural domains. UCR1 of **A'':** Dnc^PA (blue) **B'':** GFP::Dnc^PA (yellow) aligned with Dnc^PA (blue) **C''** Dnc^PA::GFP (yellow) aligned with Dnc^PA (blue) **A'''-C''':** The UCR2 of GFP::Dnc^PA is almost perfectly aligned with the domain of the untagged protein. The position of an α-helix in Dnc^PA::GFP differs from the wild-type domain. UCR2 of **A''':** Dnc^PA (orange) **B''':** GFP::Dnc^PA (yellow) aligned with Dnc^PA (orange) C''' Dnc^PA::GFP (yellow) aligned with Dnc^PA (orange). **A-C''':** Models of Dnc^PA predicted using AlphaFold2 (Jumper *et al.*, 2021), aligned and displayed using PyMOL (DeLano, 2021) PDE domain according to UniProt (The UniProt Consortium, 2021), UCR domains according to Bolger et al. (Bolger *et al.*, 1993). The arrows indicate where the domains of the tagged transgenes do not match the untagged Dnc^PA.

3.1.7 Subcellular localisation of N- or C- terminally tagged Dnc[PA] and C-terminally tagged Dnc[PG].

It has been shown that the cell body, the axon, the bouton and the nucleus are independent cAMP signalling compartments. This subcompartmentation is mediated by the PDEs (Maiellaro *et al.*, 2016). In the ovary, ectopically expressed Dnc isoforms are expressed in different cellular compartments (Ruppert, Franz *et al.*, 2017). Therefore, we wanted to investigate where these isoforms are expressed in neurons. We analysed the expression pattern of C- and N-terminally GFP-tagged Dnc[PA], and C-terminally tagged Dnc[PG], an isoform that has been shown to express a nuclear localisation signal and that is expressed in the nucleus in ovaries (Ruppert, Franz *et al.*, 2017).

To examine the subcellular localisation in the CNS and at the NMJ, we expressed the GFP-tagged transgenes in glutamatergic neurons using the *DV-Glut-Gal4* driver, a glutamatergic driver expressed in the motor neuron and all neuropils except the MB (Daniels *et al.*, 2008), and analysed the GFP expression using immunohistochemistry. As a control, we also included the membrane-bound marker mCD8::GFP (Lee and Luo, 1999).

To examine the localisation at the soma, we co-labelled the nuclear envelope with anti-lamin antibodies and the DNA with DAPI (Fig. 12 A). The control mCD8::GFP is expressed at the membrane. Dnc[PA]::GFP and GFP::Dnc[PA] are both expressed throughout the soma. Dnc[PG]::GFP is expressed not only in the nucleus but also in the soma (Fig. 12 A).

Next we examined whether the Dnc isoforms are also expressed in the axons of the neurons within the VNC and in the motor neurons (Fig. 12 B). In the VNC, we observe that all genotypes tested, the membrane marker mCD8::GFP, the differently tagged Dnc[PA] transgenes and the Dnc[PG]::GFP transgene are all expressed not only in the soma, but also in the axon. In the motor neuron, the membrane marker mCD8::GFP shows uniform staining along the axon. GFP::Dnc[PA] can be seen in fibrous and dot-like structures along the axon. Although Dnc[PA]::GFP shows a lower intensity, its expression is also seen in fibrous and dot-like structures along the axon. Dnc[PG]::GFP shows a more fibrous expression.
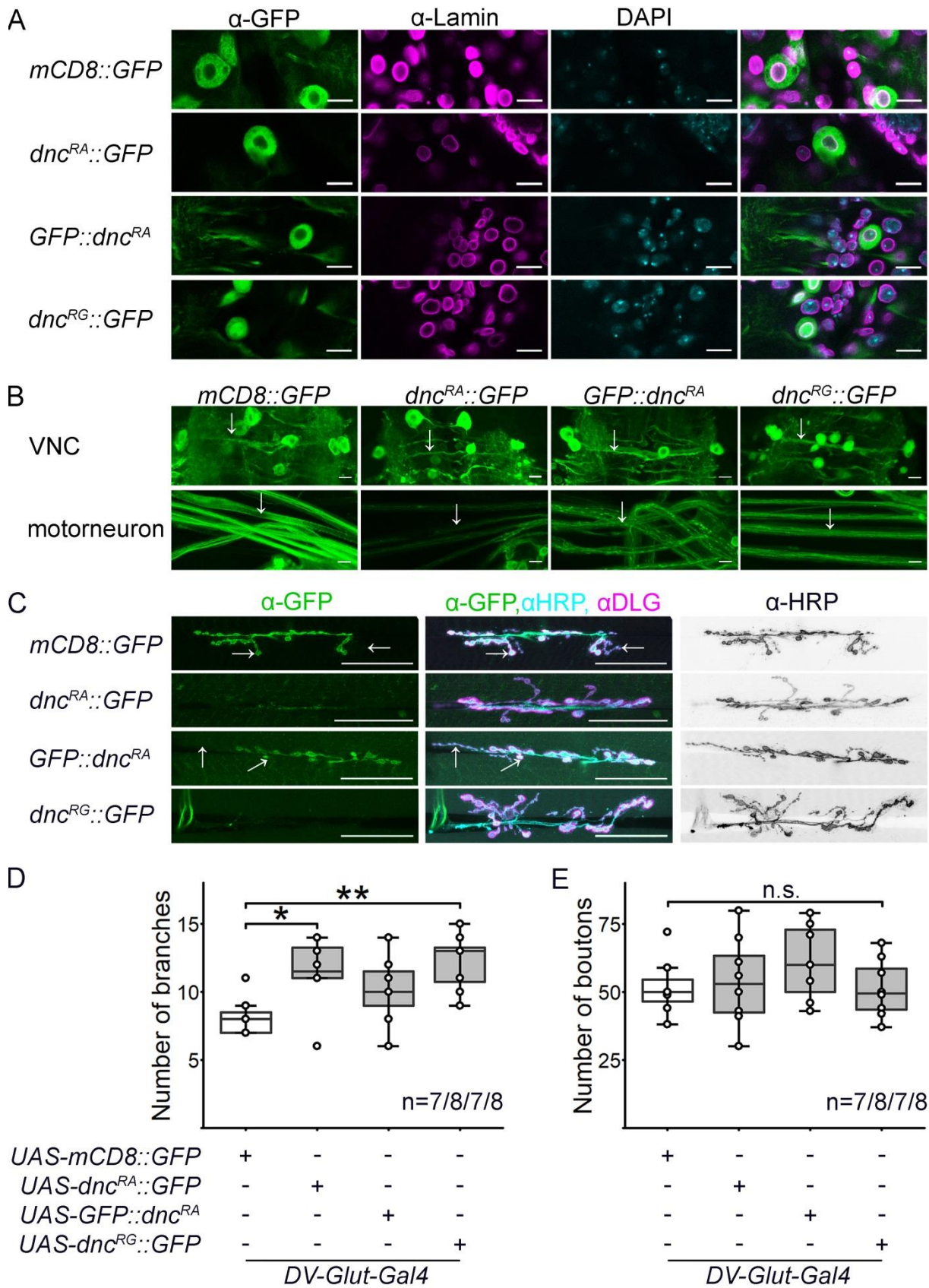
Fig. 12: Subcellular localisation of different tagged Dnc isoforms
A: While Dnc[PA]::GFP and GFP::Dnc[PA] are expressed in the soma but not in the nucleus, Dnc[PG]::GFP is expressed in both the nucleus and the soma. The membrane marker mCD8::GFP is shown for comparison. Anti-GFP labels the GFP tag (green),

anti-lamin labels the nuclear envelope (magenta) and DAPI labels the DNA (Cyan). **B**: All Dnc transgenes tested are also expressed along the axons in the VNC neuropil. All transgenes are expressed in the axons of motor neurons connecting the VNC to the body wall muscles. The expression of Dnc^{PA}::GFP and GFP::Dnc^{PA} is more dotted, the expression of Dnc^{PG}::GFP more fibrous. The arrows indicate the axons in the VNC and the motor neurons. **C**: While the membrane marker mCD8::GFP and the transgene GFP::Dnc^{PA} are expressed at the NMJ of muscles 6/7 in segment A4, Dnc^{PA}::GFP and Dnc^{PG}::GFP are not. Anti-GFP labels the corresponding transgene (green), anti-horseradish peroxydase (HRP) labels the neuronal membrane (cyan), anti-DLG labels the postsynaptic membrane (magenta). The arrows indicate a type Ib and a type Is bouton at the NMJ. mCD8::GFP and GFP::Dnc^{PA} are localised in type Ib boutons. **D**: The amount of terminal branching at the NMJ is significantly increased in larvae expressing Dnc^{PA}::GFP and Dnc^{PG}::GFP. **E**: There is no significant difference in the number of boutons at the NMJ in the larvae overexpressing the tested isoforms. **A-E**: *UAS-mCD8::GFP, UAS-dnc^{RA}::GFP, UAS-GFP::dnc^{RA}* and *UAS-dnc^{RG}::GFP* expressed in the *Drosophila* third instar larva under the control of *DV-Glut-Gal4.* **A**: Single slide of a 63x scan of cells in the VNC. **B-C**: Stacks were scanned at 63x magnification and 0.33µm optical section. Scale bars are: **A-B**: 10µm, **C**: 50µm. **D, E**: Differences were analysed by ANOVA with Tukey's post-hoc test with *: $p < 0.05$, **: $p < 0.01$ and *** $p < 0.001$.

Type Ib and Is boutons are glutamatergic, they are driven by the *DV-Glut-Gal4* driver (Daniels *et al.*, 2008; Hoang and Chiba, 2001; Johansen *et al.*, 1989). The control, the membrane marker mCD8::GFP, is expressed in the presynaptic terminals of type Ib boutons, but not in type Is boutons. Dnc^{PA}::GFP and Dnc^{PG}::GFP are not expressed in the presynaptic terminals at the NMJ. Like the control, GFP::Dnc^{PA} is expressed in type Ib presynaptic terminals.

To investigate the influence of the expression of different Dnc isoforms on synaptic development, we analysed the branching and number of boutons formed at the NMJ (Fig. 12 D, E). For the expression of *dnc^{RA}::GFP*, *GFP::dnc^{RA}* and *dnc^{RG}::GFP*, there are no significant differences in the number of boutons to the control (Fig. 12 E).

The number of branches in *dnc^{RA}::GFP* and *dnc^{RG}::GFP* is significantly higher than in the control (Fig. 12 E). Previous studies of different *dnc* mutants have observed an effect on both bouton number and branching. For branching, they have observed the same phenotype as we show for isoform-specific overexpression. *dnc^{1}* and *dnc^{M14}* have significantly increased bouton number and terminal branching at the NMJ (Davis and Kiger, 1981; Zhong *et al.*, 1992), whereas non-isoform-specific Dnc overexpression reduces the number of varicosities (Cheung *et al.*, 1999). This, together with the different results for the differently tagged Dnc^{PA} isoforms, show that the change is isoform-specific and depends on subcellular localisation.

In summary, the localisation of the GFP tag influences the subcellular localisation of Dnc^{PA} and on synaptic plasticity. Dnc^{PA}::GFP , which is more likely to be correctly localised, is mainly expressed in the soma, whereas GFP::Dnc^{PA} is expressed in all compartments except the nucleus. In Dnc^{PG}::GFP, as predicted, is expressed predominantly in the nucleus but also in the soma, indicating that the tag does not interfere with its subcellular localisation.

3.1.8 Somatic phosphodiesterase activity restores the memory phenotype of $dnc^{\Delta 143}$.

Subcellular compartmentation plays a role in cAMP signalling throughout the neuron (Maiellaro *et al.*, 2016). The Dnc isoforms are also differentially expressed throughout the neuron (Fig. 12).

Next, we wanted to investigate whether the subcellular localisation of Dnc has an impact on learning and memory. Therefore, we analysed which isoform is able to regulate learning and memory after one training cycle.

As a control, we used the *UAS-dnc^{RA}::GFP* line expressed in a w^{1118} background, the genetic background of $dnc^{\Delta 143}$. It shows a significant memory after one training cycle (Fig. 13 A). Both the *dnc^{RA}-Gal4* line and the *UAS-dnc^{RA}::GFP* expressed in $dnc^{\Delta 143}$ mutants show significantly improved memory. The experimental group expresses *dnc^{RA}::GFP* under the control of the *dnc^{RA}*-promoter in $dnc^{\Delta 143}$. It restores learning and memory to control levels (Fig. 13 A). Having shown that Dnc PDE activity in *dnc^{RA}*-specific cells is responsible for the improved memory phenotype (Fig. 4 C), this shows that Dnc expression in the soma (Fig. 12 A) is sufficient to restore the memory phenotype of $dnc^{\Delta 143}$ to wildtype levels.

To investigate whether subcellular localisation in the synapse is important for the $dnc^{\Delta 143}$ memory phenotype, we repeated the experiment expressing N-terminally tagged *GFP::dnc^{RA}* (Fig. 13 B). This construct is expressed in different domains in the neuron. While *dnc^{RA}::GFP* is restricted to the soma and the axon, *GFP::dnc^{RA}* is also expressed in the synapse.

A

AM 1:100
EA 1:50
2M NaCl

1-Cycle training | Test

Learning Index (axis 1.0 to -1.0)

*** ** * *

a a a a

n=14/12/11/14

UAS-dnc^{RA}::GFP	+	+	-	+
dnc^{RA}-Gal4	-	-	+	+
	w^{1118}		$w^{1118}, dnc^{\Delta 143}$	

B

1-Cycle training | Test

Learning Index (axis 1.0 to -1.0)

* ** * *

a a a a

n=18/18/15/14

UAS-GFP::dnc^{RA}	-	+	-	+
dnc^{RA}-Gal4	+	-	+	+
	w^{1118}		$w^{1118}, dnc^{\Delta 143}$	

C

1-Cycle training | Test

Learning Index (axis 1.0 to -1.0)

* *** ** **

a a a a

n=14/14/14/14

UAS-dnc^{RG}::GFP	-	+	-	+
dnc^{RA}-Gal4	+	-	+	+
	w^{1118}		$w^{1118}, dnc^{\Delta 143}$	
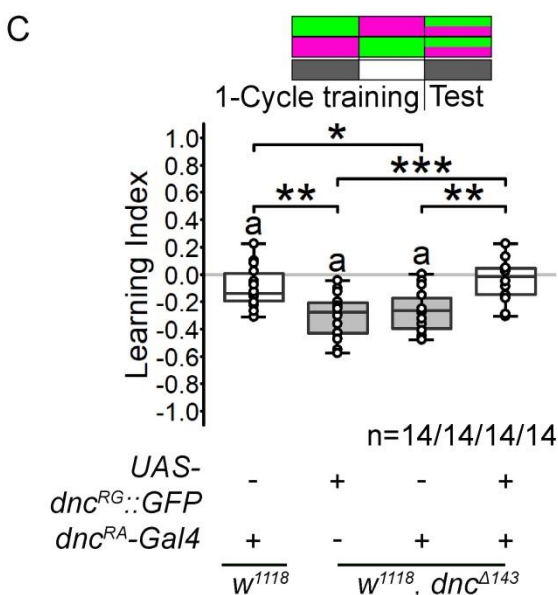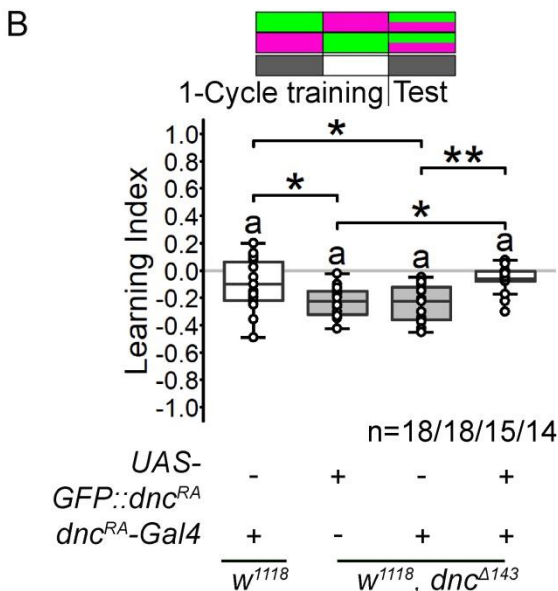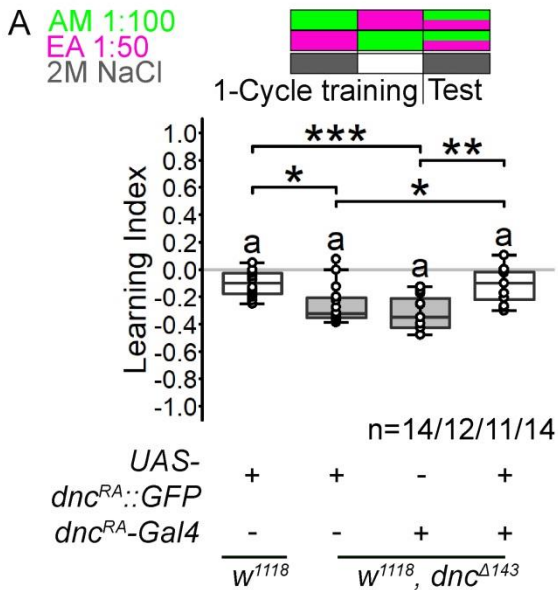
Flies carrying the *dnc^{RA}-Gal4* transgene were used as controls. They develop significant memory, but less than *dnc$^{\Delta 143}$* mutant flies carrying the *UAS-GFP::dnc^{RA}* transgene or the *dnc^{RA}-Gal4* transgene. Expression of *UAS-GFP::dnc^{RA}* under the control of the *dnc^{RA}-Gal4* driver restores learning and memory to control levels (Fig. 13 B). GFP::Dnc^{PA} is expressed in the soma, the axon and the bouton (Fig. 12 A, B, C). This shows that increased expression in all other signalling compartments is not important for the wild-type memory phenotype.

Fig. 13: Expression of different isoforms restores learning and memory performance to control levels after one cycle of training.
A: Expression of a Dnc^{PA}::GFP, **B:** GFP::Dnc^{PA} and **C:** Dnc^{PG} under the control of the *dnc^{RA}-Gal4* driver in *dnc$^{\Delta 143}$* larvae reduces learning to control levels in an olfactory one-cycle aversive learning and memory assay The letter 'a' indicates significant differences from random choice as determined using one sample t-test ($p < 0.05$). Differences between groups were analysed using ANOVA with Tukey's post-hoc test with *: $p < 0.05$, **: $p < 0.01$ and *** $p < 0.001$. Experiments shown in figures **A** and **B** were conducted by Marcel Verbrüggen (Bachelor thesis: Verbrüggen, 2021). Experiments shown in figure **C** were conducted by Victoria Brüning (Bachelor thesis: Brüning, 2022).

Dnc^{PG} contains a nuclear localisation signal (Ruppert, Franz *et al.*, 2017). As it is expressed in the nucleus and the soma (Fig. 12), its subcellular localisation is more distinct from the natural expression of untagged Dnc^{PA} than that of Dnc^{PA}::GFP and GFP::Dnc^{PA}. In a one-cycle aversive olfactory learning and memory assay, we again used the *dnc^{RA}-Gal4* driver line in *w^{1118}* as a control (Fig. 13 D). It shows low but significant memory. The *dnc^{RA}-Gal4* line and *dnc^{RG}::GFP* individually expressed in *dnc$^{\Delta143}$* mutants show a significantly improved learning and memory phenotype. The expression of *dnc^{RG}::GFP* under the control of the *dnc^{RA}-Gal4* promoter is sufficient to restore the learning and memory phenotype of *dnc$^{\Delta143}$* to wild-type levels.

Although Dnc^{PA}::GFP, GFP::Dnc^{PA} and dnc^{PG}::GFP localise subcellularly differently, they are all expressed in the soma (Fig. 12 A-C). This shows that the somatic expression of Dnc, which reduces somatic cAMP levels in the neurons driven by the *dnc^{RA}-Gal4* driver is sufficient to restore the memory phenotype to wild-type levels.

3.1.9 Overexpression of Dnc^{PA}::GFP does not alter the learning phenotype.

Since reduction of cAMP in the soma of dnc^{RA}-positive neurons regulates learning and memory, the question arises whether reduction of cAMP in these neurons by overexpression of Dnc will result in the opposite learning and memory phenotype.

To analyse a possibly improved memory, we performed an aversive olfactory one-cycle learning and memory experiment using AM and EA as odorants and 2M NaCl as reinforcer (Fig. 14 A). We expressed the *dnc^{RA}::GFP* transgene under the control of the *dnc^{RA}* promoter in *w^{1118}* larvae. Consistent with the results in Figure 13 A, the larvae encoding *UAS-dnc^{RA}::GFP* not driven by any promotor show a low but significant memory performance (Fig. 14 A). The larvae expressing Gal4 under the control of the *dnc^{RA}* promoter with no transgene expressed show no significant memory (Fig. 14 A). The larvae expressing the *dnc^{RA}::GFP* transgene under the control of the *dnc^{RA}* promoter in *w^{1118}* do not show significant memory. The memory scores are not significantly different from the controls, showing that after one training cycle, Dnc overexpression does not improve the memory phenotype. From the results we obtained with *dnc$^{\Delta143}$*, we suspected a reduction in memory performance.
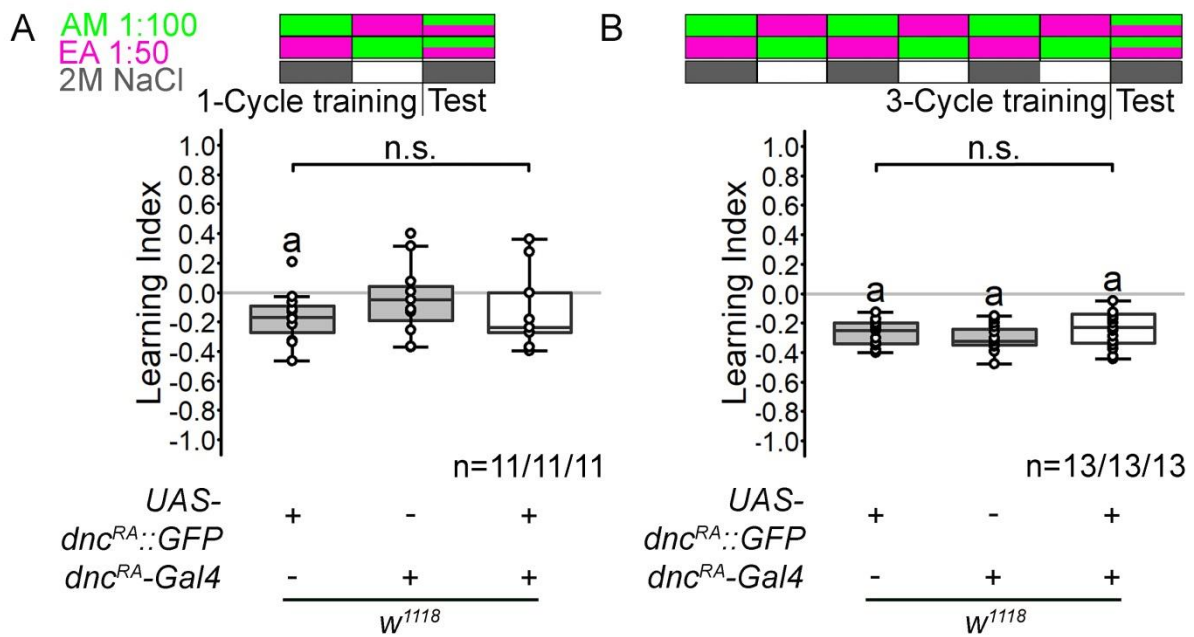
Fig. 14: Overexpression of Dnc^{PA} does not affect learning and memory
A: Overexpression of Dnc^{PA} under the control of *dnc^{RA}-Gal4* does not significantly alter associative learning in *w^{1118}* larvae after one training cycle or **B**: three training cycles. The letter 'a' indicates a significant difference from random choice as determined using one sample t-test (p < 0.05). Differences between groups were analysed using ANOVA with Tukey's post-hoc test with *: $p < 0.05$, **: $p < 0.01$ and *** $p < 0.001$. Experiments shown in **B** were conducted by Marcel Verbrüggen

To investigate whether memory performance is reduced when Dnc is overexpressed in the soma of *dnc^{RA}*-positive cells, thereby locally reducing cAMP concentration, we performed an aversive three-cycle learning and memory experiment using the same lines as in the one-cycle experiment. After three training cycles, the *UAS-dnc^{RA}::GFP*-line, the *dnc^{RA}-Gal4*-line and the cross with expressing *dnc^{RA}::GFP* under the control of the *dnc^{RA}* promoter show a significant memory performance. There are no significant differences between the lines.

Taken together, this shows that the reduction in cAMP caused by overexpression of Dnc^{PA} in *dnc^{RA}*-positive cells does not affect memory performance.

3.2 Phenotypic characterisation of dnc^{EP1395}

3.2.1 dnc^{EP1395} is a dnc^{RB}-specific mutant.

Another isoform that is significantly reduced in dnc^1 is dnc^{RB} (Fig. 3) (Ruppert, Franz *et al.*, 2017). Therefore, it is a good candidate to study the effects of other Dnc isoforms on learning and memory. We used the fly line $w^{1118}P\{EP\}dnc^{EP1395}$, originally developed by Rørth (1996) in a genetic screen. It has a P-element inserted 2 basepairs (bp) after the 3'-end of the first exon of dnc^{RB} (Fig. 15 A). This exon is located within the 5'-UTR of Dnc^{PB} (Ruppert, Franz *et al.*, 2017). To determine whether the insertion of the P-element has an effect on the expression of dnc^{RB}, we designed a qPCR with primers in the first and second exon (Fig. 15 A). For comparison, we used its genetic control, w^{1118}. We performed the qPCR on dissected larval CNS. The expression of dnc^{RB} is significantly reduced in dnc^{EP1395} compared to w^{1118} (Fig. 15 B).

We next investigated whether and how this reduced expression of dnc^{RB} (Fig. 15 B) affects the levels of Dnc^{PB} in the fly. To do this, we analysed the heads of adult flies by western blot analysis. As a control we expressed Dnc^{PB}::GFP under the control of a neuronal driver, *Appl-Gal4. Appl-Gal4* drives expression with the promoter of the *Drosophila* protein Appl, a member of the amyloid precurser protein-like family that is expressed in all neuronal cells and concentrated in the neuropil (Torroja *et al.*, 1996). We compared this expression with the dnc^{RA}-specific mutant $dnc^{\Delta 143}$ and the dnc^{RB}-specific mutant dnc^{EP1395}. The antibody used was anti-Dnc^{all}, an antibody that will be further characterised in the following sections (Fig. 18). We calculated the molecular weight detected by the western blot using a regression analysis. The western blot analysis shows that the antibody recognises 6 bands ranging in size from 80.2 to 179.2 kDa (Fig. 15 C, D). Theoretically, Dnc^{PB} should have a size of 129.4 kDa (Expasy - Compute pI/Mw tool, 2023) and Dnc^{PB}::GFP should be at 157.1kDa. Band 1 is at 179.2+/- 4.6 kDa (Fig. 15 D). Although the measured values deviate from the theoretical values, this band is unique to the overexpression of Dnc^{PB}::GFP (Fig. 19). The distance between band 1 and band 2 suggests that band 2 at 161.7kDa +/- 10.2 kDa is untagged Dnc^{PB} (Fig. 15 D). The western blot analysis shows 4 smaller bands corresponding to shorter Dnc isoforms.
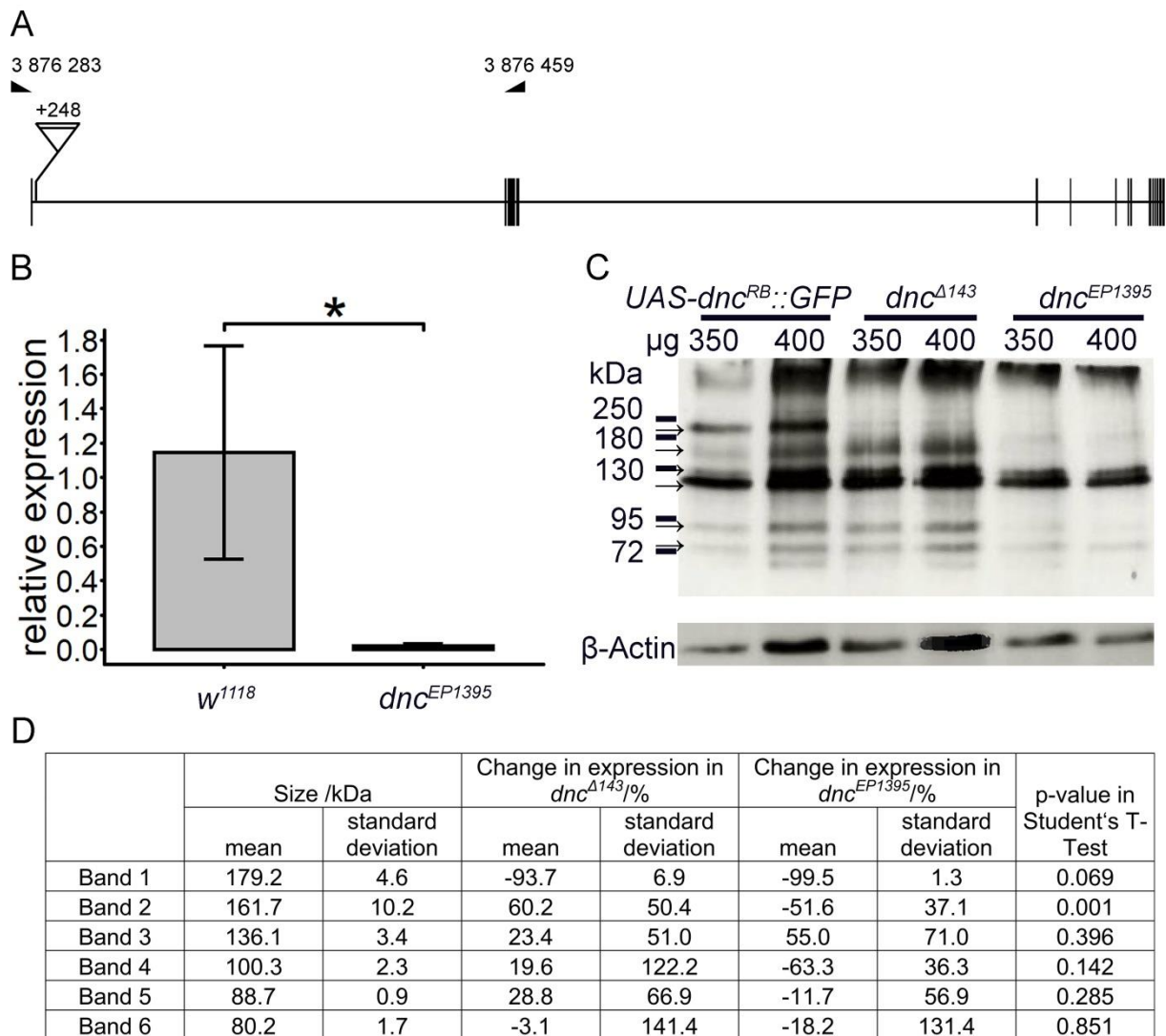
A

3 876 283   3 876 459

+248

B

C

UAS-dnc^{RB}::GFP   dnc$^{\Delta143}$ dnc^{EP1395}

µg 350 400 350 400 350 400

kDa

250
180
130

95
72

β-Actin

D

	Size /kDa		Change in expression in dnc$^{\Delta143}$/%		Change in expression in dnc^{EP1395}/%		p-value in Student's T-Test
	mean	standard deviation	mean	standard deviation	mean	standard deviation	
Band 1	179.2	4.6	-93.7	6.9	-99.5	1.3	0.069
Band 2	161.7	10.2	60.2	50.4	-51.6	37.1	0.001
Band 3	136.1	3.4	23.4	51.0	55.0	71.0	0.396
Band 4	100.3	2.3	19.6	122.2	-63.3	36.3	0.142
Band 5	88.7	0.9	28.8	66.9	-11.7	56.9	0.285
Band 6	80.2	1.7	-3.1	141.4	-18.2	131.4	0.851

Fig. 15: dnc^{EP1395} shows significantly reduced expression of dnc^{RB} and Dnc^{PB}.
A: dnc^{EP1395} has a P-element inserted 2 bp after the 3'-end of the first exon of dnc^{RB}. The primers for the qPCR in B were localised within the first and second exon of dnc^{RB}. **B**: The qPCR of larval *Drosophila* CNS as designed in **A** shows a significantly reduced expression of dnc^{RB} in dnc^{EP1395} compared to w^{1118}. **C, D**: Western blot analysis of larval *Drosophila* CNS. w^{1118}/Appl-Gal4;UASdnc^{RB}::GFP shows a strong band at 179.2 +/- 4.6 kDa corresponding to the Dnc^{PB}::GFP fusion protein and a weaker band at 161.7 +/- 10.2 kDa corresponding to the untagged Dnc^{PB}. The expression of Dnc^{PB} in dnc^{EP1395} is significantly reduced compared to dnc$^{\Delta143}$. The arrows indicate the position of the bands. Quantitative analysis of 3 western blots with two different protein concentrations, each showing that band 2, untagged Dnc^{PB} differs significantly between dnc$^{\Delta143}$ and dnc^{EP1395}. Experiments shown in this figure were conducted in collaboration with Evelin Fahle.

The concentration of the Dnc^{PB}::GFP transgene detected in dnc$^{\Delta143}$ is 93,7% lower than in w^{1118}/Appl-Gal4;UAS-dnc^{RB}::GFP. dnc^{EP1395} expresses only 0.5% of the Dnc^{PB}::GFP that w^{1118}/Appl-Gal4;UAS-dnc^{RB}::GFP expresses. When these

expressions are attributed to background staining, there are no significant differences between dnc^{EP1395} and $dnc^{\Delta143}$.

The expression of untagged Dnc^{PB} (band 2), although still detectable, is significantly reduced in dnc^{EP1395} compared to $dnc^{\Delta143}$. The concentration of Dnc^{PB} in $dnc^{\Delta143}$ is 160.2% +/- 50.4% of the concentration in w^{1118}/Appl-Gal4;UAS-dnc^{RB}::GFP. In dnc^{EP1395}, it is 48,4% +/- 37,1% of the expression in w^{1118}/Appl-Gal4;UAS-dnc^{RB}::GFP.

Taken together, we found that the mutant dnc^{EP1395} shows significantly reduced expression of the dnc^{RB} transcript and significantly reduced expression of a Dnc^{PB} with a size of 161.7 kDa. Other proteins detected by the anti-Dnc^{all} antibody were not altered. Thus, dnc^{EP1395} is a Dnc^{PB}-specific mutant.

3.2.2 dnc^{EP1395} is a better learner.

To investigate the effect of Dnc^{PB} expression on learning and memory, we analysed aversive olfactory learning and memory for w^{1118} as a control and for dnc^{EP1395} using AM and EA as odorants and 2M NaCl as a reinforcer (Fig. 16).

After one training cycle, dnc^{EP1395} learns significantly better than the control w^{1118} (Fig. 16 A). After three training cycles, both genotypes show a similar memory performance. (Fig. 15 F).
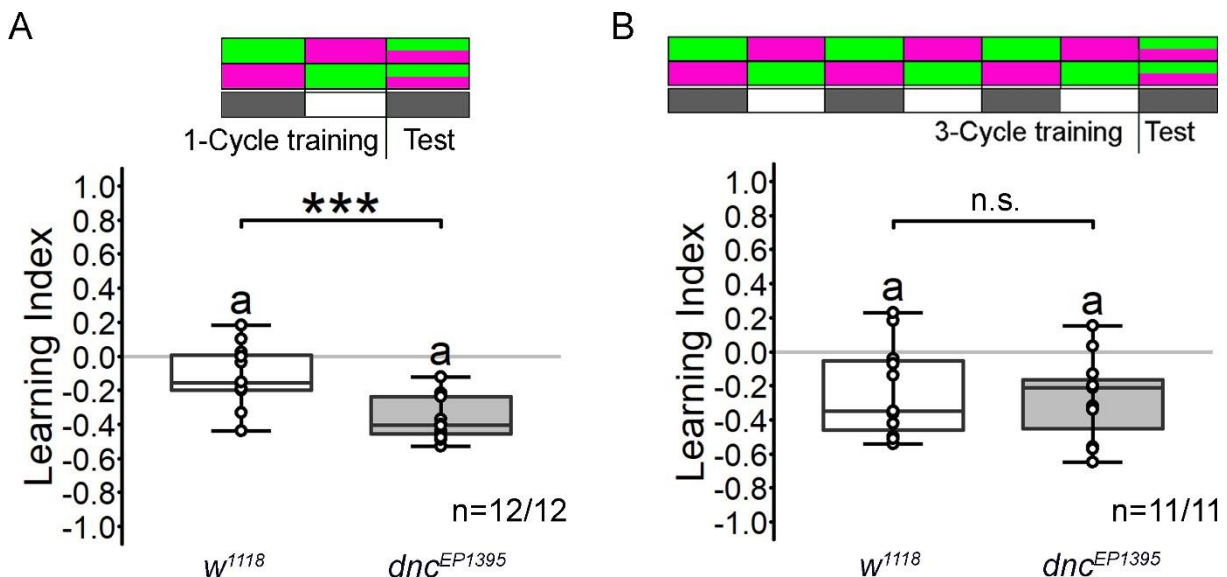

Fig. 16: dnc^{EP1395} learns better after one training cycle.
dnc^{EP1395} larvae learn significantly better than w^{1118} larvae after **A:** one training cycle, but not after **B:** three training cycles. Significant differences from random choice were determined by one sample t-test ($p < 0.05$) and labelled with the letter 'a'. Differences between groups were analysed using Student's t-test with *** $p < 0.001$.

3.3 Analysis of the expression pattern of isoform-specific and non-isoform-specific antibodies against Dunce

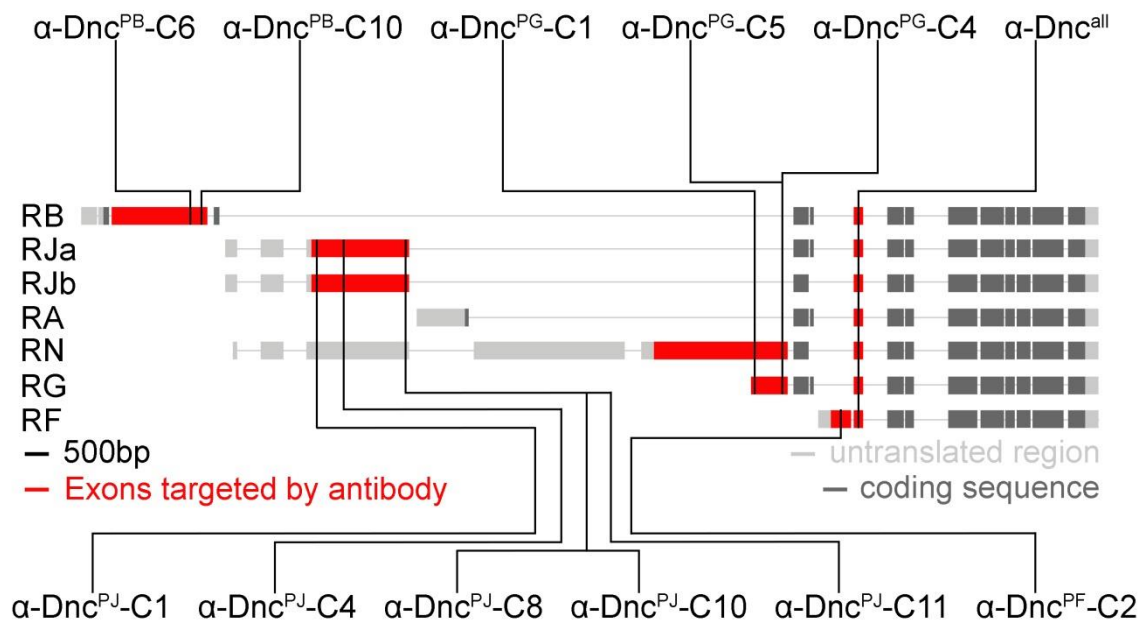### 3.3.1 Design of putative Dunce isoform-specific antibodies

Fig. 17: Antibody design for anti-Dnc^{all} and Dnc isoform-specific antibodies
The anti-Dnc^{all} antibody is a polyclonal antibody designed to bind to the first common exon shared by most isoforms. The isoform-specific antibodies are monoclonal and designed to bind to peptides in exons specific to one or two isoforms. Anti-Dnc^{PJ}-C8 and anti-Dnc^{PJ}-C10 were designed against the same peptide, whereas anti-Dnc^{PJ}-C8 / anti-Dnc^{PJ}-C10 / anti-Dnc^{PJ}-C11 and anti-Dnc^{PG}-C4 / anti-Dnc^{PG}-C5 were designed against overlapping peptides. The basic scheme of Dnc isoforms was adapted from Ruppert, Franz et al. (2017)

To study the localisation of the different Dnc isoforms, we designed several antibodies. The anti-Dnc^{all} antibody is a polyclonal antibody designed against two polypeptides encoded by an exon common to all known *dnc* isoforms except *dnc^{RL}* (FlyBase, 2023).

The putative isoform-specific antibodies are monoclonal, each designed against a polypeptide encoded by an exon specific for one or two isoforms. Figure 17 provides an overview of the localisation of the polypeptides and of the expression patterns of the respective antibodies. The polypeptides for anti-Dnc^{PG}-C4 and anti-Dnc^{PG}-C5 and for anti-Dnc^{PJ}-C8, anti-Dnc^{PJ}-C10 and anti-*Dnc^{PJ}*-C1 overlap. Anti-Dnc^{PJ}-C8 and anti-Dnc^{PJ}-C10 are designed against the same polypeptide.The antibodies and their expression patterns are described in the following sections.

### 3.3.2 Expression pattern of the anti-Dnc^{all} antibody

To study the distribution of Dnc in the larval CNS, we used a rabbit polyclonal antibody. It was designed against two polypeptides encoded by an exon common to most Dnc isoforms. Figure 17 shows which exons encode the polypeptide against which the anti-Dnc^{all} antibody was designed. We analysed the expression pattern on the Dnc^{PA}-specific mutant *dnc^{Δ143}* and on its genetic control, *w¹¹¹⁸*. We also tested the antibody on *dnc¹*, a mutant that results in reduced PDE activity, *dnc^{M14}*, a mutant with cAMP-hydrolysis even further reduced than *dnc¹* (Davis and Kiger, 1981), and their genetic control, *CS*. The anti-Dnc^{all} antibody recognises the MB, the center of learning and memory in *Drosophila* larvae (Fig. 18 A) (Heisenberg *et al.*, 1985) and in 14 clusters throughout the brain and in the VNC. The VNC has been reported as a centre for locomotor activity (Kohsaka *et al.*, 2012), but not as a relevant structure for learning and memory. Therefore, we focus on the cells in the brain. There the antibody recognises 7 clusters.

4 of these clusters are located in the mandibular neuromeres, the MDvm1 cluster, the MDvm2 cluster and the MXv cluster. They consist of one cell per cluster per side and show no significant differences between the different genotypes and their control.

The Hva cluster consists of 1 +/- 1 neuron. It is located in close proximity to the superior protocerebrum and projects towards it. The Hva-cluster was detected in *w¹¹¹⁸* in 10 out of 20 analysed hemispheres, in *dnc^{Δ143}* in 4 out of 12 analysed hemispheres and in *dnc¹* in 2 out of 10 analysed hemispheres. Like the Hd cluster, it is located close to the MB and projects towards it. Due to its high variability, no significant differences between the genotypes could be observed.

The Hd cluster consists of 3 +/- 1 neurons located in close proximity to the MB calyx and projecting towards it. Figures 2B and C show that although the Hd cluster is stained by anti-Dnc^{all} in all the mutants, it stains significantly more cells in *dnc^{Δ143}* than in its control. In *dnc^{M14}*, anti-Dnc^{all} stains significantly fewer cells than in its control. For *dnc¹* no significant differences can be detected.

The Hm cluster is located close to the AL. It consists of in average 1 +/- 1 cells, although in individual larval brains the antibody recognises none or three neurons most of the time. The anti-Dnc^{all} antibody recognises significantly fewer cells in *dnc^{Δ143}* than in its control *w¹¹¹⁸*. It also recognises significantly fewer cells in *dnc^{M14}* than in its control *CS*. No significant differences were observed between *dnc¹* and *CS*.

A

α-Dnc^{all} α-nc82
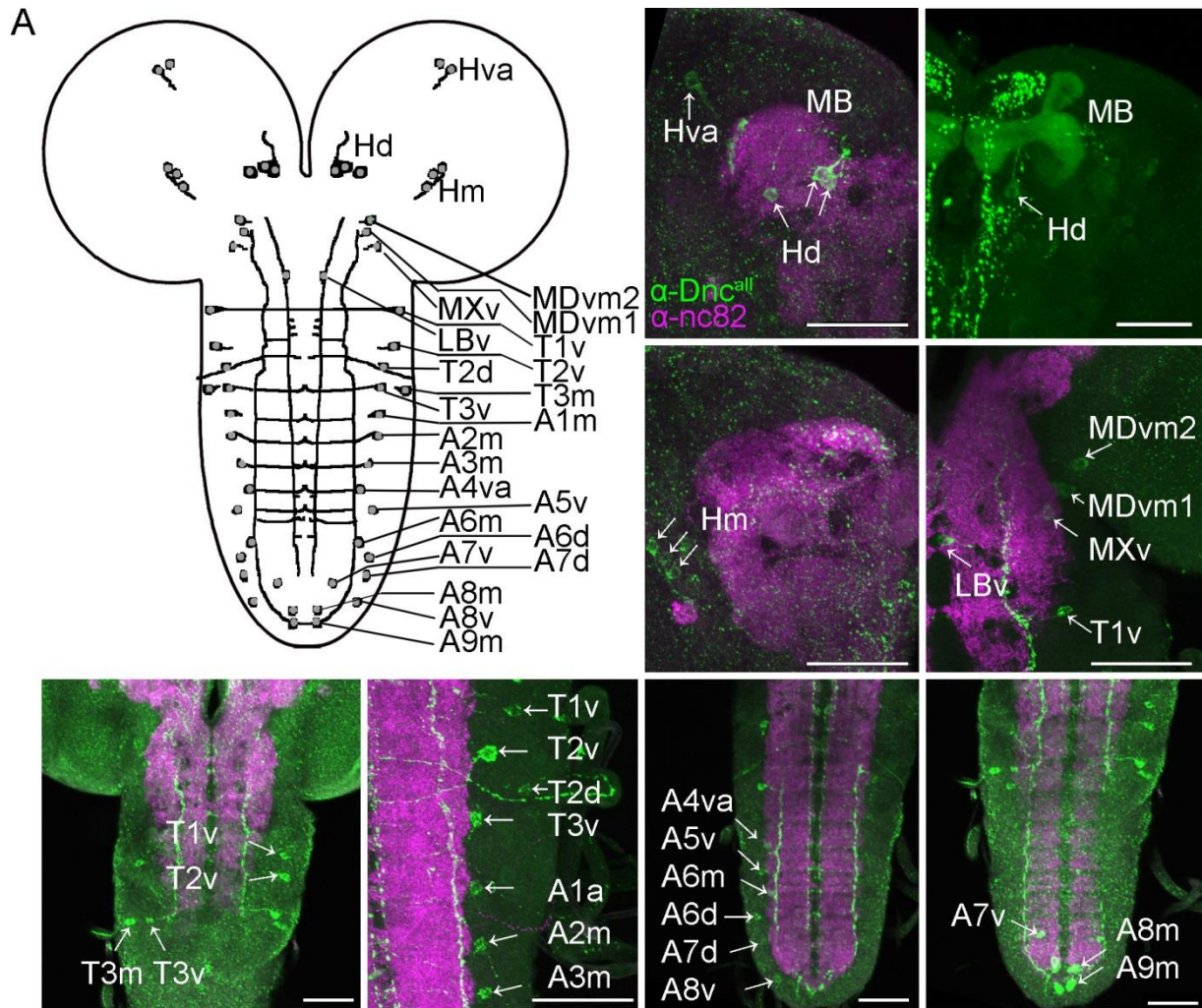
B

Genotype	Cluster	MDvm1	MXv	LBv	MDvm2	Hd	Hm	Hva
w^{1118}	Average	1	1	1	1	3	1	1
	Stddev	0.3	0.5	0.0	0.4	0.5	1.4	0.5
	n	20	20	20	20	20	20	20
$dnc^{\Delta143}$	Average	1	1	1	1	3	0	0
	Stddev	0.3	0.3	0.0	0.3	0.0	0.3	0.8
	n	12	12	12	12	12	12	12
	T-Test	ns	ns	ns	ns	*	*	ns

C

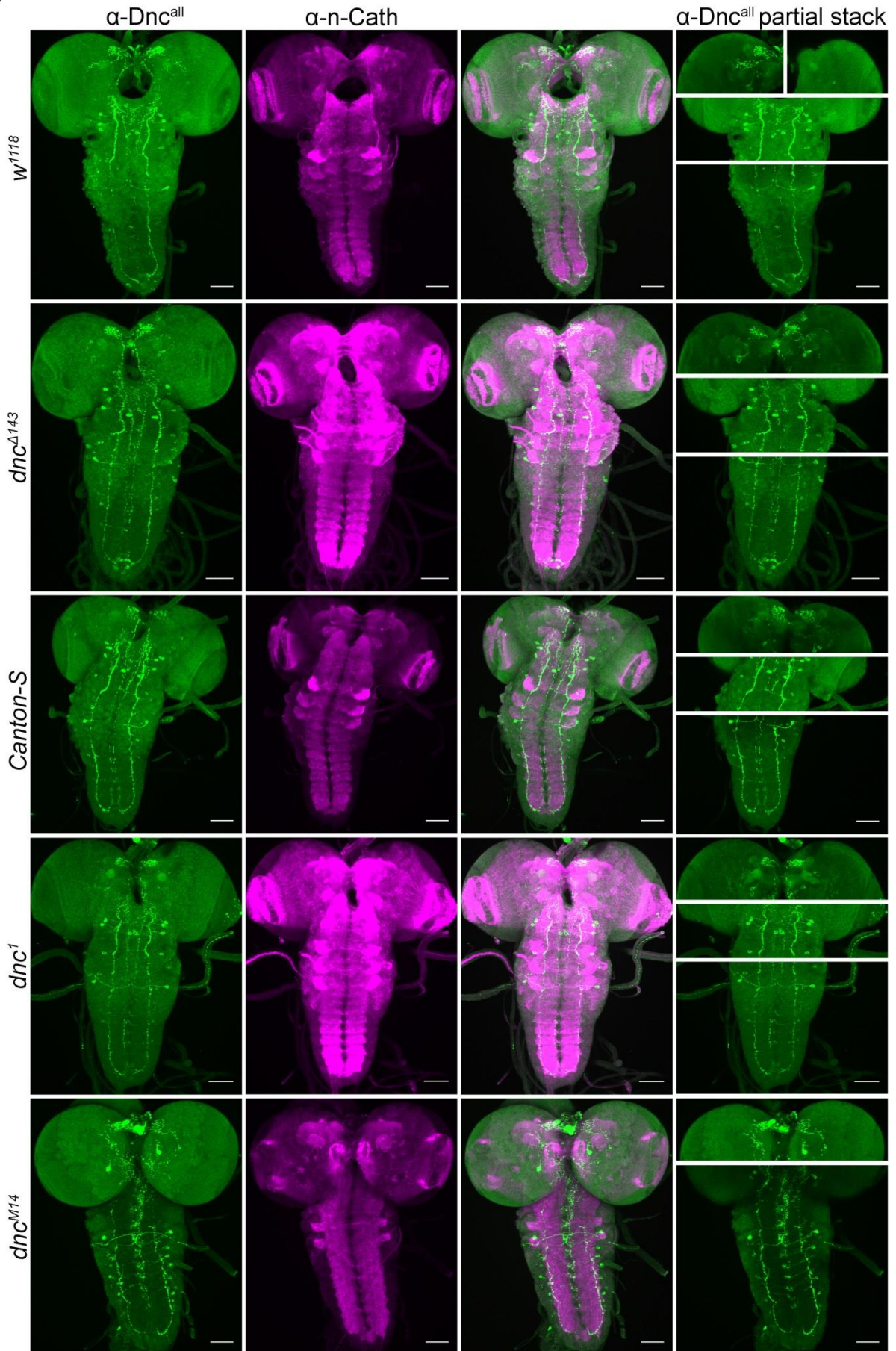| Genotype	Cluster	MDvm1	MXv	LBv	MDvm2	Hd	Hm	Hva
CS	Average	1	1	1	1	2	0	0
	Stddev	0.4	0.6	0.0	0.4	0.7	0.5	0.0
	n	14	14	14	14	14	14	14
dnc^1	Average	1	1	1	1	2	1	0
	Stddev	0	0.4	0.0	0.3	0.3	1.6	0.6
	n	10	10	10	10	10	10	10
	T-Test	ns	ns	ns	ns	ns	ns	ns
dnc^{M14}	Average	1	1	1	1	1	0	0
	Stddev	0.6	0.3	0.0	0.0	0.6	0.0	0.0
	n	12	12	12	12	12	12	12
	T-Test	ns	ns	ns	ns	**	**	ns

Fig. 18: The anti-Dnc^{all} antibody recognises 24 clusters in the *Drosophila* larval CNS.

A: The anti-Dnc^{all} antibody recognises 24 clusters of neurons in the larval CNS. Nomenclature of all clusters recognised by anti-Dnc^{all} and confocal partial stacks of their position. Grey dots indicate nuclei. w^{1118} larval CNS labelled with anti-Dnc^{all} (green), neuropile labelled with anti-nc82 (magenta). In the upper right panel, neuropile labelling is not shown for clarity. Partial stacks were scanned at 40x magnification and 1µm optical section. Scale bars are 50µm. **B**: The Hd cluster shows significantly different expression in $dnc^{\Delta143}$ than its genetic control w^{1118}. The Hm cluster shows significantly lower expression in $dnc^{\Delta143}$ than its genetic control w^{1118}. **C**: None of the clusters in the larval brain show a significantly different expression in dnc^1 than its genetic control *CS*. The Hd- and Hm cluster show significantly lower expression in dnc^{M14} than its genetic control *CS*. **D**: Immunofluorescence images of the larval CNS of Dnc mutants and their genetic background as an example of the statistics shown in B and C using Anti-Dnc^{all} and Anti-n-Cathenin (n-Cath) as a neuropil marker. Full stacks show the entire CNS and partial stacks to highlight specific regions. **B, C**: Average number of cells and standard deviation per cluster in the *Drosophila* larval brain, differences between mutants and their genetic control were analysed using Student's t-test with *: $p < 0.05$, **: $p < 0.01$. Clusters in the VNC are not shown for clarity. n indicates the number of hemispheres examined.

In conclusion, the anti-Dnc^{all} antibody recognises structures of the larval MB and multiple neurons throughout the larval CNS, of which the Hd and Hm clusters show significant differences between the mutant $dnc^{\Delta143}$ and its control w^{1118} and between the mutant dnc^{M14} and its control *CS*. No significant differences could be found for these clusters between dnc^1 and its control, *CS*. They are located in close proximity to the MB and the AL in the larval brain.

3.3.3 The anti-Dnc^{all} antibody recognises Dnc^{PB}::GFP in a western blot.

To confirm that the anti-Dnc^{all} antibody recognises Dnc, we performed a western blot analysis. We expressed the Dnc^{PB}::GFP transgene under the control of the *Appl-Gal4* driver and used the GFP-tagged membrane protein mCD8::GFP as a control (Fig. 19). The molecular weight of the proteins recognised by the antibody was calculated using regression analysis.

Using the anti-GFP antibody, we were able to detect a band at 163.1kDa for *UAS-dnc^{RB}::GFP*, and for UAS-mCD8::GFP a band at 55.3kDa (Fig. 19 A). The band at 163.1kDa corresponds to the Dnc^{PB}::GFP transgene. Its measured size is similar to the 179.2 +/-4.6 kDa measured for the same transgene in the western blot in Figure 15. As noted above (see chapter 3.2.1), this is not the predicted size, but is consistent with our previous experiments and could be due to phosphorylation. The band at 55.3kDa for UAS-mCD8::GFP corresponds to the mCD8::GFP transgene.
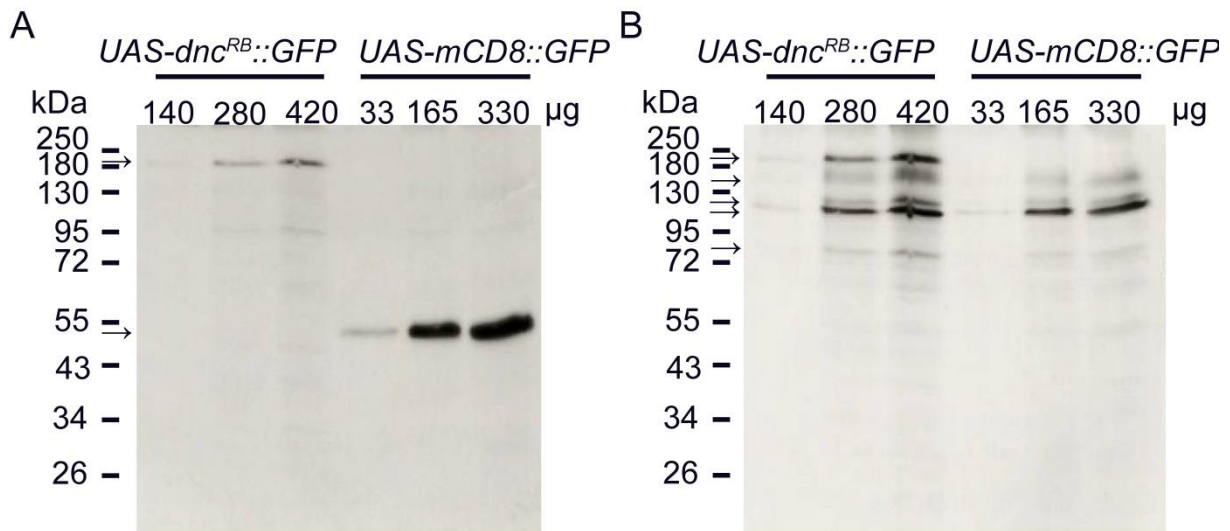
Fig. 19: **Anti-Dnc^all antibody binds to Dnc^PB::GFP.**
A, B: Western blot analysis of *UAS-dnc^RB::GFP* and *UAS-mCD8::GFP* driven by the *Appl-.Gal4* driver with anti-GFP (**A**) and anti-Dnc^all (**B**). **A**: For *UAS-dnc^RB::GFP* a band at 163.1kDa is detected corresponding to the Dnc^PB::GFP fusion protein. *UAS-mCD8::GFP* shows a band at 55.3kDa corresponding to the mCD8::GFP fusion protein. **B**: A band at 163.5kDa can be detected for *UAS-dnc^RB::GFP* but not for *UAS-mCD8::GFP* corresponding to the Dnc^PB::GFP fusion protein. Additional bands at 143.1kDa, 122.1kDa, 113.5kDa and 87.9kDa can be detected for both *Appl-Gal4;UAS-dnc^RB::GFP* and *Appl-Gal4;UAS-mCD8::GFP* corresponding to untagged Dnc^PB and other Dnc isoforms. Experiments shown in this figure were conducted by Evelin Fahle.

Figure 19 B shows the same blot incubated with anti-Dnc^all antibody. For *UAS-dnc^RB::GFP* we can detect bands at 163.5kDa, 143.1kDa, 122.1kDa, 113.5kDa and 87.9kDa. For *UAS-mCD8::GFP* we can detect the same bands with the exception of the band at 163.5kDa. This band corresponds to Dnc^PB::GFP. The other bands correspond to untagged Dnc isoforms.

This shows that the anti-Dnc^all antibody recognises several proteins of the above mentioned sizes and recognises the Dnc^PB::GFP fusion protein. Thus, anti-Dnc^all recognises Dnc isoforms. These experiments and the experiments with *dnc^EP1395* show that anti-Dnc^all is at least specific for Dnc^PB. It is therefore a Dnc-specific antibody.
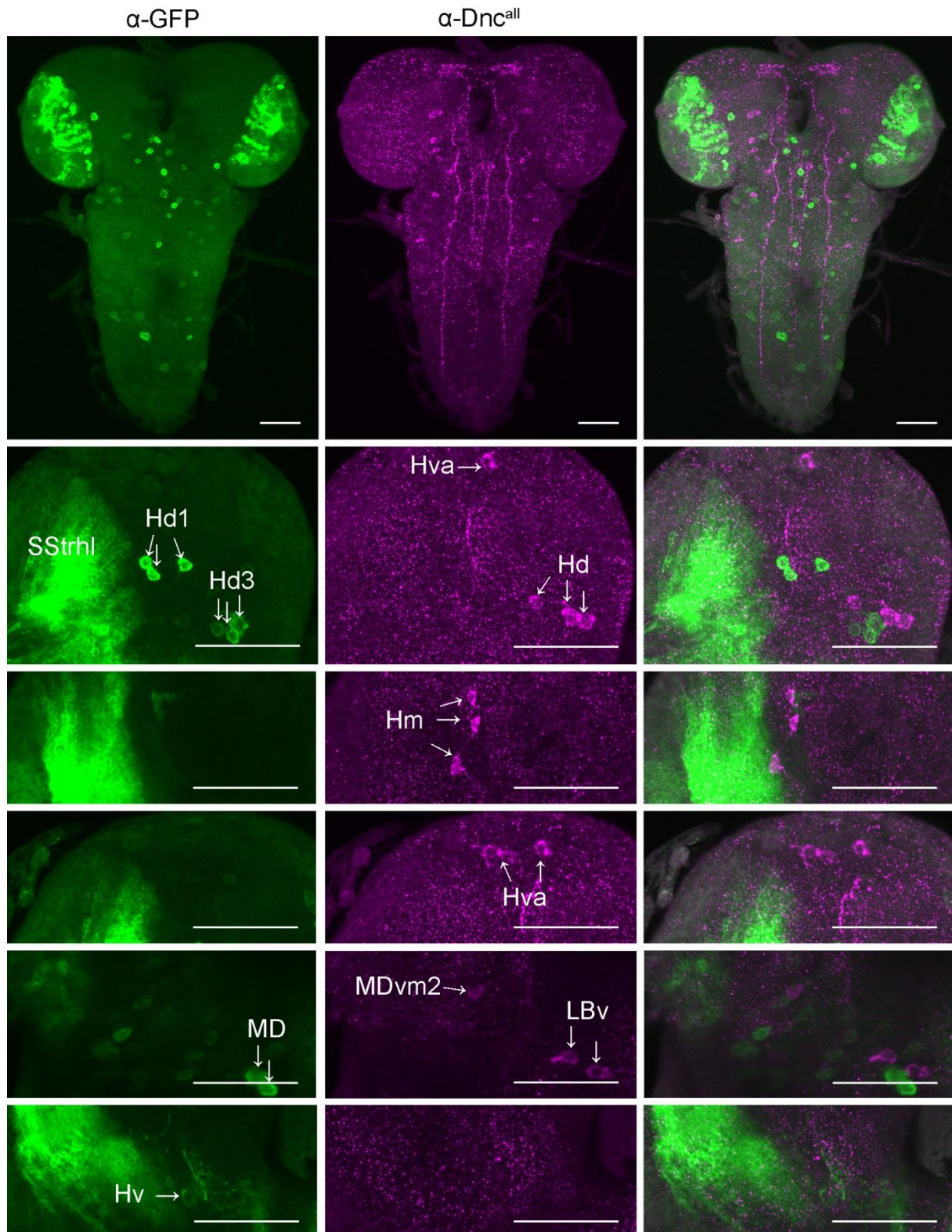
α-GFP   α-Dnc[all]

Fig. 20: **The anti-Dnc[all] antibody does not label *dnc[RA]*-positive cells.**
UASmCD8::GFP expressed in the larval CNS under the control of the *dnc[RA]-Gal4*
driver labelled with α-GFP (green) and α-Dnc[all] (magenta). The clusters recognized
by α-GFP were labelled according to the nomenclature introduced in Figure 10, the

clusters recognized by α-Dnc[all] were labelled after the nomenclature introduced in Figure 18. No colocalisation was observed. Full and partial stacks were scanned at 20x and 40x magnification and 1 μm optical section. Scale bars are 50μm. The 40x scans were conducted by Marie Müller.

To investigate whether the anti-Dnc[all] antibody recognises neurons that are targeted by the dnc^{RA}-Gal4 driver line, we performed a colocalisation study (Fig. 20).

There is no colocalisation. This leads to the conclusion that the anti-Dnc[all] antibody, although directed against a common peptide common to most isoforms (Fig. 17), does not recognise all Dnc isoforms in their natural configuration, possibly because the peptides are masked. The dnc^{RA}-Gal4 promoter drives an isoform in which the peptide anti-Dnc[all] is designed against is masked.

3.3.5 The cells recognised by the anti-Dnc[all] antibody are neither dopaminergic nor serotonergic nor *hugin*-positive.

To further characterise the cells recognised by anti-Dnc[all], we investigated whether they are dopaminergic. Dopaminergic neurons have been characterised as essential for olfactory aversive and appetitive learning and memory in *Drosophila* larvae (Selcho *et al.*, 2009). They have been shown to innervate the MB (Selcho *et al.*, 2009). The localisation and phenotype make the Hd cluster a promising candidate for expression in dopaminergic cells.

To investigate whether the anti-Dnc[all] antibody recognises dopaminergic neurons, a colocalisation studiy was performed in w^{1118} larvae using the anti-Dnc[all] antibody in combination with an antibody against tyrosine hydroxylase (TH), an enzyme specific for dopaminergic neurons. None of the neurons were recognised by both anitbodies, indicating that the anti-Dnc[all] antibody does not recognise dopaminergic neurons (Fig. 21).

In adult *Drosophila*, a serotonergic projection neuron that projects to the MB peduncle was found to be responsible for defective LTM formation in dnc^1 (Scheunemann *et al.*, 2018). In the larva, the serotonergic system has been reported to modulate larval aversive olfactory learning and memory (Huser *et al.*, 2017).

To test whether the anti-Dnc[all] antibody recognizes serotonergic neurons, colocalisation studies were performed in w^{1118} larvae using the anti-Dnc[all] antibody in combination with an antibody against serotonin (5-hydroxyltryptamine, 5-HT). None of the neurons were recognised by both anitbodies, indicating that the anti-Dnc[all] antibody does not recognise serotonergic neurons (Fig. 22).
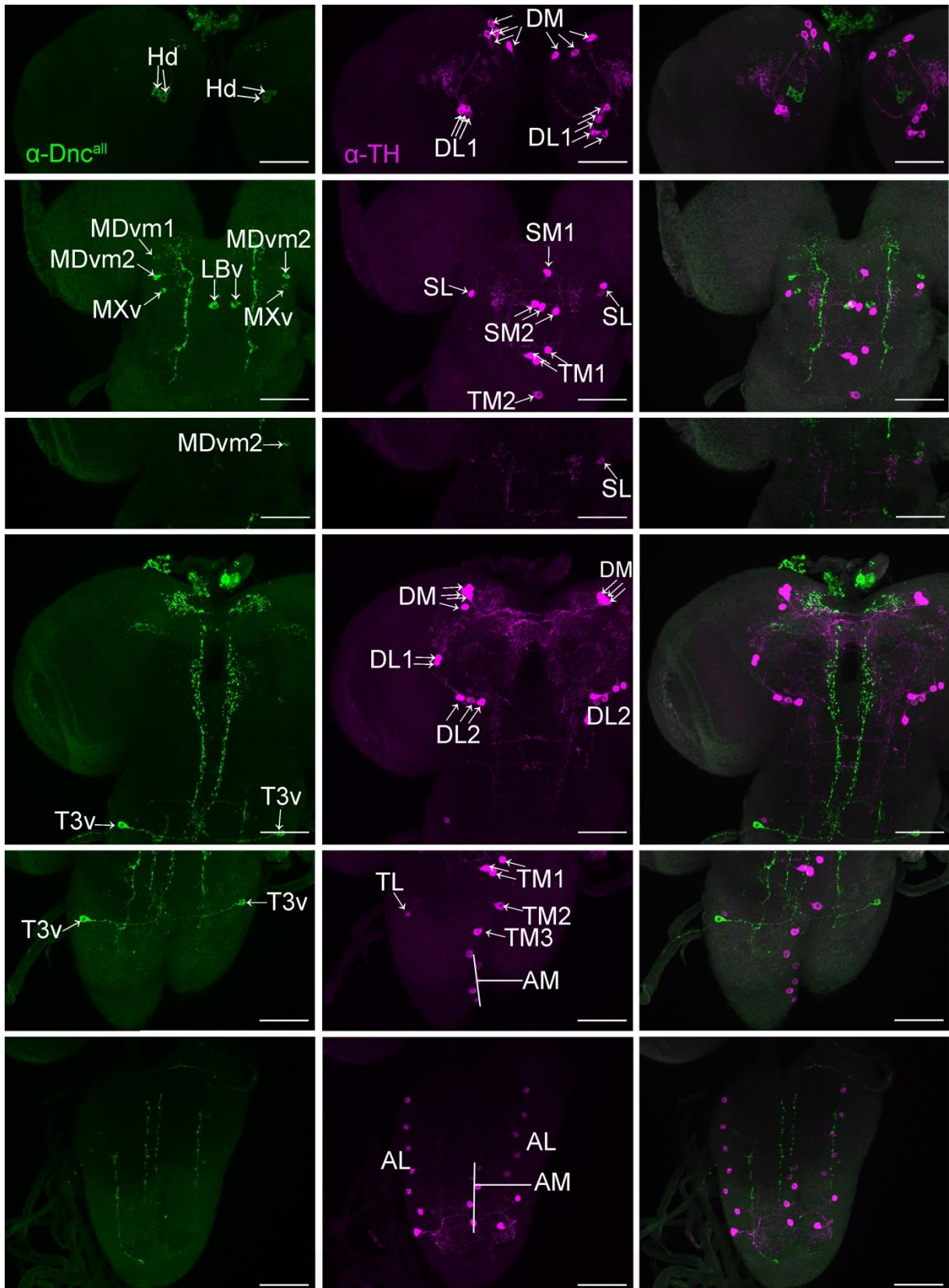
Fig. 21: Anti-Dnc^{all} does not recognise dopaminergic neurons.
A: No colocalisations can be observed. *w¹¹¹⁸* larval CNS labelled with anti-Dnc^{all} (green), clusters labelled according to Figure 18 and anti-TH (magenta), clusters labelled according to Selcho et al (Selcho *et al.*, 2009). Partial stacks were scanned at 40x magnification and 1μm optical section. Scale bars are 50μm.
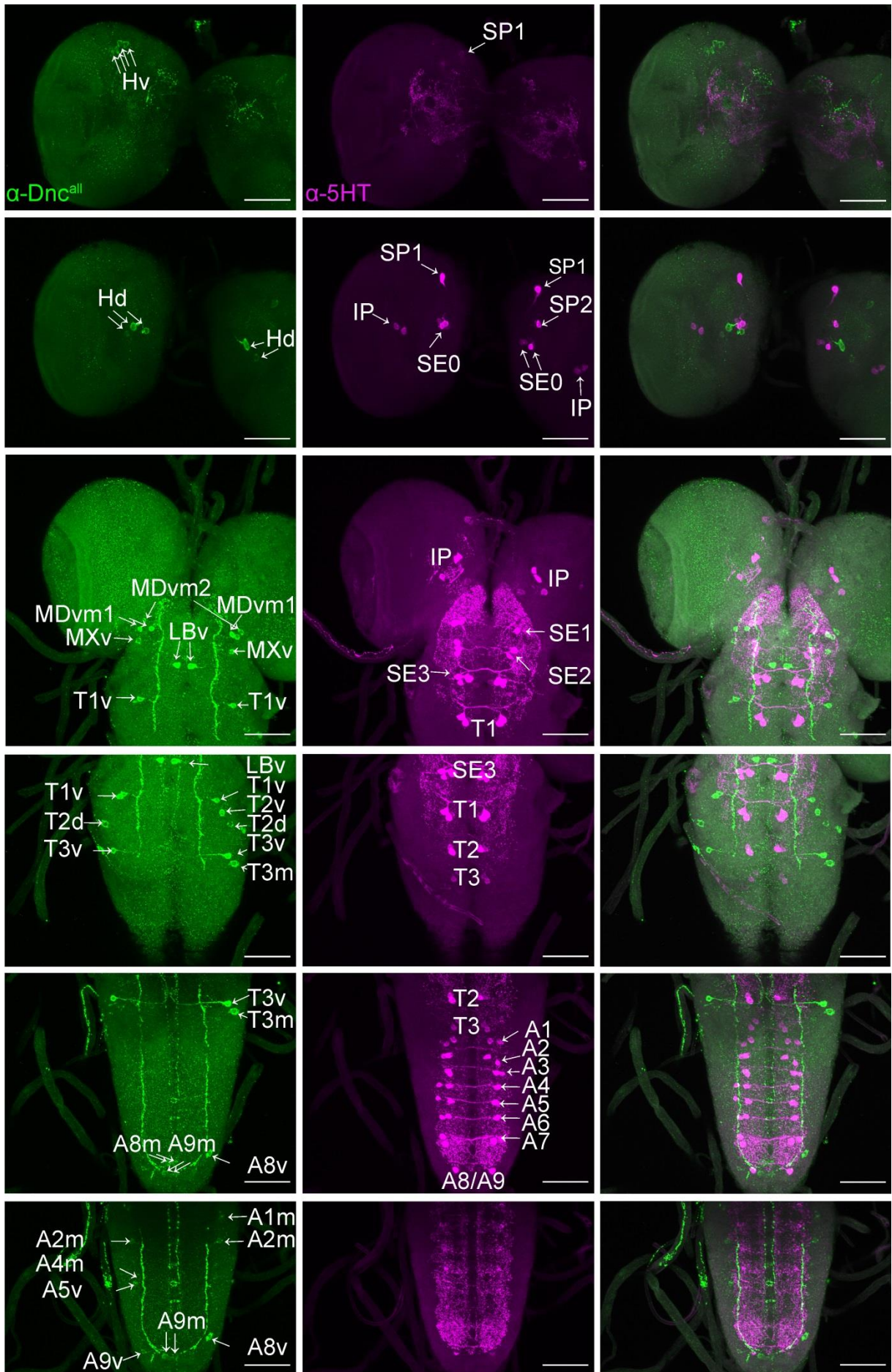
Fig. 22: Anti-Dnc^{all} does not recognise serotonergic neurons.

A: w^{1118} larval CNS labelled with anti-Dnc^{all} (green) and anti-5-HT (magenta). No colocalisations can be observed. Anti-Dnc^{all} clusters labelled according to nomenclature (Fig. 18), anti-5-HT labelled according to Huser et al (Huser *et al.*, 2012). Partial stacks were scanned at 40x magnification and 1µm optical section. Scale bars are 50µm.
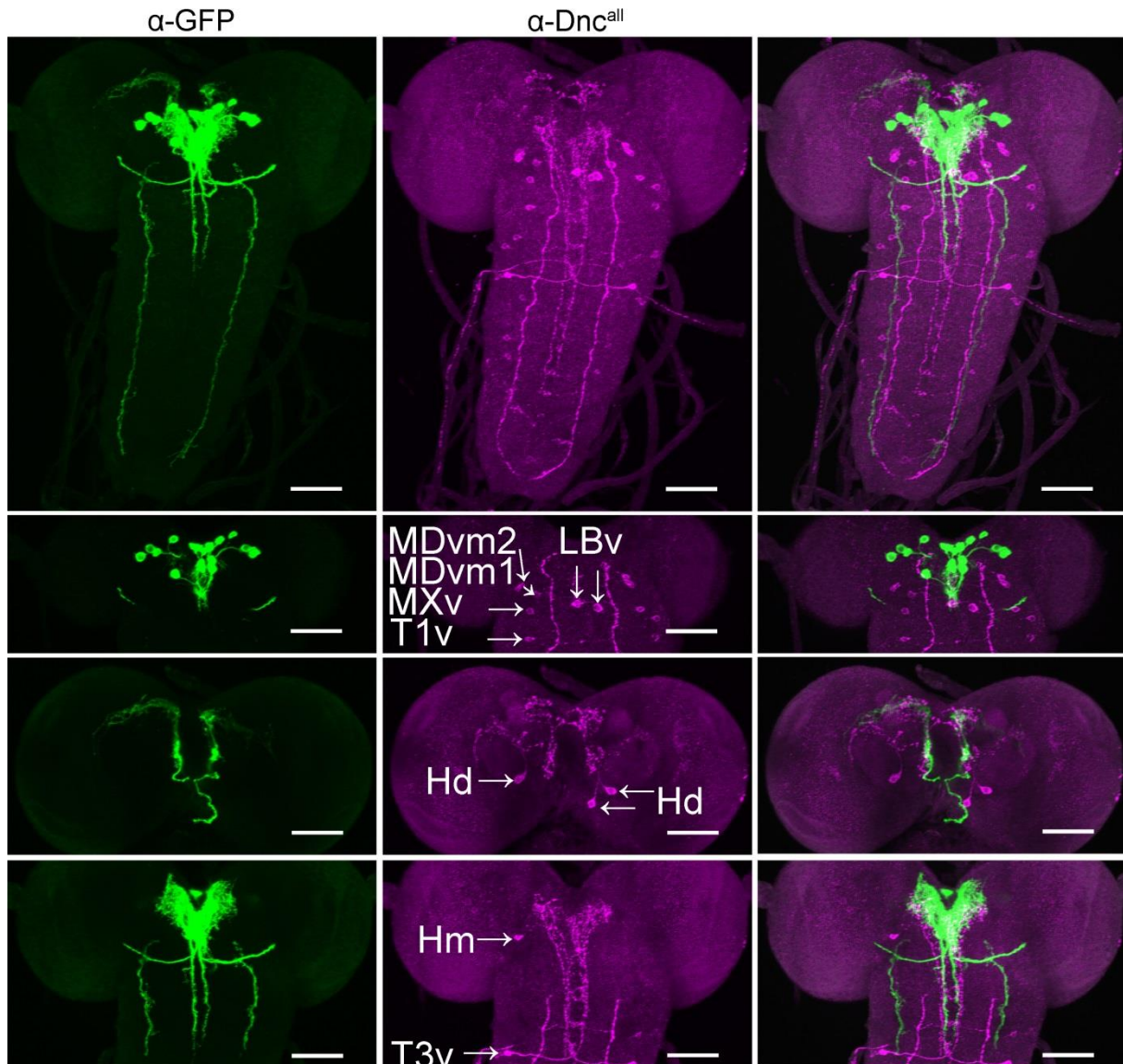

Fig. 23: Anti-Dnc^{all} does not recognise *hug* neurons.

UASmCD8::GFP expressed in the larval CNS under the control of the *HugS3-Gal4* driver, labelled with α-GFP (green) and α-Dnc^{all} (magenta). α-Dnc^{all} clusters were labelled according to the nomenclature introduced in Figure 18. Full and partial stacks were scanned at 20x magnification and 1 µm optical section. Scale bars are 50µm.

Other distinct neurons in the larval CNS are *hugin (hug)* neurons, which are peptidergic neurons that play a role in larval feeding behaviour (Melcher and Pankratz, 2005). To determine if the anti-Dnc^{all} antibody recognises *hug* neurons,

colonisation studies were performed on *HugS3-Gal4/UAS-mCD8::GFP* larvae using an anti-GFP antibody in combination with the anti-Dnc[all] antibody. None of the neurons were recognised by both antibodies, indicating that the anti-Dnc[all] antibody does not recognise *hug* neurons (Fig. 23).

In conclusion, the anti-Dnc[all] antibody is not expressed in serotonergic, dopaminergic or *hug*-positive peptidergic neurons.

3.3.6 Characterisation of putative peptide antibodies against Dnc[PB]

To investigate the localisation of the individual isoforms, isoform-specific peptide antibodies were designed. They were designed against polypeptides encoded by exons present only in one or two isoforms (Fig. 17) and were generated by Abmart using a library-based approach (Wang *et al.*, 2020).

For Dnc[PB] we have obtained two putative antibodies, one of which is anti-Dnc[PB]-C6. It recognises several clusters in the larval brain and VNC (Fig. 24), including clusters in the deutocerebrum and tritocerebrum, in the labium, three clusters in the thoracic ganglion and three clusters in the abdominal ganglion (Fig. 24 A, B).

The neurons of the labium (LBv cluster) are also recognised by the anti-Dnc[all] antibody. In addition, the T2v, T2d and T3v clusters in the thoracic segments of the VNC are anti-Dnc[all] and anti-Dnc[PB]-C6 positive (Fig. 24 A, B). At the cellular level, like anti-Dnc[all], anti-Dnc[PB]-C6 detects the soma and not the nucleus (Fig. 24 C).

To ensure that anti-Dnc[PB]-C6 is specific for the peptide against which it was designed, we blocked the epitope binding in the CNS by adding increasing concentrations of the peptide against which the antibody was selected. The peptide was added at concentrations 10 and 100 times higher than the antibody. To control that the procedure was working, a larval CNS was labelled with the anti-Dnc[PB]-C6 antibody without added peptide (Fig. 24 D). The intensity of the fluorescence signal was reduced by blocking the antibody-antigen interaction with a 10-fold excess of peptide and abolished by a 100-fold excess of peptide. Thus, anti-Dnc[PB]-C6 recognises in vivo the peptide sequence to which the antibody was designed.

Since Dnc[PB]-deficient larvae are defective in olfactory learning and memory, one candidate for possible defects is *hug*-specific neurons, peptidergic neurons that play a role in larval feeding behaviour (Melcher and Pankratz, 2005). As with the anti-Dnc[all] antibody, we used *UAS-mCD8::GFP* driven by the *HugS3-Gal4* driver to visualise *hug* neurons. We used the anti-GFP antibody to label the *hug* neurons and the anti-Dnc[PB]-C6 antibody to visualise the Dnc[PB]-positive neurons.
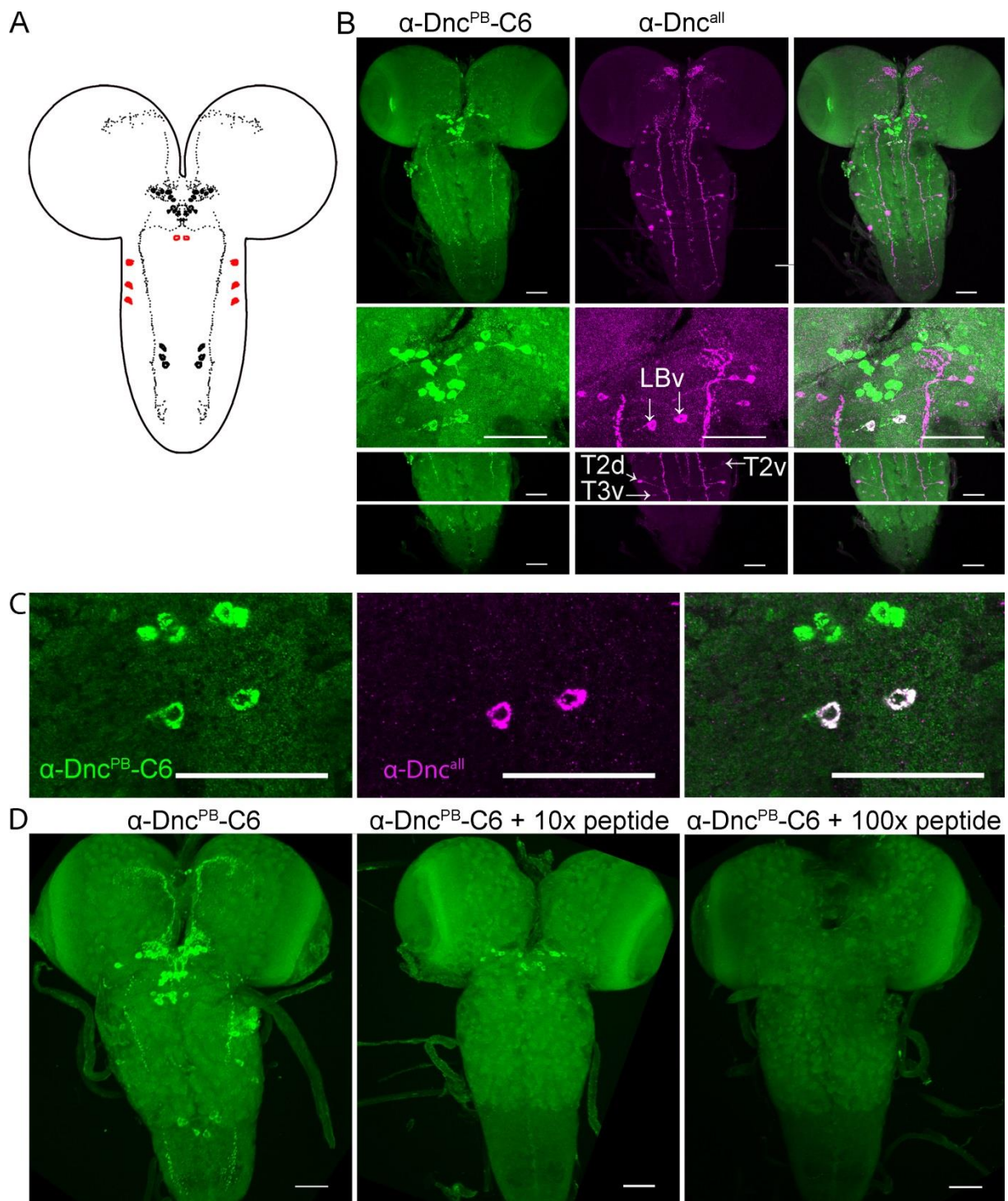
Fig. 24: Putative Dnc^PB-specific anti-Dnc^PB-C6 recognises the same neurons as anti-Dnc^all in the LBv cluster, T2d, T2v and T3v clusters.
A: Cartoon of neurons recognised by the anti-Dnc^PB-C6 antibody in the larval CNS. Neurons recognised by both anti-Dnc^PB-C6 and anti-Dnc^all are all shown in red, neurons uniquely recognised by anti-Dnc^PB-C6 are shown in black. **B**: w^{1118} larval CNS labelled with Anti-Dnc^PB-C6 (green) and anti-Dnc^all (magenta). Clusters recognised by both α-Dnc^all and anti-Dnc^PB-C6 are labelled according to the nomenclature for anti-Dnc^all introduced in Figure 18. **C**: Anti-Dnc^PB-C6 detects regions of the soma of the LBv cluster in w^{1118}. **D**: Recognition of cells by anti-Dnc^PB-

C6 is blocked by addition of the peptide to which the antibody was generated. w^{1118} larval CNS labelled with anti-Dnc^{PB}-C6, and addition of 10x higher concentration of peptide than the antibody and 100x higher concentration than the antibody. Full stacks were scanned at 20x magnification and 1µm optical section. Partial stacks were scanned at 40x magnification and 1µm optical section and for **C** at 63x magnification and 0.33µm optical section. Scale bars are 50µm.

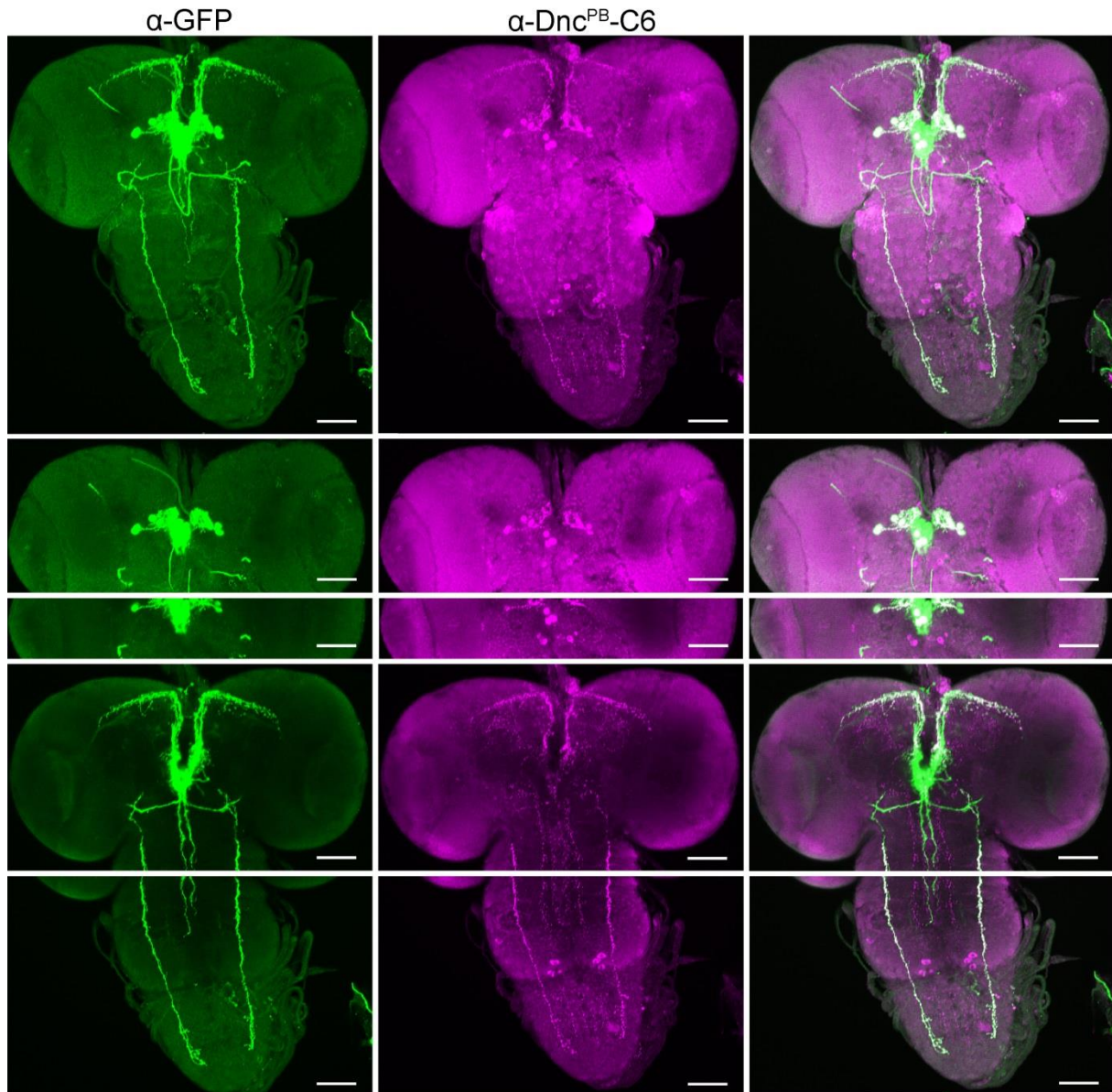**Fig. 25: Anti-Dnc^{PB}-C6 recognises *hug*-positive neurons.**
The majority of anti-Dnc^{PB}-C6-positive neurons are driven by *HugS3-Gal4*. *UASmCD8::GFP* expressed in the larval CNS under the control of the *HugS3-Gal4* driver, labelled with anti-GFP (green) and anti-Dnc^{PB}-C6 (magenta). Full and partial stacks were scanned at 20x magnification and 1 µm optical section. Scale bars are 50µm.

In Figure 25 we show that the majority of the clusters recognised by the anti-Dnc^{PB}-C6 in the hemispheres are *hug*-positive. However, there are two clusters in each hemisphere, including the LBv cluster, that are not *hug*-positive. Three clusters in the abdominal segments of the VNC are anti-Dnc^{PB}-C6-positive but they are not *hug*-positive. In the thoracic clusters T2d, T2v and T3v there is also no expression of *hug*. This shows that Dnc^{PB} plays a role in peptidergic neurons. It further leads to the assumption that *hug* neurons play a role in the behaviour phenotype of Dnc^{PB} mutants (Fig. 15), however this has to be further investigated in the future in larval learning and memory experiments expressing *dnc^{RNAi}* in *hug* neurons.
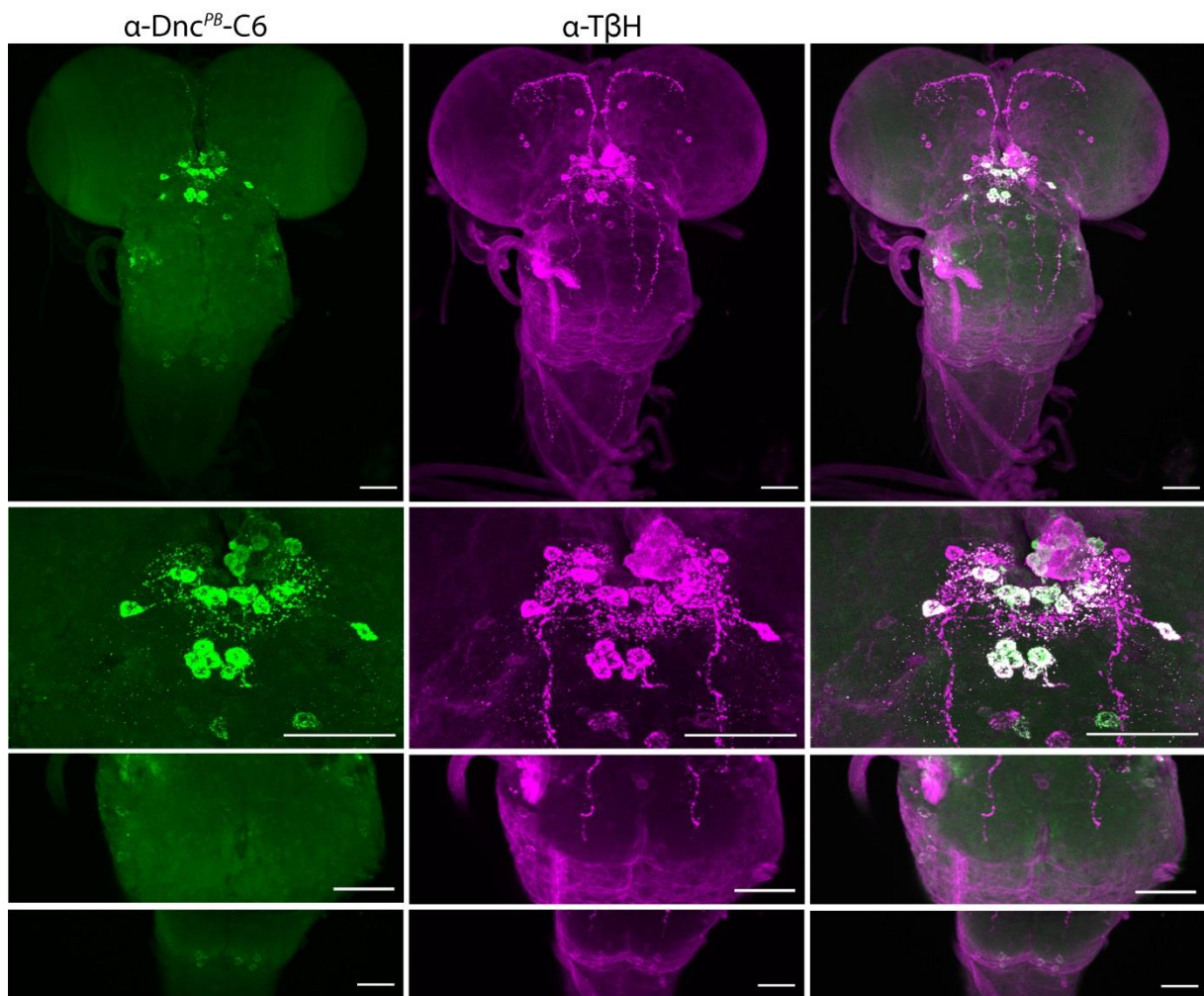
Fig. 26: Anti-Dnc^{PB}-C6 detects cells that are Tβh-positive.
w^{1118} larval CNS labelled with anti-Dnc^{PB}-C6 (green) and anti- Tyramine β-hydroxylase (TβH) (magenta). All anti-Dnc^{PB}-C6-positive neurons colocalise with anti-TβH-positive neurons. Full stacks are scanned at 20x magnification and 1 µm optical section, partial stacks are scanned at 60x magnification and 0.33µm optical section. Scale bars are 50µm.

TβH catalises the final step in octopamine synthesis in *Drosophila melanogaster* (Livingstone and Tempel, 1983), a neurotransmitter that has been shown to play a role in learning and memory (Berger *et al.*, 2023; Perisse *et al.*, 2013; Schwaerzel *et al.*, 2003). The Anti-TβH antibody recognises octopaminergic cells, but also other cells (Monastirioti *et al.*, 1996). To analyse whether the neurons recognised by anti-Dnc[PB]-C6 are Tβh-positive neurons, we used an anti-TβH antibody by Cibik and the anti-Dnc[PB]-C6 antibody on a larval VNC in an immunohistochemical experiment (Cibik, 2007).

We show that most of the neurons recognised by anti-Dnc[PB]-C6 are also recognised by anti-TβH (Fig. 26). All cells in the hemispheres that are recognised by anti-Dnc[PB]-C6 are also TβH-positive, although there are TβH-positive cells that are anti-Dnc[PB]-C6-negative. In the labium, the LBv cluster, which also does not recognise *hug*-positive cells but colocalises with anti-Dnc[all] (Fig. 24, 25) does not colocalise with anti-TβH. In the VNC, the clusters in both the thoracicic and abdominal segments that are positive for anti-Dnc[PB]-C6 are also positive for anti-TβH (Fig. 26).

In summary, the anti-Dnc[PB]-C6 antibody recognises the soma in several clusters within the larval CNS. Four of the clusters recognised by anti-Dnc[PB]-C6 colocalise with anti-Dnc[all]. Most of the anti-Dnc[PB]-C6-positive clusters are also *hug*-positive and Tβh-positive.

To further investigate the localisation of Dnc[PB] in the larval CNS, we generated a second putative peptide antibody against the same isoform, anti-Dnc[PB]-C10. As shown in Figure 17, this peptide antibody was designed against a polypeptide encoded by the 4th exon of *dnc[RB]*, the same exon against which the polypeptide anti-Dnc[PB]-C6 was designed. Anti-Dnc[PB]-C10 was designed against a polypeptide sequence more C-terminal than anti-Dnc[PB]-C6.

We show that anti-Dnc[PB]-C10 recognises two clusters in the larval brain, an expression pattern entirely different from that of anti-Dnc[PB]-C6 (Fig. 27 A, B). It does not colocalise with anti-Dnc[all]. Using a competition experiment similar to that designed for the anti-Dnc[PB]-C6 antibody, we tested whether the binding of the antibody could be outcompeted by the peptide it was designed against, and thus whether it is specific for this peptide. We show that already 10 times the concentration of the antibody added to the peptide is sufficient to eliminate the recognition of the antigene, confirming that the antibody is specific for the polypeptide (Fig. 27 C).

To investigate whether anti-Dnc^{PB}-C10, like the other putative Dnc^{PB}-specific antibody anti-Dnc^{PB}-C6, recognises *hug*-positive cells, we examined colocalisation by crossing the *Hug-Gal4.S3* line with *UAS-mCD8::GFP*. We then used the anti-GFP antibody and the anti-Dnc^{PB}-C10 antibody. We show that none of the *hug* neurons are recognised by anti-Dnc^{PB}-C10 (Fig. 26).
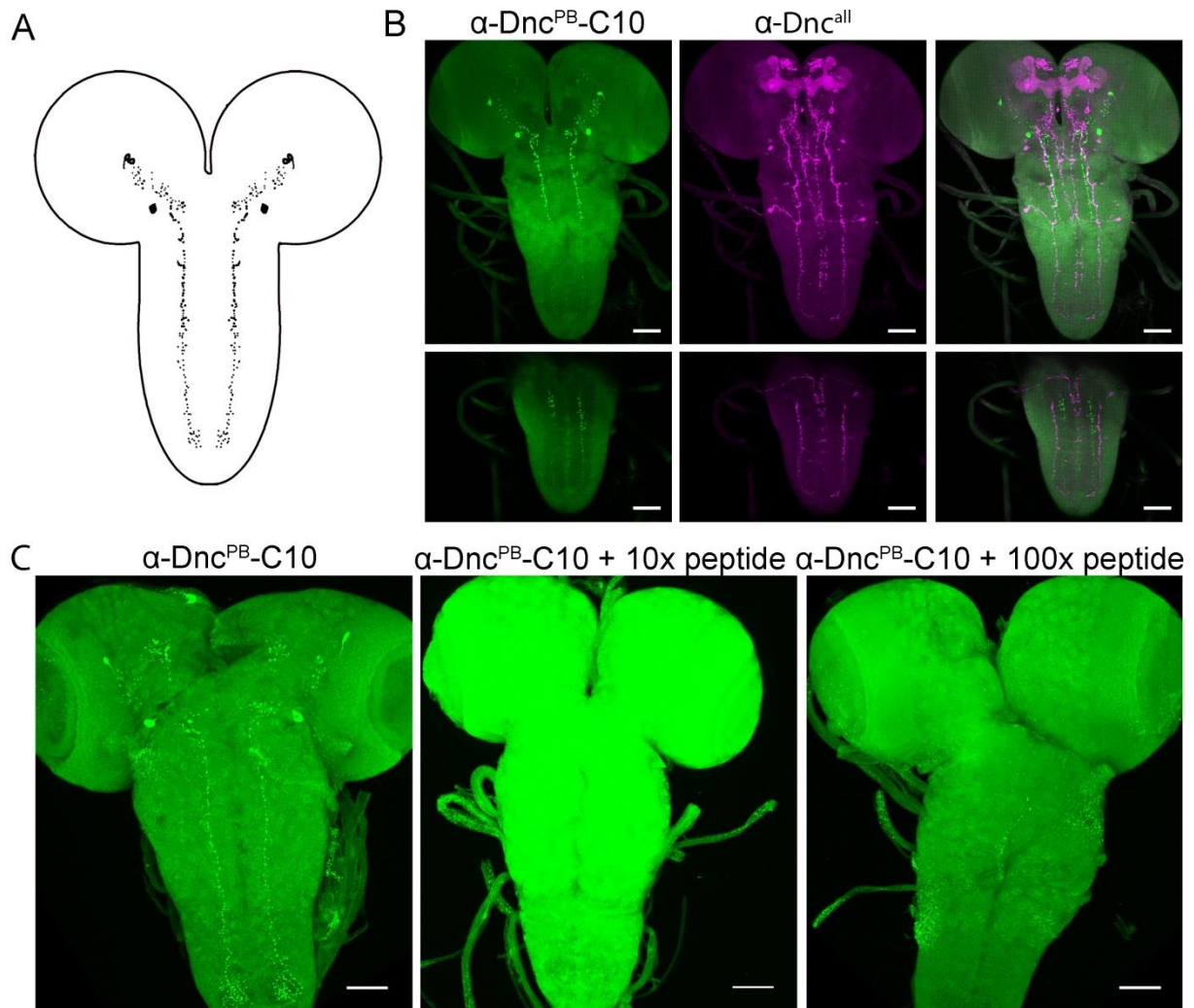

Fig. 27: Putative Dnc^{PB}-specific anti-Dnc^{PB}-C10 does not recognise structures recognised by anti-Dnc^{all}.
A: Cartoon of neurons recognised by the anti-Dnc^{PB}-C10 antibody in the larval CNS. **B**: No colocalisations were observed in *w^{1118}* larval CNS labelled with anti-Dnc^{PB}-C10 (green) and anti-Dnc^{all} (magenta). **C**: Recognition of cells by anti-Dnc^{PB}-C10 is blocked by adding peptide to which the antibody was generated. *w^{1118}* larval CNS labelled with anti-Dnc^{PB}-C6 and addition of 10x higher concentration of peptide than antibody and 100x higher concentration than the antibody. Full and partial stacks were scanned at 20x magnification and 1µm optical section. Scale bars are 50µm.

In conclusion, although anti-Dnc^{PB}-C6 and anti-Dnc^{PB}-C10 are peptide antibodies directed against sequences encoded by the same exon, and competition

experiments confirm their specificity for the polypeptides, their expression patterns are very different. While anti-Dnc[PB]-C6 partially colocalises with anti-Dnc[all] and anti-TβH and recognises *hug* neurons, anti-Dnc[PB]-C10 does not colocalise with anti-Dnc[all] and does not recognise *hug* neurons.
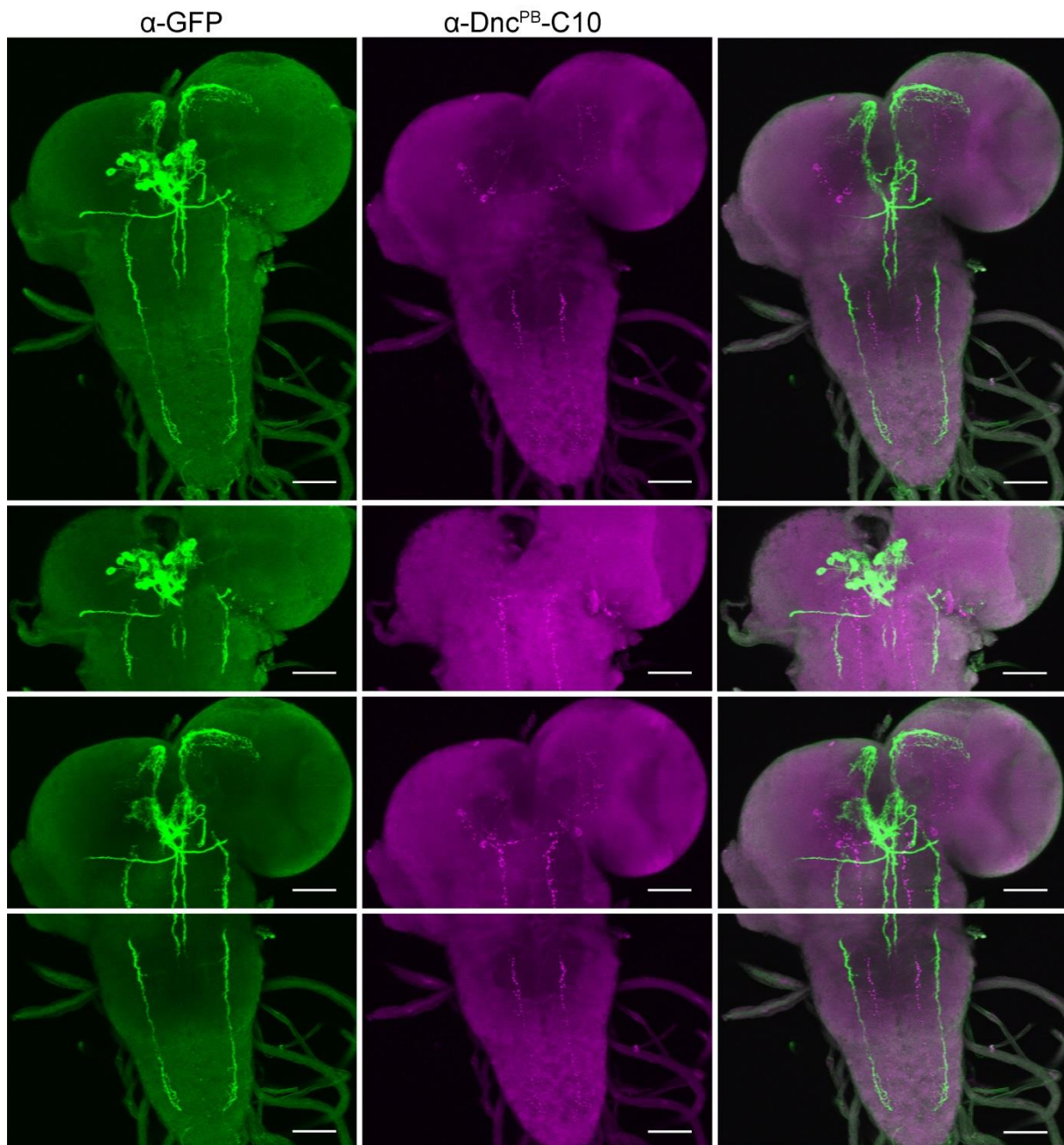

Fig. 28: Anti-Dnc[PB]-C10 does not recognise *hug* neurons.
None of the anti-Dnc[PB]-C6-positive neurons are driven by *HugS3-Gal4*. *UASmCD8::GFP* expressed in the larval CNS under the control of the *HugS3-Gal4* driver labelled with anti-GFP (green) and anti-Dnc[PB]-C10 (magenta). Full and partial stacks were scanned at 20x magnification and 1 μm optical section. Scale bars are 50μm.

3.3.7 Characterisation of putative peptide antibodies against Dnc^{PJ}

To investigate the expression of Dnc^{PJ} in the larval CNS, we generated five putative isoform-specific peptide antibodies against polypeptides encoded by an exon unique to dnc^{RJ} (Fig. 17).

One of these antibodies is anti-Dnc^{PJ}-C1. It recognises several clusters in the larval CNS (Fig. 29). A cluster of three neurons can be observed in the lateral protocerebrum, four clusters of several neurons in the tritocerebrum and a cluster of one neuron per side in the labium. A further cluster of three neurons is observed in the thoracic region of the VNC. The antibody also recognises a characteristic pattern of axons in both the brain and the VNC (Fig. 29 A, B). Although anti-Dnc^{PJ}-C1 recognises neurons in a similar pattern to anti-Dnc^{PB}-C6, it does not colocalise with anti-Dnc^{all} (Fig. 29 A, B).

Like the anti-Dnc^{PB}-C6, anti Dnc^{PJ}-C1 recognises the soma but not the nucleus of neurons (Fig. 29 C). We performed a competition experiment similar to the one with anti-Dnc^{PB}-C6 and anti-Dnc^{PB}-C10 by adding the peptide to the antibody during immunohistochemical staining. The addition of 10 times the concentration of the antibody to the peptide mostly outcompeted the binding of the antibody, 100 times the concentration of the antibody could completely block the binding of the anti-Dnc^{PJ}-C1 antibody to the epitope, confirming that anti-Dnc^{PJ}-C1 binds in vivo the polypeptide it was designed against (Fig. 29 D).

With an expression pattern similar to that of anti-Dnc^{PB}-C6, we investigated whether anti-Dnc^{PJ}-C1 also recognises *hug*-specific neurons.

Therefore, we used *UAS-mCD8::GFP* driven by the *HugS3-Gal4* driver to visualise *hug* neurons. We used the anti-GFP antibody to label the *hug* neurons and the anti-Dnc^{PJ}-C1 antibody to visualise the Dnc^{PB}-positive neurons.

We show that most of the clusters recognised by anti-Dnc^{PJ}-C1 are *hug*-positive (Fig. 30). In the CNS there are several anti-Dnc^{PJ}-C1-positive clusters that are not *hug*-positive, one in the superior protocerebrum and one in the ventromedial cerebrum (Fig. 30). The cluster in the labium is not driven by the *Hug-Gal4* driver. The cells recognised by anti-Dnc^{PB}-C1 in the abdominal segments of the VNC are *hug*-positive (Fig. 30).
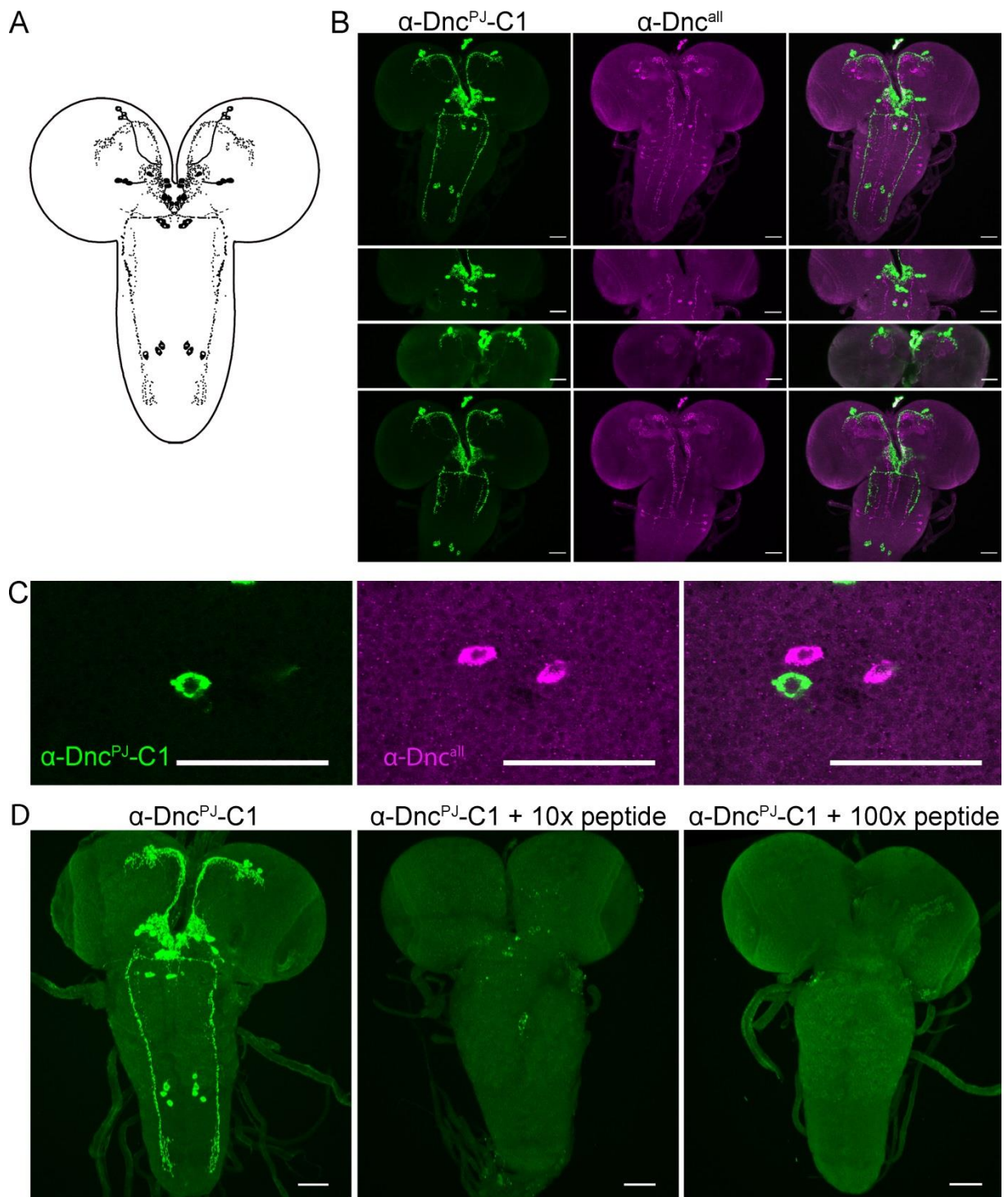
Fig. 29: Putative Dnc^{PJ}-specific anti-Dnc^{PJ}-C1 does not recognise structures detected by anti-Dnc^{all}.

A: Cartoon of neurons recognised by the anti-Dnc^{PJ}-C1 antibody in the larval CNS. **B**: No colocalisations were observed in *w^{1118}* larval CNS labelled with anti-Dnc^{PJ}-C1 (green) and anti-Dnc^{all} (magenta). **C**: Anti-Dnc^{PJ}-C1 detects regions of the soma of a neuron near the LBv cluster in *w^{1118}*. **D**: Recognition of cells by anti-Dnc^{PJ}-C1 is blocked by adding the peptide against which the antibody was generated. *w^{1118}* larval CNS labelled with anti-Dnc^{PJ}-C1 and addition of 10x higher concentration of peptide than the antibody and 100x higher concentration than the antibody. **B, D**: Full and partial stacks were scanned at 20x magnification and 1 µm optical section. **C**: Partial

stacks were scanned at 63x magnification and 0.33 µm optical section. Scale bars are 50µm.

In summary, anti-Dnc^{PB}-C1 recognizes the somatic region of numerous cells within the larval CNS, with no colocalisation with anti-Dnc^{all}. Most of the cells recognized are *hug*-positive. The majority of cells that anti-Dnc^{RB}-C6 and anti-Dnc^{RJ}-C1 identify overlap, as demonstrated by the fact that anti-Dnc^{RB}-C6 and anti-Dnc^{RJ}-C1 both recognize *hug*-positive cells (Fig. 25, 30).

The second antibody that we have developed to study the localisation of Dnc^{PJ} is anti-Dnc^{PJ}-C4. As shown in Figure 17, this antibody was designed against a polypeptide encoded by the 3rd exon of *dnc^{RJ}*, the same exon encoded by the polypeptide anti-Dnc^{PJ}-C1, but anti-Dnc^{PJ}-C4 was designed against a sequence more C-terminal than anti-Dnc^{PJ}-C1.

We show that anti-Dnc^{PJ}-C4 recognises several clusters in the larval CNS, one cluster in the labium, three clusters in the thoracic region of the VNC and two clusters in the abdominal region of the VNC. The expression pattern is completely different from that of anti-Dnc^{PJ}-C1 (Fig. 31 A, B).

Unlike anti-Dnc^{PJ}-C4, some of the neurons recognised by anti-Dnc^{PJ}-C1 are also recognised by anti-Dnc^{all}. The cluster recognised in the labium corresponds to the LBv cluster, which is also recognised by anti-Dnc^{all}. The clusters in the thoracic segments of the VNC also align with the clusters recognised by anti-Dnc^{all}. They can be identified as T2v, T2d and T3v (Fig. 31 A, B). The cells visualised in the brain and in the abdominal region of the VNC do not colocalise with anti-Dnc^{all}.

Like anti-Dnc^{PJ}-C1 and the Dnc^{PB}-specific antibodies, anti-Dnc^{PJ}-C4 recognises the soma and not the nucleus of the neurons (Fig. 31 C). We performed a competition experiment similar to the one performed with anti-Dnc^{PB}-C6, anti-Dnc^{PB}-C10 and anti-Dnc^{PJ}-C1 by adding the peptide to the antibody during the immunohistochemistry experiment. Adding 10 times the concentration of the antibody to the peptide mostly outcompeted anti-Dnc^{PJ}-C4, 100 times the concentration of the antibody could completely block the binding of the anti-Dnc^{PJ}-C4 antibody to the antigene, confirming that the anti-Dnc^{PJ}-C4 binds in vivo to the polypeptide it was designed against (Fig. 31 D).

In summary, the anti-Dnc^{PJ}-C4 antibody recognises a variety of cells in the *Drosophila* larval CNS, some of which colocalise with anti-Dnc^{all}. It recognises the soma of neurons and a different pattern in the CNS to anti-Dnc^{PJ}-C1.
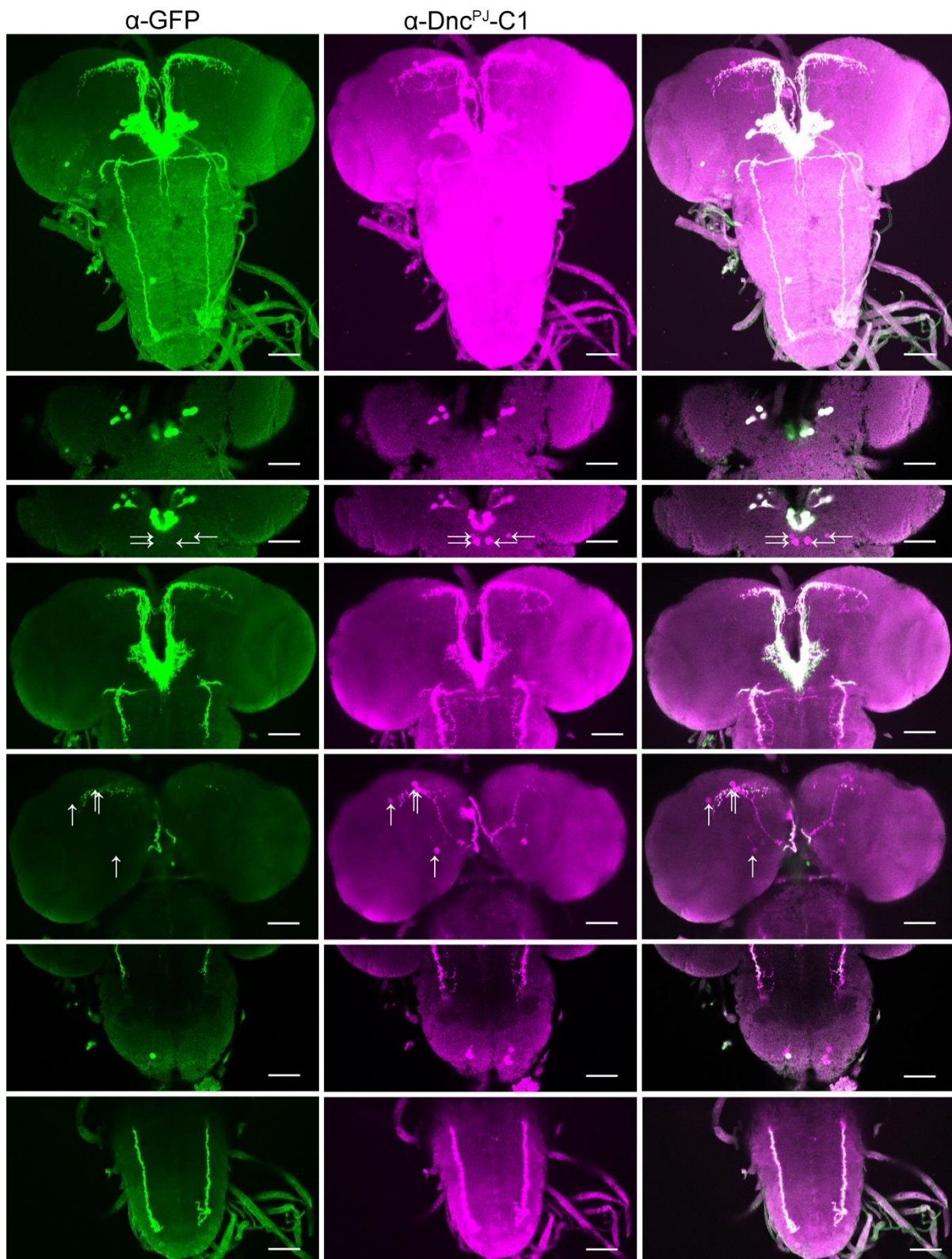
Fig. 30: Anti-Dnc^{PJ}-C1 partially, but not exclusively, recognises neurons targeted by the *hug-Gal4*.
The majority of anti-Dnc^{PJ}-C6-positive neurons are driven by *HugS3-Gal4. UASmCD8::GFP* expressed in the larval CNS under the control of the *HugS3-Gal4* driver, labelled with anti-GFP (green) and anti-Dnc^{PB}-C1 (magenta). The arrows indicate anti-Dnc^{PJ}-C6-positive neurons that are not driven by *HugS3-Gal4*. Full and

partial stacks were scanned at 20x magnification and 1 μm optical section. Scale bars are 50μm.
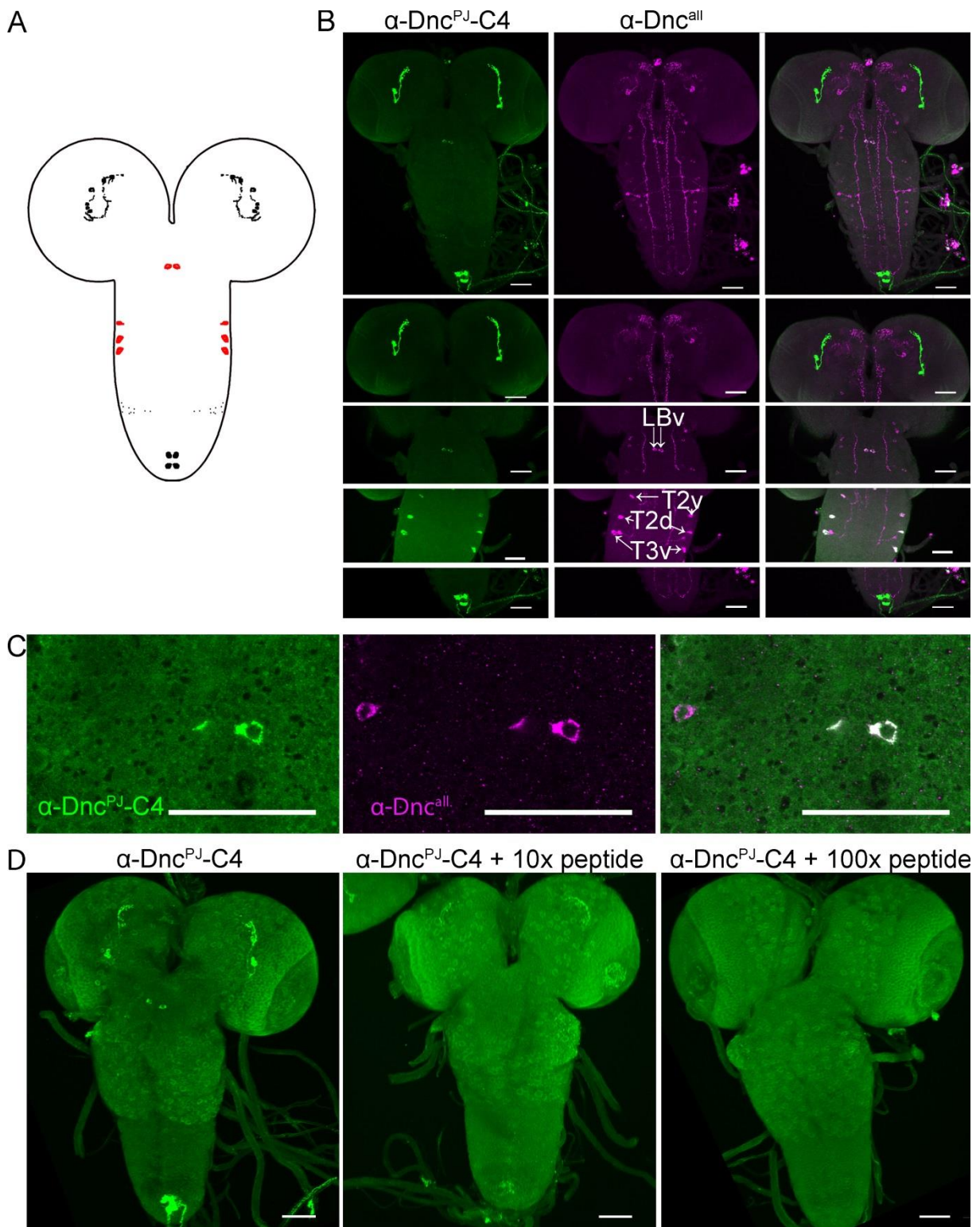
Fig. 31: The putative Dnc^{PJ}-specific anti-Dnc^{PJ}-C4 recognises four clusters that are also recognised by anti-Dnc^{all}.
A: Cartoon of neurons recognised by the anti-Dnc^{PJ}-C4 antibody in the larval CNS. Neurons recognised by both anti-Dnc^{PJ}-C4 and anti-Dnc^{all} are shown in red, neurons recognised uniquely by anti-Dnc^{PJ}-C4 are shown in black. **B**: w^{1118} larval CNS

labelled with anti-Dnc^{PJ}-C4 (green) and anti-Dnc^{all} (magenta). Clusters recognised by both α-Dnc^{all} and anti-Dnc^{PJ}-C4 are labelled according to the nomenclature for anti-Dnc^{all} introduced in Figure 18. **C**: Anti-Dnc^{PJ}-C4 detects regions of the soma of the LBv cluster in w^{1118}. **D**: Recognition of cells by anti-Dnc^{PJ}-C4 is blocked by addition of the peptide to which the antibody was generated. w^{1118} larval CNS labelled with anti-Dnc^{PJ}-C4, and addition of 10x higher concentration of peptide than the antibody and 100x higher concentration than the antibody. **B, D**: Full and partial stacks were scanned at 20x magnification and 1 µm optical section. **C**: Partial stacks were scanned at 63x magnification and 0.33 µm optical section. Scale bars are 50µm.
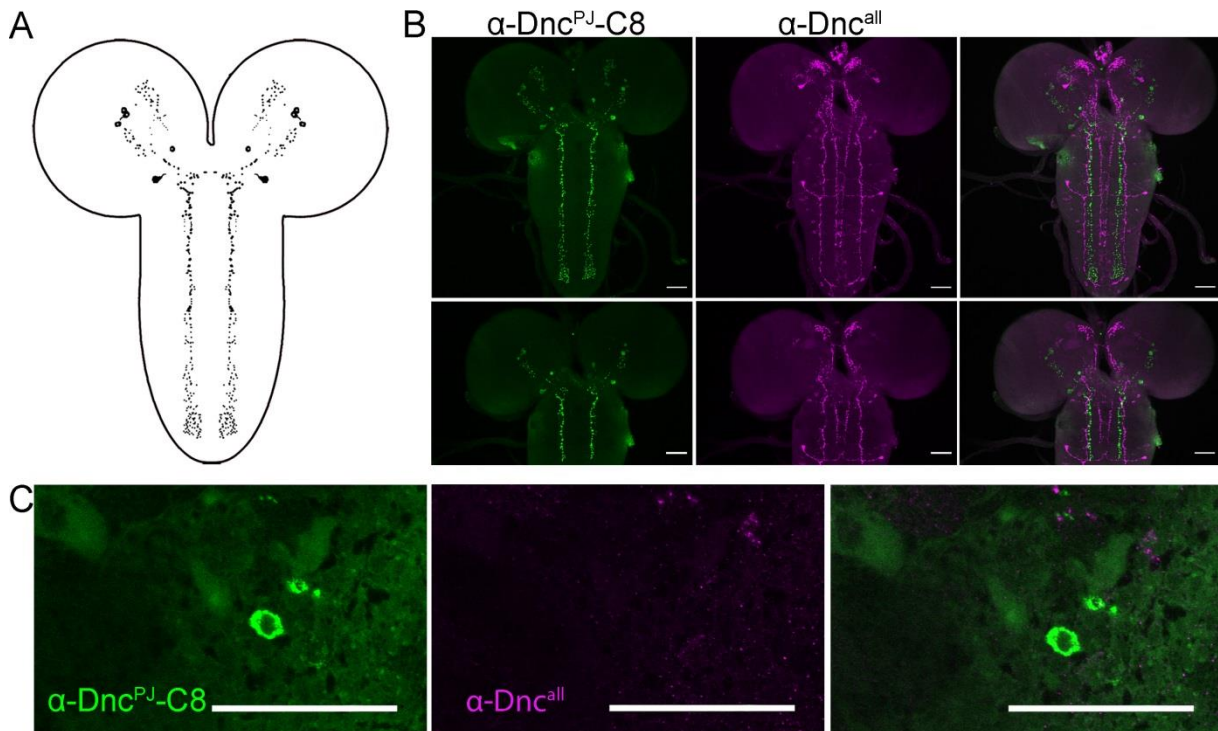
Fig. 32: Putative Dnc^{PJ}-specific anti-Dnc^{PJ}-C8 does not recognise structures detected by anti-Dnc^{all}.
A: Cartoon of neurons recognised by the anti-Dnc^{PJ}-C8 antibody in the larval CNS. **B**: No colocalisations were observed in w^{1118} larval CNS labelled with anti-Dnc^{PJ}-C8 (green) and anti-Dnc^{all} (magenta). **C**: Anti-Dnc^{PJ}-C8 detects regions in the soma **B**: Full and partial stacks were scanned at 20x magnification and 1 µm optical section. **C**: Partial stacks were scanned at 63x magnification and 0.33 µm optical section. Scale bars are 50µm.

To further investigate the localisation of Dnc^{PJ}, we designed a third peptide antibody, anti-Dnc^{PJ}-C8. It was designed against a polypeptide encoded by the 3rd exon of dnc^{RJ}, the same exon that the anti-Dnc^{PJ}-C1 and anti-Dnc^{PJ}-C4 polypeptides were designed against, but further C-terminal (Fig. 17).

Anti-Dnc^{PJ}-C8 recognises several clusters in the *Drosophila* larval brain, but no clusters in the VNC. Instead, it recognises a series of terminal varicosities in the VNC.

Optically, the expression pattern of anti-Dnc^{PJ}-C8 is more similar to that of anti-Dnc^{PB}-C10 than to any of the other antibodies against Dnc^{PJ}. If a colocalising antibody or Gal4-driver line is found in the future, this could be investigated further.

None of the clusters detected colocalise with anti-Dnc^{all} (Fig. 32 A, B). Like anti-Dnc^{all}, but also the other Dnc^{PB} or Dnc^{PJ} specific antibodies, it recognises the soma but not the nucleus of the neurons (Fig. 32 C).
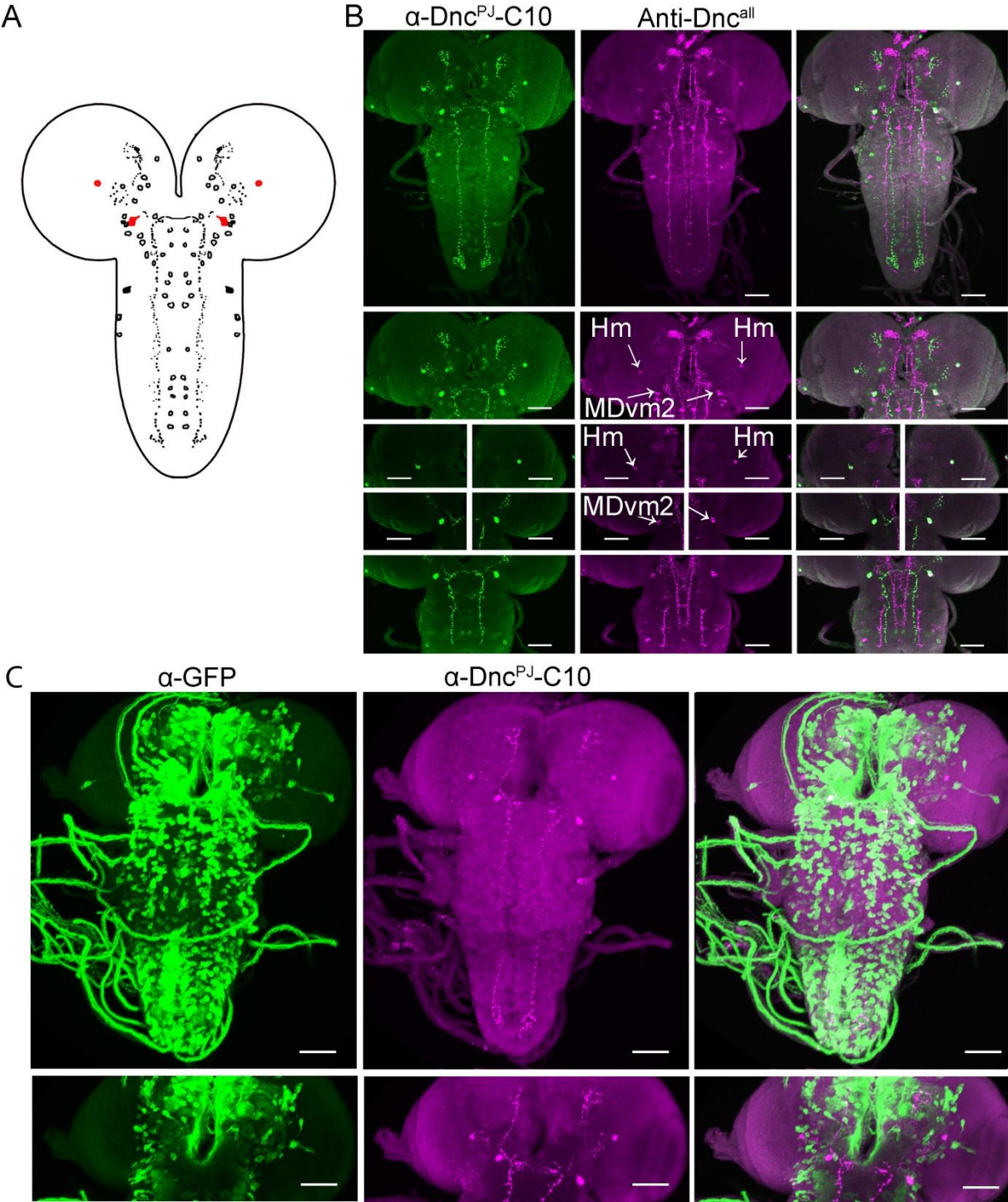
Fig. 33: Putative Dnc^PJ-specific anti-Dnc^PJ-C10 recognises two clusters that are also detected by anti-Dnc^all. It does not recognise glutamatergic neurons.
A: Cartoon of neurons recognised by the anti-Dnc^PJ-C10 antibody in the larval CNS. Neurons recognised by both anti-Dnc^PJ-C10 and anti-Dnc^all are shown in red, neurons recognised uniquely by anti-Dnc^PJ-C10 are shown in black. **B**: Anti-Dnc^all and anti-Dnc^PJ-C10 colocalise in two clusters. w^{1118} larval CNS labelled with anti-Dnc^PJ-C10 (green) and anti-Dnc^all (magenta). Clusters recognised by both α-Dnc^all and anti-Dnc^PJ-C10 are labelled according to the nomenclature for anti-Dnc^all introduced in Figure 18. **C**: The anti-Dnc^PJ-C10 antibody does not recognise glutamatergic neurons. *UASmCD8::GFP* expressed in the larval CNS under the control of the *DV-Glut-Gal4* driver labelled with anti-GFP (green) and anti-Dnc^PJ-C10 (magenta). Full and partial stacks were scanned at 20x magnification and 1 µm optical section. Scale bars are 50µm.

To further investigate the localisation of Dnc^PJ, we designed another peptide antibody, anti-Dnc^PJ-C10. It was designed against the same peptide as the anti-Dnc^PJ-C8 antibody (Fig. 17).

We show that anti-Dnc^PJ-C10 has an expression pattern similar, but not identical, to that of anti-Dnc^PJ-C8. Anti-Dnc^PJ-C10 recognises more clusters throughout the CNS than anti-Dnc^PJ-C8. Two of the clusters also recognised by the anti-Dnc^PJ-C10 are also recognised by anti-Dnc^all, in the hemisphere in the Hm cluster and in the mandibular neuromer in the MDvm2 cluster (Fig. 33 A, B).

Glutamate is one of the major excitatory neurotransmitters in vertebrates and has been described in the larval CNS by Daniels et al (Daniels *et al.*, 2008). They show that glutamate is expressed in a large number of neurons in the VNC, also in the CNS, but not in the MB (Daniels *et al.*, 2008). To analyse whether the anti-Dnc^PJ-C10 recognises glutamatergic neurons, we expressed mCD8::GFP under the control of the glutamatergic driver *DV-Glut-Gal4*. Anti-Dnc^PJ-C10 does not recognise glutamatergic neurons (Fig. 33 C).

In summary, the anti-Dnc^PJ-C10 recognizes multiple clusters throughout the larval CNS, some of which are anti-Dnc^all-positive and none of which are glutamatergic.

To further investigate the localisation of Dnc^PJ, we generated another peptide antibody, anti-Dnc^PJ-C11. It was designed against a peptide that partially overlaps with the peptide against which anti-Dnc^PJ-C8 and anti-Dnc^PJ-C10 were designed (Fig. 17). To investigate its expression, we performed immunohistochemistry using anti-Dnc^all and the anti-Dnc^PJ-C11.

We show that the expresssion pattern of anti-Dnc^PJ-C11 is completely different from anti-Dnc^PJ-C8 and anti-Dnc^PJ-C10, it is similar to anti-Dnc^PJ-C4. It recognises three

clusters in the abdominal region of the VNC and two clusters in the larval brain. Anti-Dnc^{PJ}-C11 does not colocalise with the anti-Dnc^{all} antibody (Fig. 34).
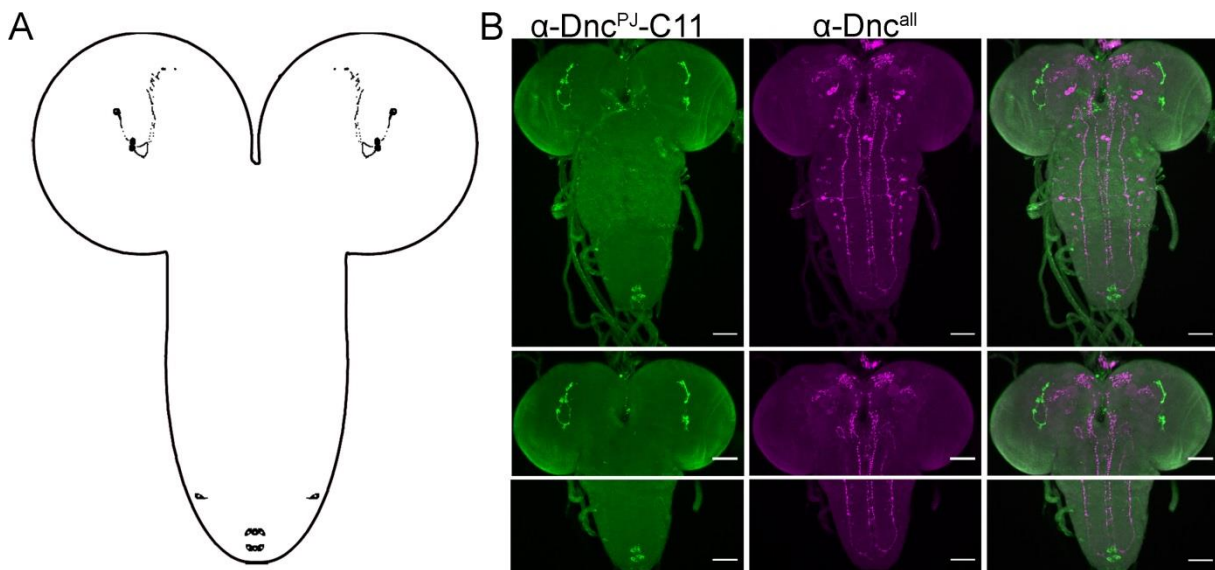

Fig. 34: The putative Dnc^{PJ}-specific anti-Dnc^{PJ}-C11 does not recognise structures detected by anti-Dnc^{all}.
A: Cartoon of neurons recognised by the anti-Dnc^{PJ}-C11 antibody in the larval CNS.
B: No colocalisations were observed in w^{1118} larval CNS labelled with anti-Dnc^{PJ}-C8 (green) and anti-Dnc^{all} (magenta). Full stacks were scanned at 20x magnification and 1 µm optical section, partial stacks were scanned at 40x magnification and 1 µm optical section. Scale bars are 50µm.

In summary, although anti-Dnc^{PJ}-C1, anti-Dnc^{PJ}-C4, anti-Dnc^{PJ}-C8, anti-Dnc^{PJ}-C10 and anti-Dnc^{PJ}-C11 are peptide antibodies designed against sequences encoded by the same exon, anti-Dnc^{PJ}-C8 and anti-Dnc^{PJ}-C10 are raised against the same polypeptide, and for anti-Dnc^{PJ}-C1 and anti-Dnc^{PJ}-C4 we were able to confirm their specificity for the polypeptides, their expression patterns are very different. While anti-Dnc^{PJ}-C4 and anti-Dnc^{PJ}-C10 partially colocalise with anti-Dnc^{all}, anti-Dnc^{PJ}-C1 recognises *hug* neurons and, like anti-Dnc^{PJ}-C8 and anti-Dnc^{PJ}-C11, does not colocalise with anti-Dnc^{all}.

3.3.8 Characterisation of putative peptide antibodies against Dnc^{PG}

To investigate the expression of Dnc^{PG} in the larval CNS, we designed three putative isoform-specific peptide antibodies against polypeptides encoded by the first exon of *dnc^{RG}*. This exon overlaps with the longer 5th exon of *dnc^{RN}*, therefore all antibodies designed against Dnc^{PG} may also bind to Dnc^{PN} (Fig. 17).
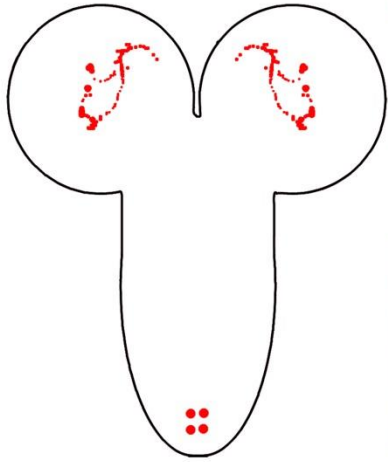
A

B
α-Dnc^PG-C1   α-Dnc^all

Hm

A8m
A9m

C
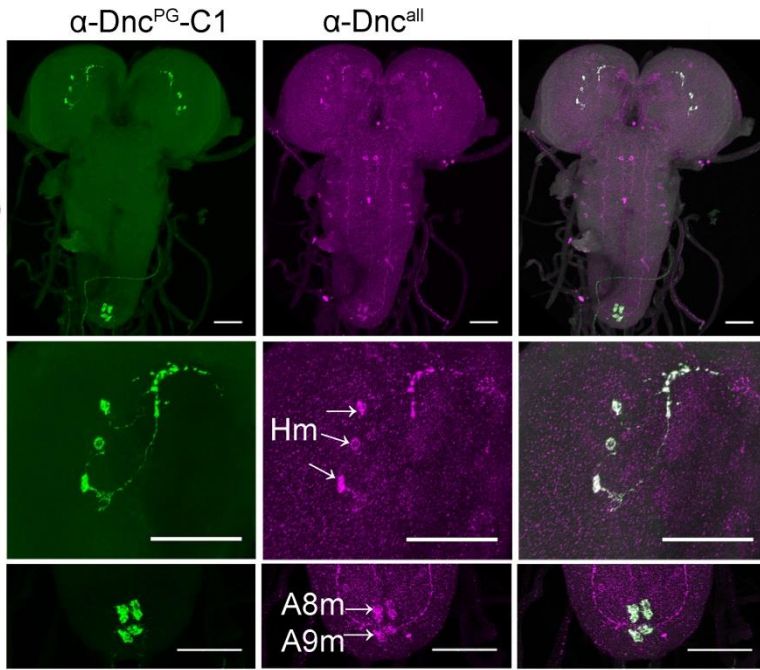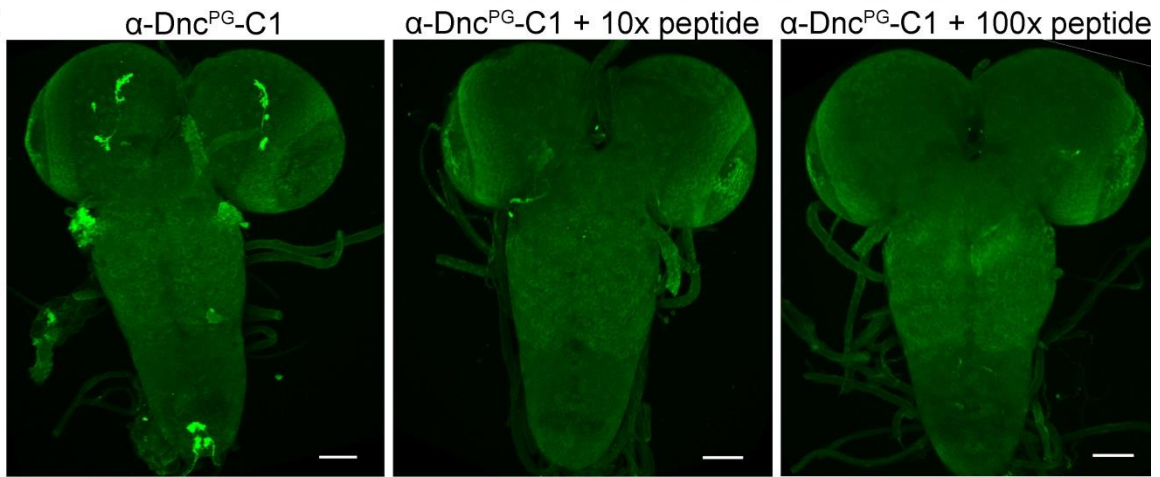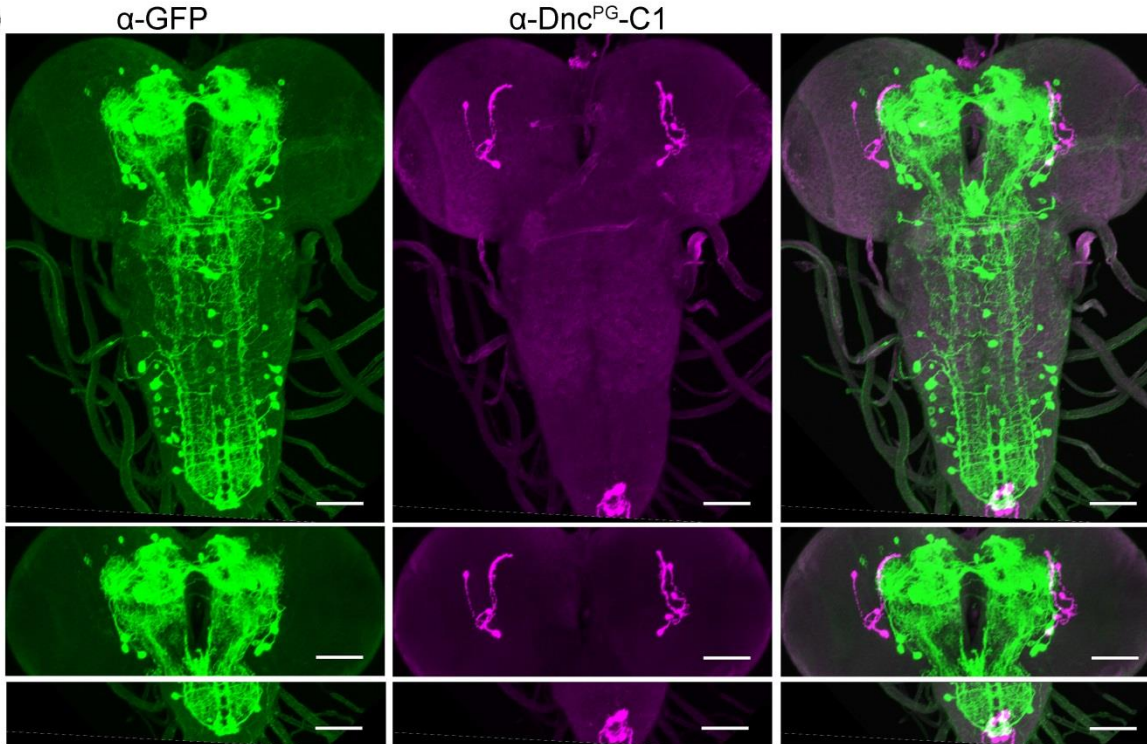α-Dnc^PG-C1   α-Dnc^PG-C1 + 10x peptide   α-Dnc^PG-C1 + 100x peptide

D
α-GFP   α-Dnc^PG-C1

81

Fig. 35: All clusters recognised by the putative Dnc^{PG}-specific anti-Dnc^{PG}-C1 are also recognised by anti-Dnc^{all}. It does not recognise dopaminergic neurons.

A: Cartoon of neurons recognised by the anti-Dnc^{PG}-C1 antibody in the larval CNS. Neurons recognised by both anti-Dnc^{PG}-C1 and anti-Dnc^{all} are shown in red. **B**: w^{1118} larval CNS labelled with anti-Dnc^{PG}-C1 (green) and anti-Dnc^{all} (magenta). Clusters recognised by both α-Dnc^{all} and anti-Dnc^{PG}-C1 are labelled according to the nomenclature for anti-Dnc^{all} introduced in Figure 18. **C**: Recognition of cells by anti-Dnc^{PG}-C1 is blocked by addition of the peptide to which the antibody was generated. w^{1118} larval CNS labelled with anti-Dnc^{PG}-C1 and addition of 10x higher concentration of peptide than the antibody and 100x higher concentration than the antibody. **D**: Anti-Dnc^{PG}-C1 antibody does not recognise dopaminergic neurons. *UASmCD8::GFP* driven by the *TH-Gal4* driver labelled with anti-GFP (green) and anti-Dnc^{PG}-C1 (magenta). Full stacks were scanned at 20x magnification and 1 µm optical section. Partial stacks were scanned at 40x and 63x magnification and 1 and 0.33µm optical section. Scale bars are 50µm. Experiments shown in figure **A** and **B** were conducted by Marie Müller (Bachelor Thesis: Müller, 2021).

The anti-Dnc^{PG}-C1 antibody was developed against a polypeptide encoded by a sequence close to the 5' end of this exon. To study its expression, we performed immunohistochemistry with anti-Dnc^{all} and anti-Dnc^{PG}-C1.

We show that anti-Dnc^{PG}-C1 recognises two clusters in the abdominal region of the VNC and a cluster of three neurons in the brain.

All neurons recognised by anti-Dnc^{PG}-C1 colocalise with the anti-Dnc^{all} antibody. The clusters in the larval brain can be identified as the Hm cluster and the clusters in the abdominal region of the VNC can be identified as the A8m and the A9m cluster (Fig. 35 A, B).

To investigate whether the antibody is specific for the peptide against which it was designed, we performed a competition experiment similar to that performed with anti-Dnc^{PB}-C6, anti-Dnc^{PB}-C10, anti-Dnc^{PJ}-C1 and anti-Dnc^{PJ}-C4 by adding the peptide to the antibody during the immunohistochemistry experiment. The addition of 10 times the concentration of the antibody already outcompetes the binding of the antibody to its antigen in the larval CNS. This confirms that anti-*dnc^{RG}*-C1 is specific for the polypeptide against which it is directed.

As mentioned above, dopaminergic neurons play a role in learning and memory in *Drosophila* larvae (Selcho *et al.*, 2009). We were therefore particularly interested in these neurons. To analyse whether anti-Dnc^{PG}-C1 recognises dopaminergic neurons, we used mCD8::GFP driven by the *TH-Gal4* driver and labelled it using anti-GFP to visualise dopaminergic cells and anti-*Dnc^{PG}*-C1. We show that anti-Dnc^{PG}-C1 does not label dopaminergic neurons, neither in the brain nor in the VNC (Fig. 35 D).

Fig. 36: The putative Dnc^{PG}-specific anti-Dnc^{PG}-C4 does not recognise structures detected by anti-Dnc^{all}. It also does not recognise dopaminergic neurons.

A: Cartoon of neurons recognised by the anti-Dnc^{PG}-C4 antibody in the larval CNS. **B**: No colocalisations were observed in w^{1118} larval CNS labelled with anti-Dnc^{PG}-C4 (green) and anti-Dnc^{all} (magenta). **C**: The anti-Dnc^{PG}-C1 antibody does not recognise dopaminergic neurons. *UASmCD8::GFP* driven by the *TH-Gal4* driver labelled with anti-GFP (green) and anti-Dnc^{PG}-C5 (magenta). Full stacks were scanned at 20x magnification and 1 µm optical section. Partial stacks were scanned at 40x magnification and 1µm optical section. Scale bars are 50µm. Experiments shown in figure **A** and **B** were conducted by Marie Müller (Bachelor Thesis: Müller, 2021).

In summary, anti-Dnc^{PG}-C1 labels clusters in the larval brain and in the VNC that colocalise with anti-Dnc^{all}. The antibody is specific for the peptide against which it was developed and does not label dopaminergic neurons.

To further investigate the localisation of Dnc^{PG}, we developed a second antibody. Anti-Dnc^{PG}-C4 was designed against a polypeptide encoded by a sequence localised further to the 3'-end of the first exon of dnc^{RG} than anti-Dnc^{PG}-C1. This exon overlaps with the 5th exon of dnc^{RN}, giving rise to the possibility that all antibodies designed against Dnc^{PG} may also to bind to Dnc^{PN} (Fig. 17). To study its expression, we performed immunohistochemistry using anti-Dnc^{all} and anti-Dnc^{PG}-C4.

We show that anti-Dnc^{PG}-C4 recognises four clusters, three clusters in the protocerebrum and one cluster in the labium. It also recognises a pattern of terminal varicosities throughout the larval VNC. None of the labelled clusters colocalise with the anti-Dnc^{all} antibody (Fig. 36 A, B).

To analyse whether anti-Dnc^{PG}-C4 recognises dopaminergic neurons, we used mCD8::GFP driven by the *TH-Gal4* driver and labelled with anti-GFP to visualise dopaminergic neurons and anti-Dnc^{PG}-C4. We show that anti-Dnc^{PG}-C4 does not label dopaminergic neurons (Fig. 36 C).

The third putative antibody that we designed to investigate the localisation of Dnc^{PG} was anti-Dnc^{PG}-C5. It was designed against a polypeptide that overlaps with the polypeptide against which anti-Dnc^{PG}-C4 was designed (Fig. 17).

To study its expression, we performed immunohistochemistry using anti-Dnc^{all} and anti-Dnc^{PG}-C5. We show that anti-Dnc^{PG}-C5 recognises four clusters, three clusters in the protocerebrum and one cluster in the labium. It also recognises a pattern of terminal varicosities throughout the larval VNC (Fig. 36 A, B). Thus, its expression pattern is similar to that of anti-Dnc^{PG}-C4.

As with anti-Dnc^{PG}-C4, none of the clusters labelled by anti-Dnc^{PG}-C5 colocalise with the anti-Dnc^{all} antibody (Fig. 37 A and B).

To analyse whether anti-Dnc^{PG}-C5 recognises dopaminergic neurons, we used mCD8::GFP driven by the *TH-Gal4* driver and labelled with anti-GFP to visualise dopaminergic cells and anti-Dnc^{PG}-C5. We show that anti-Dnc^{PG}-C5 does not label dopaminergic neurons (Fig. 37 C).

In summary, we have generated three putative peptide antibodies against Dnc^{PG}. One of these antibodies, anti-Dnc^{RG}-C1, recognises neurons that are also recognised by anti-Dnc^{all}. Anti-Dnc^{RG}-C4 and anti-Dnc^{RG}-C5 show a similar expression pattern

and do not recognise neurons that are recognised by anti-Dnc[all]. None of the antibodies recognise dopaminergic neurons.

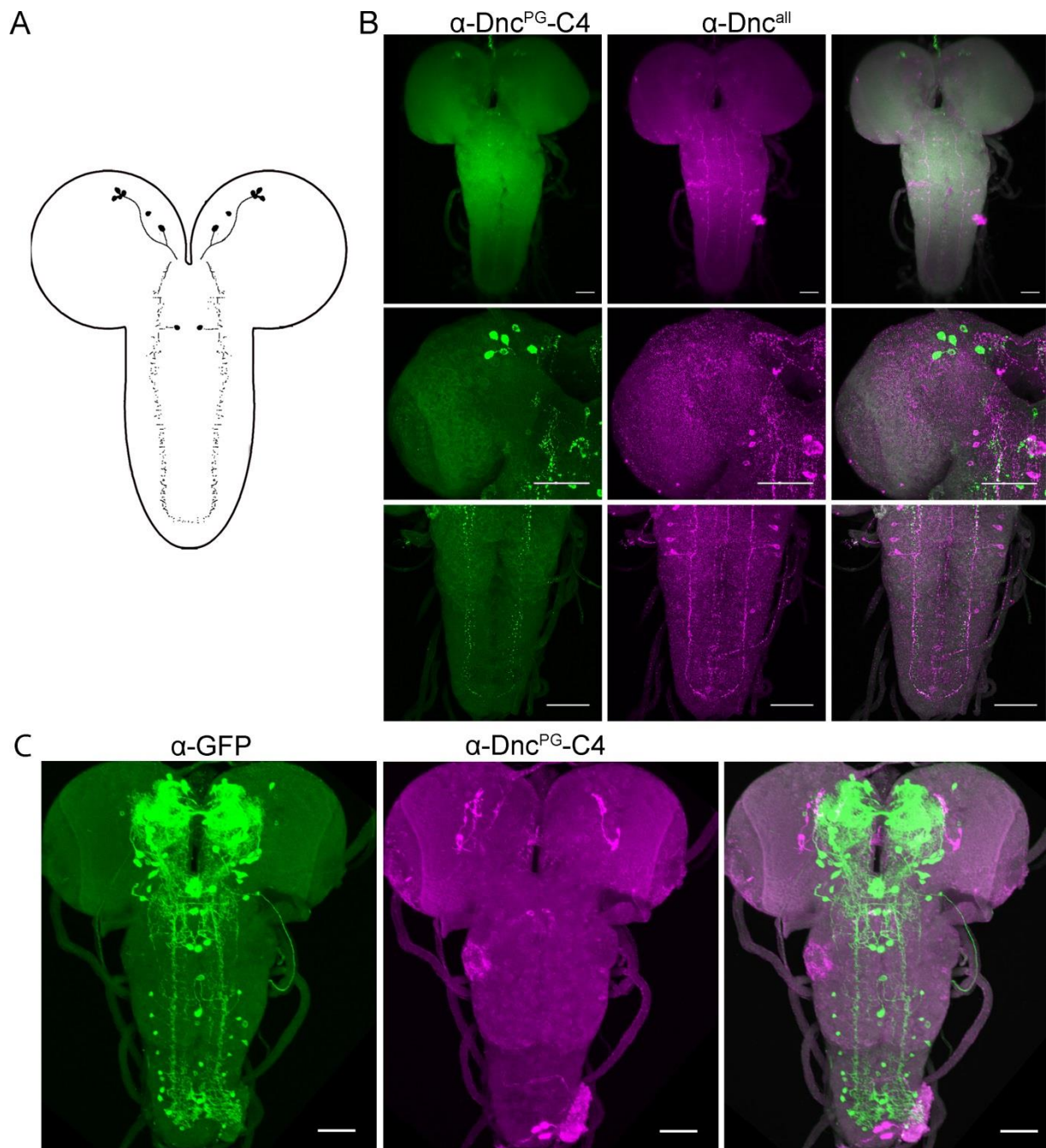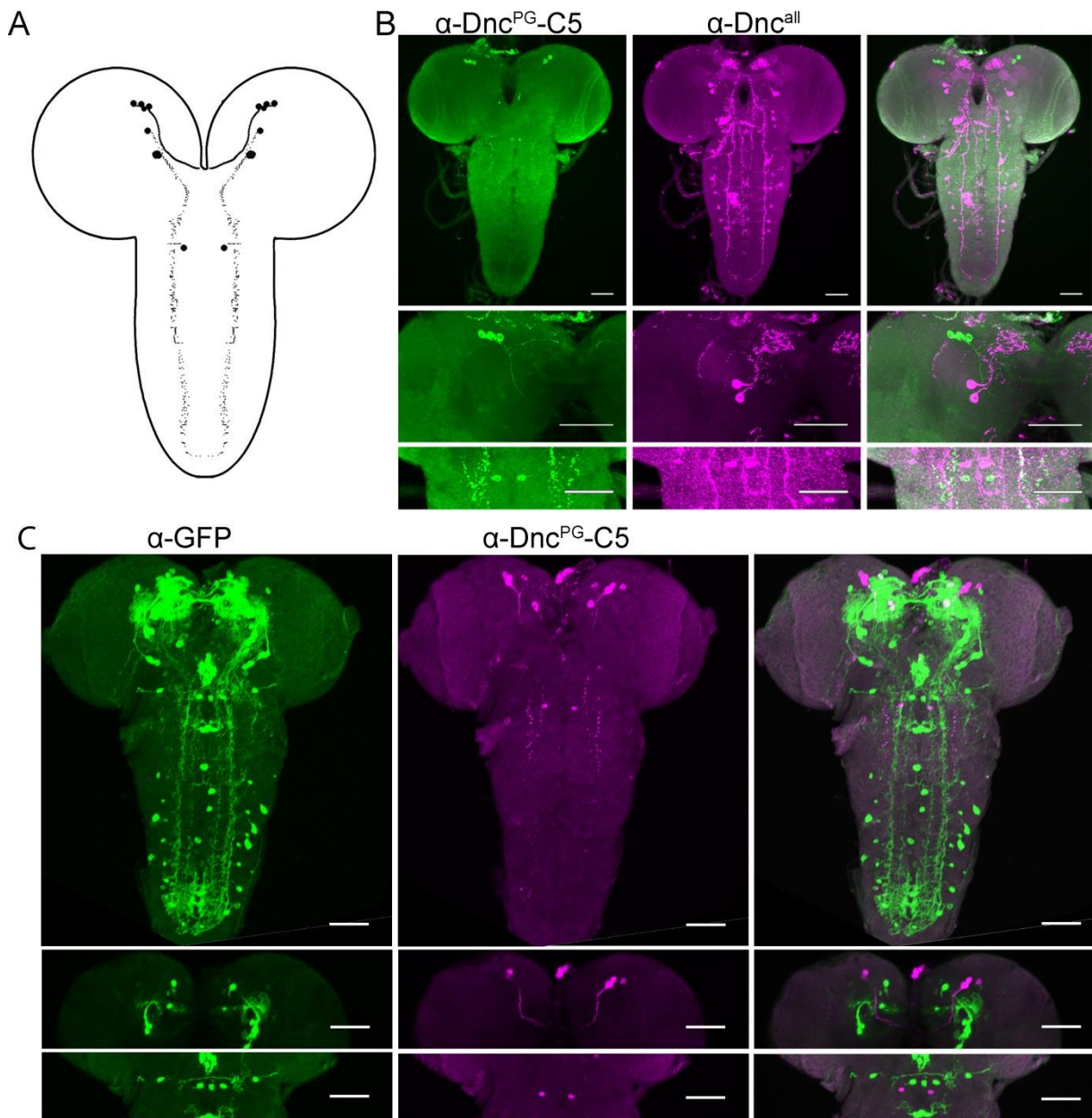**Fig. 37: The putative Dnc[PG]-specific anti-Dnc[PG]-C5 does not recognise structures detected by anti-Dnc[all]. It also does not recognise dopaminergic neurons.**
A: Cartoon of neurons recognised by the anti-Dnc[PG]-C5 antibody in the larval CNS.
B: No colocalisations were observed in *w[1118]* larval CNS labelled with anti-Dnc[PG]-C5 (green) and anti-Dnc[all] (magenta). **C**: Anti-Dnc[PG]-C5 does not recognize dopaminergic neurons. *UASmCD8::GFP* driven by the *TH-Gal4* driver labelled with anti-GFP (green) and anti-Dnc[PG]-C5 (magenta). Full stacks were scanned at 20x magnification and 1 µm optical section. Partial stacks were scanned at 40x magnification and 1 µm optical section. Scale bars are 50 µm. Experiments shown in figure **A** and **B** were conducted by Marie Müller (Bachelor Thesis: Müller, 2021).

3.3.9 Expression pattern of a putative peptide antibody against Dnc[PF]

To investigate the expression of Dnc[PF] in the larval CNS, we designed a putative isoform-specific antibody against a polypeptide encoded by the first exon of *dnc[RF]* (Fig. 17).

We show that the anti-Dnc[PF]-C5 antibody recognises five clusters within the brain and a series of terminal varicosities throughout the VNC. None of the cells identified by the putative anti-Dnc[PF]-C2 antibody overlap with the cells detected by the anti-Dnc[all] antibody (Fig. 38 A and B).
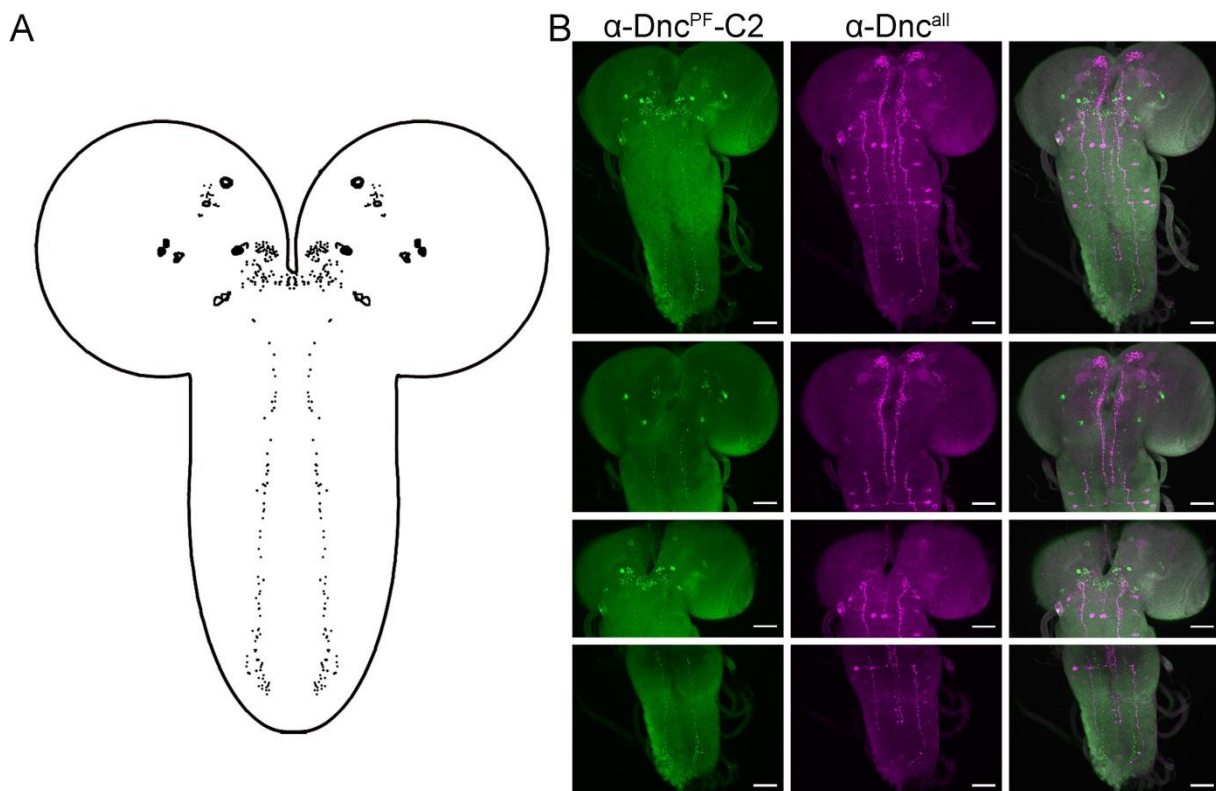
Fig. 38 The putative Dnc[PF]-specific anti-Dnc[PF]-C2 does not recognise structures detected by anti-Dnc[all].
A: Cartoon of neurons recognised by the anti-Dnc[PF]-C2 antibody in the larval CNS.
B: No colocalisations were observed *w[1118]* larval CNS labelled with anti-Dnc[PG]-C5 (green) and anti-Dnc[all] (magenta). Stacks were scanned at 20x magnification and 1 µm optical section. Scale bars are 50 µm.

3.3.10 Summary of the characterisation of putative Dunce isoform-specific antibodies

α-Dnc^PG^-C5

α-Dnc^PG^-C4

α-Dnc^PG^-C1

α-Dnc^PB^-C6

α-Dnc^PB^-C10

α-Dnc^all^

RB
RJa
RJb
RA
RN
RG
RF

— 500bp

— Exons targeted by antibody

— untranslated region

— coding sequence

α-Dnc^PJ^-C1

α-Dnc^PJ^-C4

α-Dnc^PJ^-C8

α-Dnc^PF^-C2

α-Dnc^PJ^-C11

α-Dnc^PJ^-C10

Fig. 39: Antibody design for anti-Dnc^{all} and putative Dnc isoform-specific antibodies and expression patterns in the larval CNS.
Antibody design of the different putative isoform-specific antibodies and of anti-Dnc^{all} as shown in Figure 17. Cartoon of neurons recognised by the different isoform-specific antibodies and of anti-Dnc^{all} in the larval CNS. Neurons recognised by both isoform-specific antibodies and anti-Dnc^{all} are shown in red. w^{1118} larval CNS labelled with anti-Dnc^{all} or putative isoform-specific antibodies (green). As in Figure 17, the scheme of Dnc isoforms was adapted from Ruppert, Franz et al. (2017). The cartoons and scans are adapted from Fig. 18, 24, 27, 29, 31, 32, 33, 35, 36, 37, 38.

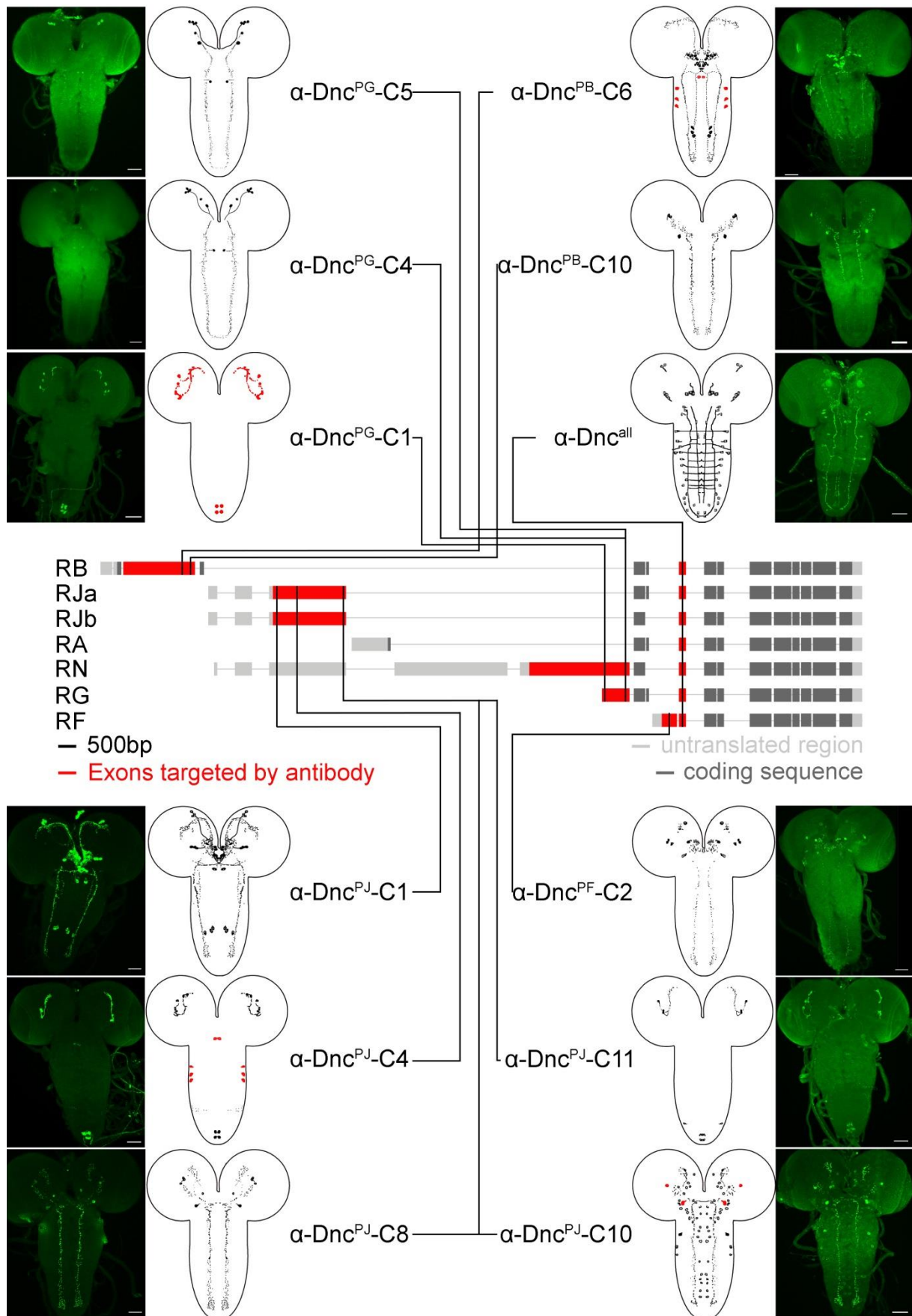In the previous chapters we showed that we were able to generate putative peptide antibodies against four different Dnc isoforms, Dnc^{PB}, Dnc^{PJ}, Dnc^{PG} and Dnc^{PF}. For all these isoforms, we used the same strategy: we chose an exon specific for one or, in the case of Dnc^{PG}, two isoforms and had the company Abmart generate antibodies against polypeptides encoded by these exons (Fig. 17, 39). To confirm the specificity of the antibodies for the polypeptide against which they were designed, we chose a competition assay by adding an excess of the polypeptide to the antibody solution. Using this method, we were able to confirm antibodies against three of the isoforms studied, namely anti-Dnc^{RB}-C6, anti-Dnc^{RB}-C10, anti-Dnc^{RJ}-C1, anti-Dnc^{RJ}-C4 and anti-Dnc^{RG}-C1.

Another antibody previously developed in our group is the polyclonal anti-Dnc^{all} antibody, which was designed to bind to two polypeptides encoded by the first exon common to all Dnc isoforms except for dnc^{RL}. In this project we were able to characterise its expression pattern in the larval CNS (Fig. 18) and confirm by western blot that it recognises Dnc (Fig. 19). Although anti-Dnc^{RB}-C6, anti-Dnc^{RJ}-C4, Dnc^{RJ}-C10 and anti-Dnc^{RG}-C1 recognise neurons that are also recognised by anti-Dnc^{all}, anti-Dnc^{RB}-C10, anti-Dnc^{RJ}-C1, anti-Dnc^{RJ}-C8, anti-Dnc^{RJ}-C11, anti-Dnc^{RG}-C4, anti-Dnc^{RG}-C5 and anti-Dnc^{RF}-C2 do not recognise neurons that are recognised by anti-Dnc^{all} (Fig. 39).

Anti-Dnc^{RB}-C6 and anti-Dnc^{RJ}-C1 recognise *hug* neurons (Fig. 25, 30), anti-Dnc^{RB}-C6 also recognises TβH-positive neurons (Fig. 26). Interestingly, the different putative isoform-specific antibodies show a wide variety of expression patterns, even antibodies that recognise the same isoform or even the same or overlapping polypeptides. For some antibodies, such as anti-Dnc^{RB}-C6 and anti-Dnc^{RJ}-C1, the similarities to an antibody recognising a different isoform appear to be larger than to different antibodies recognising the same isoform (Fig. 39). This shows that more factors than just isoforms need to be considered when studying Dnc.

4 Discussion

The aim of this project is to investigate the role of Dnc isoforms and their localisation in memory formation. To date, Dnc is considered to be a PDE which plays a defined role in memory: Dnc mutants are unable to perform STM (Widmann *et al.*, 2016). Here, we show that Dnc is more than that. We show that Dnc isoforms have specific functions in learning and memory. dnc^{RA}-deficient $dnc^{\Delta143}$ and dnc^{RB}-deficient dnc^{EP1395} have the opposite phenotype to dnc^1, showing improved memory.

We have shown that somatic expression in dnc^{RA}-specific neurons is necessary to restore the wild-type memory phenotype in Dnc^{PA}-deficient larvae. Expression of two different Dnc isoforms in these neurons, with different subcellular localisation, can restore the control memory phenotype. Overexpression of Dnc^{PA} in these cells has no effect on memory performance.

We characterised the cells in which the Dnc activity is required to restore the control memory phenotype. These include a cluster of neurons that project into the AL.

We also developed several antibodies against sequences encoded by exons unique to one isoform or shared by several isoforms. The expression patterns differed greatly from each other, between isoforms and even between antibodies against the same isoform, showing that there is a strong difference between isoforms and even between proteins of the same isoform.

These results show that the Dnc PDE should always be considered at the isoform level, and also at the cellular and subcellular level, rather than as a single PDE that influences PDE activity and with that the cAMP concentration throughout the entire animal.

4.1 The role of different Dunce isoforms in memory mutants

4.1.1 Odorant choice is crucial for reproducible learning and memory experiments in Drosophila larvae.

Although the general trend that dnc^1 performs worse than the control in memory experiments remains unchanged, it is clear that Widmann et al. (2016) show significantly worse memory performance after one training cycle for dnc^1, but not after three training cycles, whereas we show significantly worse memory performance after three training cycles (Fig. 4). To show that this is due to the pair of odorants used, we reproduced their results using the same odorants as them, BA and AM (Fig. 6).

Olfactory memory in *Drosophila* larvae is concentration dependent (Mishra *et al.*, 2013). In general, low concentrations of an odorant activate few ORNs and higher concentrations activate multiple ORNs (Si *et al.*, 2019). EA is recognised by the Or42b receptor and at higher concentrations is also recognised by Or42a. AM, the odorant used in both paradigms, initially activates Or35a, Or85c and Or45a and at higher concentrations activates a variety of ORNs including Or24a. BA activates Or45b and Or24a at a low odorant concentration. At higher concentrations, it also activates Or30a and Or35a (Si *et al.*, 2019).

A likely explanation for why the AM/BA odorant pair requires fewer repetitions than the AM/EA pair is that the higher concentration of BA used elicits a greater number of ORNs to respond than the lower concentration of EA, resulting in a higher memory response and thus fewer training cycles required.

This highlights the importance of carefully selecting the odorant for learning and memory experiments in *Drosophila melanogaster* larvae. As AM/EA are more similar in concentration to each other than AM/BA and do not activate the same ORNs, this odorant pair is the better choice for larval olfactory memory experiments.

4.1.2 The dnc^1 memory phenotype is not caused by Dnc^{PA} or Dnc^{PB}.

Although *dnc^1* is considered the typical mutant for STM formation in *Drosophila* larvae (Widmann *et al.*, 2016), previous publications show that this mutant has altered expression of several *dnc* isoforms, with *dnc^{RA}* and *dnc^{RB}* being examples of two of these isoforms (Fig. 3 A) (Ruppert, Franz *et al.*, 2017). The hypothesis that the reduction in *dnc^{RA}* expression is the reason for the STM phenotype of *dnc^1* has been thoroughly investigated in this work. By showing that *dnc$^{\Delta 143}$* has the opposite memory phenotype of *dnc^1*, and thus an improved STM (Fig. 4 A, B), and that reintroduction of Dnc PDE into Dnc^{PA}- positive neurons restores the memory to wild-type levels in *dnc$^{\Delta 143}$* (Fig. 4 C), but not in *dnc^1* (Fig. 7), we can conclude that it is not the reduced expression of Dnc^{PA} that causes the reduced STM phenotype of *dnc^1*.

Like *dnc^{RA}*, *dnc^{RB}* is also reduced in *dnc^1* (Fig. 3 A) (Ruppert, Franz *et al.*, 2017). We established *dnc^{EP1395}* as a Dnc^{PB}-specific mutant (Fig. 14). Like Dnc^{PA}, Dnc^{PB} has an inhibitory effect on the formation of associative aversive memory (Fig. 15). However, further experiments are needed to determine where and how this isoform affects memory in *Drosophila* larvae. To confirm that the memory phenotype of *dnc^{EP1395}* is caused by the reduction of Dnc^{PB}, the memory phenotype of *dnc^{EP1395}* needs to be restored by expressing *dnc^{RB}* in *dnc^{RB}*-specific neurons. Similar to the experiments

we performed to dissect the memory phenotype of $dnc^{\Delta 143}$, a series of decay, extinction, and reversal experiments like those performed for $dnc^{\Delta 143}$ (Fig. 9) should be performed in the future. Future cold shock experiments could further dissect the long-term components of the memory phenotype. To investigate the spatial component of Dnc^{PB}, several experiments expressing a Dnc^{PB} transgene under the control of driver lines and comparison with the expression pattern of the Dnc^{PB}-specific antibodies would be required.

Although some experiments can be peformed to further investigate the memory phenotype, our results narrow down the dnc^1 memory phenotype to the isoforms dnc^{RJ}, significantly reduced in dnc^1, or dnc^{RG}/dnc^{RN}, significantly increased in dnc^1 (Ruppert, Franz *et al.*, 2017). These findings illustrate that Dnc should not be considered a PDE whose mutants lead to specific phenotypes such as defective STM. Instead, Dnc should be considered a collection of isoforms with specific functions.

4.1.3 Memory phenotype of $dnc^{\Delta 143}$

The possible explanations for an improved memory phenotype in $dnc^{\Delta 143}$ are improved associative memory formation or reduced habituation. Habituation leads to a reduced response to a stimulus with repeated exposure. If there was a lack of habituation or even sensitisation in $dnc^{\Delta 143}$, there would be a significant difference between w^{1118} and $dnc^{\Delta 143}$ not only in the one-cycle but especially in the three-cycle associative aversive memory experiment. The repeated exposure in the three-cycle experiment would lead to habituation in w^{1118} and a significant difference to $dnc^{\Delta 143}$ which would be even more pronounced than in the one-cycle aversive memory experiment. This is not the case (Fig. 4 A, B). Therefore, associative memory formation is enhanced in $dnc^{\Delta 143}$.

For the extinction and reversal experiment, the exact mechanism in larvae has not yet been shown (Lesar *et al.*, 2021; Mancini *et al.*, 2019). We suggest a similar mechanism as in adults where an appetitive memory is formed alongside the aversive memory (Felsenberg *et al.*, 2018). In the extinction and reversal experiment (Fig. 9), we observed that the memory formed was significantly altered by the appetitive memory formed (Fig. 9). This indicates that not only the aversive memory, but also the appetitive memory is enhanced in $dnc^{\Delta 143}$. According to the prediction error theory, memory is formed after the first presentation of the stimulus and then the error is minimised with repetitions (Rescorla and Wagner, 1972; review: Cognigni

et al., 2018).This mechanism is defective in *dnc$^{\Delta 143}$*. Therefore, Dnc^{PA} is required to inhibit premature memory formation and plays a role in determining the relevance of incoming information.

Further experiments will be needed to determine which forms of memory other than STM are affected in *dnc$^{\Delta 143}$*. Decay experiments with different time frames could be used to investigate the learning curve of *dnc$^{\Delta 143}$*. Cycloheximide could be used to study the effect on LTM, cold shock to study the effect on ARM.

4.2 Expression of different isoforms in the central nervous system

4.2.1 Dunce is a highly complex and highly modified protein.

In this project, we used several antibodies to investigate in which neurons different Dnc isoforms are localised.

The putative antibodies designed against Dnc^{PB}, Dnc^{PJ}, Dnc^{PG} and Dnc^{PF} detect different expression patterns in the larval CNS, even within an isoform, antibodies against overlapping polypeptides and antibodies against the same polypeptide. We were able to confirm that most of the isoform-specific antibodies bind the polypeptide against which they were designed (Fig. 24, 27, 29, 21, 35). The method we used, the competition of binding to the antigen by adding the polypeptide against which it was designed, confirms for several of the peptide antibodies that they recognise their antigen in its natural configuration (Skliris *et al.*, 2009; review: Bordeaux *et al.*, 2010). There are two possible explanations for the different expression patterns. One is that there is a large number of unannotated Dnc isoforms that are recognized by the antibodies.

However, the second explanation is much more likely. The structure and complexation of the Dnc PDE makes the antigen accessible only in some of the neurons in which it is expressed. Dnc has the potential to bind cAMP, be phosphorylated (Houslay *et al.*, 2017; MacKenzie *et al.*, 2000) and form multimers and complexes with AKAPs (Baillie and Houslay, 2005; Dodge *et al.*, 2001; Richter and Conti, 2004, 2002; Taskén *et al.*, 2001; Xie *et al.*, 2014). Monoclonal antibodies bind specifically to a single epitope (review: Nelson, 2000). These antibodies are highly susceptible to small structural changes that inhibit access to the antigen in an epitope, thereby eliminating all staining. As a result, isoform-specific monoclonal antibodies only bind to a subpopulation of cells that express that isoform. Antibodies designed against the same polypeptide may bind to the same antigene, but because

they are monoclonal, they do so with different kinetics, recognising their isoforms only with no or very small conformational changes.

Polyclonal peptide antibodies also reveal the complexity of Dnc. In the larval CNS, an anti-Dnc antibody by Nighorn et al recognises the MB with no difference between the lobes and, at a much lower level, the rest of the neuropil and in cell bodies near the MB (Nighorn *et al.*, 1991).

Like the antibody by Nighorn et al (1991), the anti-Dnc[all] antibody also recognises the MB (Fig. 18). However, we did not observe the other neuropil structures observed by Nighorn et al (Nighorn *et al.*, 1991). This may be due to differences in the antibody or to a difference in imaging technique, with modern confocal microscopes picking up smallest signals at a high resolution and resolving a diffuse signal across the neuropil to individual neurons and varicosities, or to the antibodies recognising different isoforms or even only a sub-population of complexes formed by these isoforms.

Our anti-Dnc[all] antibody and the antibody designed and used by Nighorn et al are both polyclonal and raised in rabbits against polypeptide sequences, but with a different strategy (Nighorn *et al.*, 1991). The antibody used by Nighorn et al was designed against a polypeptide translated from a 264 bp fragment in the region highly conserved between several PDEs (Bolger *et al.*, 1993; Nighorn *et al.*, 1991). It can be localised C-terminal to the PDE domain (The UniProt Consortium, 2021), while the anti-Dnc[all] antibody was raised against two polypeptides encoded by the same exon. It is localised 5' of the exon that encodes the PDE domain and is the first exon highly conserved between isoforms (Fig. 18). This exon also encodes part of UCR1 (Bolger *et al.*, 1993).

Using a western blot, we confirmed that the antibody binds to Dnc[PB] with all its post-translational modifications (Fig. 19), whereas Nighorn et al. only confirmed that it recognises the unmodified polypeptide (Nighorn *et al.*, 1991). As the western blot uses SDS and therefore completely denatures the protein, this does not guarantee that the antibody recognises the correctly folded protein in complex with interaction partners in its natural environment (review: Bordeaux *et al.*, 2010). We were able to show that the antibody recognises several neurons in the CNS, confirming that anti-Dnc[all] at least partially recognises the protein against which it was designed (Fig. 18). No colocalisation of the anti-Dnc[all] antibody with cells driven by the *dnc[RA]-Gal4* line was observed (Fig. 20). Although in a colocalisation with Dnc[PB] specific antibodies only some of the cells recognised by anti-Dnc[all] are also recognised by the isoform-

93

specific antibodies (Fig. 24, 27), the western blot shows that anti-Dnc[all] recognises Dnc[PB] (Fig. 19), demonstrating the influence of the tertiary structure formed.

In the western blot, the difference between the calculated molecular weight of Dnc[PB]::GFP and the observed band indicates a strong post-translational modification. Several phosphorylation sites for Dnc[PB] have been published in iProteinDB (Hu *et al.*, 2019). Phosphorylation of proteins can cause a significant change in their reported size in a western blot analysis due to altered binding to sodium dodecyl sulfonate (Lee *et al.*, 2013).

PDEs also have the potential to bind cAMP, to form homo- and heteromultimers and complexes with AKAPs (Baillie and Houslay, 2005; Dodge *et al.*, 2001; Houslay *et al.*, 2017; MacKenzie *et al.*, 2000; Richter and Conti, 2004, 2002; Taskén *et al.*, 2001; Xie *et al.*, 2014). Post-translational modification has been shown to mask antigens in mice (Chen *et al.*, 1999). The interaction of the antibody with Dnc is a protein-protein interaction. The same also applies for complexes like multimeres. This kind of interaction depends on interface size and hydrophobicity and is selected by the binding constant (review: Jones and Thornton, 1996). If the other interactions are stronger or the structure of the protein inhibits accessibility for the antibody, it is possible that the anti-Dnc[all] antibody only recognises some of the cells with specific isoforms or complexes, but not all of the isoforms or complexes. This explains why anti-Dnc[all] only partially overlaps with Dnc[PB]-specific antibodies, although the western blot shows that anti-Dnc[all] recognises Dnc[PB].

The same limitation also applies to the antibody used by Nighorn et al, as it was developed using a similar strategy (Nighorn *et al.*, 1991). Since Nighorn et al found clear differences between the MB lobes in the adult fly; an interesting follow-up experiment is the characterisation of the anti-Dnc[all] antibody in the adult fly.

In summary, Dnc is a highly complex and highly modified protein. Our experiments show that antibodies only partially recognise the expression of the isoforms in a physiological setting. The expression pattern of the anti-Dnc[all] antibody partially overlaps with previous findings with a putative antibody by Nighorn et al (Nighorn *et al.*, 1991).

4.2.2 Neurons driven by the *dnc[RA]* promotor are important for learning and memory.

As *dnc[Δ143]* is one of the isoform-specific mutants with improved memory, we are particularly interested in the localisation of Dnc[PA] (Fig. 4). Dnc[PA] is expressed in 21

clusters throughout the CNS (Fig. 10). In the *Drosophila* larval CNS, it is the AL, the MB and the lateral horn that are most important for memory formation (Chu-Wang and Axtell, 1971; Gerber *et al.*, 2004; Tanaka *et al.*, 2012). None of the clusters driven by the dnc^{RA} promoter are expressed in the vicinity of the lateral horn (Fig. 10). The Hd3 cluster, localised close to the MB, does not come into contact with it (Fig. 10 C), which means that the Hd3 cluster is neither a Kenyon cell nor an input or output neuron, and thus it is highly unlikely that this neuron has an influence on the memory performance of the larva. Therefore, the cluster that is most likely to have an influence on the performance of the olfactory memory is the Hv cluster. It projects to the AL (Fig. 10 D).

There are several types of neurons in the antennal lobe. The olfactory signal travels from the dorsal organ to the AL via the ORNs and is transmitted to the projection neurons that connect the AL to the MB (Ramaekers *et al.*, 2005). The local interneurons have arborizations that cover the entire AL thereby identifying the Hv cluster as a local interneuron (Ramaekers *et al.*, 2005). It has been hypothesized that they cause a transformation of the signal from the ORNs (Ramaekers *et al.*, 2005). Although Figure 10 clearly shows that the Hv cluster contains neurons projecting to the AL, it remains to be investigated whether these neurons are the cause of the $dnc^{\Delta 143}$ memory phenotype. Therefore, a possible future experiment would be their colocalisation with common neurotransmitter systems and in case of a colocalisation the expression of the dnc^{RNAi} line in that neurotransmitter system.

Expression in the Hv cluster provides a possible mechanism by which it affects memory formation. In *Drosophila* larvae, it has been shown that habituation is not caused by changes in sensory neurons such as receptor adaptation, but by central synaptic mechanisms localised in the AL that require the activity of local interneurons (Larkin *et al.*, 2010). Therefore, at first glance, the importance of the Hv cluster, a local interneuron at the AL, suggests that the mutation affects habituation rather than associative memory. However, we show that it is associative memory formation that is improved in $dnc^{\Delta 143}$ (Fig.9). In adult flies, associative memory has been shown to take place in the MB. Protocerebral anterior medial (PAM) DANs signal a positive reward, protocerebral posterior lateral 1 (PPL1) DANs signal a negative reward, projection neurons signal the olfactory stimulus (Claridge-Chang *et al.*, 2009; Liu *et al.*, 2012). Additional feedback between DANs and MBONs allows for re-evaluation of the memory (Eschbach *et al.*, 2020; Felsenberg *et al.*, 2018, 2017; Mohamed *et al.*,

2023; Springer and Nawrot, 2021). However, the earliest associative memory has been shown to form in the adult *Drosophila* AL by altering olfactory representation (Yu *et al.*, 2004). This requires the US to be transmitted to the AL, possibly by local interneurons (Yu *et al.*, 2004). In Dnc^{PA}-deficient *dnc$^{\Delta143}$* larvae, the PDE in the soma of the Hv cluster, the local interneuron that transmits the US to the AL is defective, thereby amplifying early memory in the AL and transmitting an altered signal to the MB. This hypothesis provides a plausible explanation for the memory phenotype of *dnc$^{\Delta143}$* (Fig. 4). Since memory in the MB is formed prediction-based and is then constantly re-evaluated (Rescorla and Wagner, 1972; review: Cognigni *et al.*, 2018), the altered odorant representation plays a role after one training cycle, but not after three cycles, as the larva has had time to reassess the value of the odorant. Given the improvement in early memory formation in *dnc$^{\Delta143}$*, the role of Dnc^{PA} can be summarised as inhibition of premature memory formation.

4.2.3 The antibodies against Dnc^{PB} detect antigens in neurons that may be associated with olfactory learning.

dnc^{EP1395} is the other isoform we show to have an improved memory phenotype, making us particularly interested also in the localisation of Dnc^{PB} (Fig. 4, 16). For this isoform, we were able to design two monoclonal antibodies against peptides encoded by a unique exon. They show two different expression patterns, visualising cells that may play a role in STM (Fig. 19). Anti-Dnc^{PB}-C6 and anti-Dnc^{PB}-C10 are putative antibodies against Dnc^{PB}, each recognising only a subpopulation of Dnc^{PB}-positive cells.

The anti-Dnc^{PB}-C6 antibody recognises cells of which the majority is driven by *HugS3-Gal4* line (Fig. 25). *hug*-expressing neurons have been shown to be the central relay for gustatory information, projecting to key organs regulating feeding and growth and to higher brain centres (Melcher and Pankratz, 2005). This makes these neurons candidates for a role in Dnc^{PB} function in memory.

Anti-*dnc^{RB}*-C6 also partially colocalises with anti-TβH, an antibody directed against octopaminergic neurons. In larvae, these neurons have been shown to modulate locomotion (Selcho *et al.*, 2012). In adult Drosophila, Berger et al recently published a preprint showing that octopaminergic neurons integrate internal energy storage into memory formation (Berger *et al.*, 2023). These neurons therefore are additional candidates through which Dnc^{PB} may influence memory formation. To further verify which neurons are responsible for the *dnc^{EP1395}* memory phenotype, an interesting

follow-up experiment would be to express the *dnc^RNAi* line in the *dnc^RB-Gal4* driver line and the *HugS3-Gal4* driver line in memory experiments and compare the memory phenotypes with *dnc^EP1395*.

4.3 Subcellular localisation of Dunce isoforms

4.3.1 The Dunce isoforms are subcellularly differentially localised within the neuron.

Maiellaro et al showed the importance of PDE activity on subcellular cAMP concentration (Maiellaro *et al.*, 2016). Within the neuron, three signalling compartments have been identified: the cell body, the axon and the bouton (Maiellaro *et al.*, 2016). In mice, it has recently been shown that PDE4D5, a homologue of Dnc that is localised in the nucleus, down-regulates cAMP in the nucleus and thereby inhibits the consolidation of memory (Martinez *et al.*, 2023). There the externalization of the PDE prolongs the nuclear cAMP signal and facilitates LTM formation (Martinez *et al.*, 2023). Although similar results have not yet been found in *Drosophila*, it has been proposed that differently localised Dnc isoforms influence aversive memory through spatial regulation of cAMP dynamics (Gervasi *et al.*, 2010). As the differential subcellular localisation of different Dnc isoforms in *Drosophila* was previously only shown in ovaries (Ruppert, Franz *et al.*, 2017), we were able to show that this is also the case in neurons (Fig. 12 A, B).

In the axon there is a difference between the tagged isoforms. While Dnc^PG::GFP shows a fibrous distribution in the axon similar to that shown for tubulin (Hurd and Saxton, 1996), both Dnc^PA transgenes show a more dotted distribution. This suggests axonal transport of vesicles containing Dnc^PA, whereas Dnc^PG is located in the axon, possibly attached to microtubules, but not transported in vesicles (Fig. 12 B).

The GFP-tag is a 30kDa protein arranged in a β-barrel configuration (Arpino *et al.*, 2012; Prasher *et al.*, 1992), which is attached to the isoforms studied. In yeast, a GFP-tag has been shown to influence the localization of microtubule-forming proteins (Skube *et al.*, 2010). To investigate the influence of the GFP-tag on Dnc^PA, we used AlphaFold to simulate the structure of the two Dnc^PA transgenes (Jumper *et al.*, 2021), with the GFP-tag attached to either the C- or N-terminus. With no structural changes in the PDE domain, both transgenes appear to be functional. We show that the N-terminally tagged Dnc^PA has few structural changes in the UCRs, whereas the C-terminally tagged Dnc^PA has changes in the UCRs but no changes in the N-

terminus (Fig. 11). Structurally, Dnc is homologous to mammalian PDE4D (Bolger *et al.*, 1993). Therefore, insights into the structure of mammalian PDE4 are likely to also apply to Dnc. The N-terminal region of a PDE is responsible for the interaction with AKAPs and β-arrestin and thus for subcellular localisation (Baillie and Houslay, 2005; Dodge *et al.*, 2001; Liliental and Chang, 1998; Taskén *et al.*, 2001; Yarwood *et al.*, 1999); the UCRs are important for oligomerisation and regulation of PDE activation (MacKenzie *et al.*, 2000; Richter and Conti, 2004, 2002). Mammalian PDE4D has been shown to form homo- and hetero-oligomers (Bolger *et al.*, 2015). This leads us to conclude that Dnc^{PA}::GFP is correctly localised but possibly incorrectly oligomerised and GFP::Dnc^{PA} is correctly oligomerised but possibly incorrectly localised.

The difficulty with this strict categorisation is the oligomerisation. If the Dnc isoform forms a heterooligomer with another isoform, or a homooligomer with the untagged version of the same isoform, these oligomerisation partners can interact with proteins such as AKAPs, leading to correct localisation for that isoform. Therefore, we cannot be certain how the tagged N-terminus and the differently configured UCRs influence localisation.

To study the localisation of untagged Dnc^{PA}, the development of a Dnc^{PA}-specific antibody would be the perfect method, but we did not succeed in this. Therefore, a possible follow-up experiment would be to develop a transgene with a smaller tag, such as a His or Flag tag, and compare its localisation to that of the GFP-tagged transgenes.

4.3.2 Somatic Dunce is required for a normal memory phenotype

Given that nuclear PDE levels have been shown to play a role in LTM consolidation in mice (Martinez *et al.*, 2023), we hypothesised that subcellular localization would have a strong influence on the inhibition of premature memory formation in *Drosophila*. We show that the expression of differentially tagged Dnc^{PA} or Dnc^{PG} is sufficient to restore the memory phenotype of *dnc$^{\Delta143}$* to wild-type levels (Fig. 13). The soma is where their expression overlaps and therefore where Dnc PDE-expression is required for the inhibition of premature memory (Fig. 12 A).

Overexpression in other compartments such as the nucleus for Dnc^{PG} does not affect the memory phenotype (Fig. 13). Overexpression of Dnc in the soma also has no effect on the memory phenotype (Fig. 14).Several different feedback loops have been identified for mammalian PDE4D. Phosphorylation of PDEs can up- or down-

regulate PDE-activity, depending on its mechanism and localisation (Dodge-Kafka *et al.*, 2005). PDE4D3 and other PDE4 subfamilies have been reported to be activated through a PKA-PDE feedback loop leading to phosphorylation in the UCR1, thereby significantly increasing PDE activity (MacKenzie *et al.*, 2002; Oki *et al.*, 2000).

In mammalian cardiac myocytes, another feedback loop has been described (Mika *et al.*, 2015). The Ca^{2+}/calmodulin-dependent kinase II (CaMKII) activates PDE4D via phosphorylation of UCR1, PDE4D hydrolises cAMP and thereby reduces CaMKII activation (Mika *et al.*, 2015).

Although these feedback loops have not yet been shown in *Drosophila*, the subunits of the PDE and other signalling pathways are highly conserved. Therefore, similar mechanisms that inactivate the overexpressed Dnc isoform are a possible explanation for the lack of a memory phenotype in the overexpression experiments. Thus, sufficient Dnc expression in the soma is essential to restore $dnc^{\Delta 143}$ memory to a wild-type phenotype, with additional expression in other compartments being down-regulated by a feedback loop.

In summary, although the fly is able to compensate for overexpression of Dnc in different compartments, sufficient expression in the soma is necessary for a wild-type memory phenotype.

4.3.3 Dunce localisation influences synaptic development.

Many different factors and mechanisms have been shown to be involved in neuronal development (review: Menon *et al.*, 2013). Dnc has been shown to have an influence. Previous publications show a reduced number of varicosities upon Dnc overexpression (Cheung *et al.*, 1999) and an increased number of varicosities in Dnc mutants (Zhong *et al.*, 1992). It is not Dnc^{PA} or Dnc^{PG} that leads to an increased number of varicosities (Fig. 12 E). However, the expression of Dnc^{PG}::GFP and Dnc^{PA}::GFP leads to increased branching at the NMJ. For Dnc mutants, previous publications have always shown an effect on both number of varicosities and branching (Zhong *et al.*, 1992; Zhong and Wu, 2004). This shows that the change in morphology is isoform-specific, probably due to the subcellular localisation of Dnc.

It has been shown that cAMP influences synaptic plasticity at two levels, via FasII and CREB (Davis *et al.*, 1996; Schuster *et al.*, 1996a; b). In the nucleus, CREB is required to initiate further transcription of functional components of synaptic plasticity (Davis *et al.*, 1996). Increased pre- or postsynaptic FasII levels lead to reduced bouton formation, whereas symmetrically increased pre-and postsynaptic FasII levels

lead to a significantly increased number of boutons (Ashley *et al.*, 2005; Schuster *et al.*, 1996a; b).

This model by Schuster, Davis et al provide a possible explanation for how the Dnc isoforms influence synaptic plasticity (Davis *et al.*, 1996; Schuster *et al.*, 1996a; b). According to this model, both Dnc^{PG} and the Dnc^{PA} transgenes, although localised in the soma and, in the case of Dnc^{PG}, in the nucleus, do not affect CREB and thus the overall number of varicosities. Instead, they may affect FasII locally, thereby influencing synaptic growth.

Synapse growth has been shown to occur in several ways, either by branching or by adding new boutons to an existing branch (Zito *et al.*, 1999). When boutons are added to an existing branch, the growing larva stretches the NMJ apart and more synapses are formed either between or at the end of existing synapses by budding, division or de novo generation (Zito *et al.*, 1999). During budding, a complex consisting of FasII, dX11 and the fly homolog of Amyloid precursor protein (APPL) forms at the membrane and binds to members of the exocytic family to initiate the budding process (Ashley *et al.*, 2005). Although FasII is predominantly localised in boutons (Zito *et al.*, 1997), in addition to its influence on bouton formation, FasII plays a role in axon growth by regulating pioneer-follower interactions in the growing axon (Sánchez-Soriano and Prokop, 2005). This interaction is necessary for motor neurons to reach their target muscles (Bate, 1976; review: Forghani *et al.*, 2023). Dnc^{PG}::GFP, which is expressed in the nucleus, soma and axon (Fig. 9 A), and Dnc^{PA}::GFP, which is expressed in the soma and the axon, are not expressed in the boutons (Fig. 12 A-C). By affecting the subcellular localisation of cAMP, they may influence the local FasII concentration, thereby facilitating bouton branching, whereas GFP::Dnc^{PA}, which is expressed in the bouton and down-regulates cAMP in the bouton, does not affect bouton formation.

Two interesting follow-up experiments could further narrow down where cAMP influences NMJ-formation. FasII levels at the NMJ and in the axon of the isoform-specific overexpression lines could be studied using an anti-FasII antibody (Koh *et al.*, 1999). cAMP could be localised subcellularly using Förster resonance energy transfer (FRET) (Maiellaro, 2022).

5 Conclusion

Our findings on the Dnc PDE provide a unique insight into the molecular basis of memory formation. Previous publications over the last 47 years have largely come to the same conclusion, namely that the Dnc PDE is important for STM, because Dnc mutants have reduced PDE function and higher cAMP levels and therefore show impaired STM in larval and adult *Drosophila* (Aceves-Piña and Quinn, 1979; Davis and Kiger, 1981; Dudai *et al.*, 1976). Our research modernises the view on Dnc by showing that Dnc should not be regarded as a single PDE with an effect on overall PDE activity and cAMP concentration, but as a collection of isoforms with individual functions in memory formation.

We show that Dnc^{PA} is an important factor in inhibiting premature memory formation. Dnc^{PB} also has an inhibitory effect on memory formation. Although these two isoforms are reduced in *dnc¹* (Ruppert, Franz *et al.*, 2017), we show that they lead to the opposite phenotype.

At the cellular level, we show that the Dnc isoforms are differentially localised within the larval CNS. However, the Dnc isoforms are differentially folded and form complexes, making it difficult to visualise all cells expressing an isoform using peptide antibodies. We localise Dnc^{PA} in several neurons throughout the CNS, with the most likely neuron responsible for the memory phenotype being a projection neuron that projects to the AL.

Previous publications illustrate the importance of PDEs for subcellular cAMP concentration and its possible impact on memory formation (Gervasi *et al.*, 2010; Maiellaro *et al.*, 2016). For Dnc^{PA}, the localisation in the soma of the correct cells is important for memory formation, the additional localisation in other compartments does not affect the memory phenotype. However, the subcellular localisation of Dnc is tightly regulated. Even GFP tags, which cause to a small change in the tertiary structure, have a large effect on subcellular localisation. This suggests that Dnc isoforms are highly regulated and interact strongly with scaffolding proteins.

For Dnc^{PA}, our findings suggest the following role in memory formation: Since the earliest memory formation occurs in the AL (Yu *et al.*, 2004), the Hv cluster, a local interneuron, transmits signals from the US to the AL. There, Dnc^{PA} hydrolyses the somatic cAMP, thereby terminating the signal, preventing premature memory formation and playing an important role in filtering out important information.

Understanding Dnc in detail is a major step towards understanding learning and memory, and therefore towards one day understanding the entire process from signal to memory. As PDEs are highly conserved between species, the basic principles we uncover in *Drosophila* in this project will also help to decipher memory formation in humans.

6 Supplementary Appendix

6.1 Peptide sequences

Table 2: **Peptide sequences against which the antibodies were designed**

Antibody	Peptide sequence
Anti-dnc^{all}	LPQRRESFYRSDSDF
	VENGQGARSPLEGGSP
Anti-dnc^{PB}-C6	QPQTSPLPHIKE
Anti-dnc^{PB}-C10	HQTSLKEHQPLP
Anti-dnc^{PJ}-C1	PSEVDPDEVRSM
Anti-dnc^{PJ}-C4	AGTTGQQSKQDS
Anti-dnc^{PJ}-C8	KRAQGRSPLSPR
Anti-dnc^{PJ}-C10	PRISFPGSDSDL
Anti-dnc^{PJ}-C11	PRISFPGSDSDL
Anti-dnc^{PG}-C1	MATEAEGEEFDV
Anti-dnc^{PG}-C4	SDLMTSDRRSST
Anti-dnc^{PG}-C5	TSDRRSSTATEY
Anti-dnc^{PF}-C2	DRDNMFSIKSQR

6.2 Primer sequences

Table 3: qPCR primer sequences

Primer	Nucleotide sequence
Forwards	GCCTAACAAAACACAAAACCCG
Reverse	GTAAATCGCGCCAATCGCAT

7 References

Aceves-Piña, E. O. and Quinn, W. G. 1979. Learning in Normal and Mutant *Drosophila* Larvae. *Science*, **206**: 93–96.

Aleman-Meza, B., Jung, S. -K. and Zhong, W. 2015. An automated system for quantitative analysis of Drosophila larval locomotion. *BMC Developmental Biology*, **15**: 11.

AlphaFold Google Colaboratory. 2022. https://colab.research.google.com/github/ deepmind/alphafold/blob/main/notebooks/AlphaFold.ipynb#scrollTo=rowN0bV YLe9n, access: 07/14/2022

Alshuaib, W. B., Hasan, M., Cherian, S. P. and Fahim, M. A. 2004. Increased Calcium Influx Through Acetylcholine Receptors in *Dunce* Neurons. *International Journal of Neuroscience*, **114**: 115–128.

Andersen, C. L., Jensen, J. L. and Ørntoft, T. F. 2004. Normalization of Real-Time Quantitative Reverse Transcription-PCR Data: A Model-Based Variance Estimation Approach to Identify Genes Suited for Normalization, Applied to Bladder and Colon Cancer Data Sets. *Cancer Research*, **64**: 5245–5250.

Apostolopoulou, A. A., Köhn, S., Stehle, B., Lutz, M., Wüst, A., Mazija, L., Rist, A., Galizia, C. G., Lüdke, A. and Thum, A. S. 2016. Caffeine Taste Signaling in *Drosophila* Larvae. *Frontiers in Cellular Neuroscience*, **10**.

Apostolopoulou, A. A., Mazija, L., Wüst, A. and Thum, A. S. 2014. The neuronal and molecular basis of quinine-dependent bitter taste signaling in *Drosophila* larvae. *Front. Behav. Neurosci.*, **8**.

Arnold, J. B., Daroczi, G., Werth, B., Weitzner, B., Kunst, J., Auguine, B., Rudis, B., Wickham, H., Talbot, J. and London, J. 2021. ggthemes. *R package*

Arpino, J. A. J., Rizkallah, P. J. and Jones, D. D. 2012. Crystal Structure of Enhanced Green Fluorescent Protein to 1.35 Å Resolution Reveals Alternative Conformations for Glu222. *PLoS One*, **7**: e47132.

Ashley, J., Packard, M., Ataman, B. and Budnik, V. 2005. Fasciclin II Signals New Synapse Formation through Amyloid Precursor Protein and the Scaffolding Protein dX11/Mint. *J. Neurosci.*, **25**: 5943–5955.

Asztalos, Z., Arora, N. and Tully, T. 2007. Olfactory Jump Reflex Habituation in *Drosophila* and Effects of Classical Conditioning Mutations. *Journal of Neurogenetics*, **21**: 1–18.

Baillie, G. S. and Houslay, M. D. 2005. Arrestin times for compartmentalised cAMP signalling and phosphodiesterase-4 enzymes. *Current Opinion in Cell Biology*, **17**: 129–134.

Balling, A., Technau, G. M. and Heisenberg, M. 1987. Are the structural changes in adult *Drosophila* mushroom bodies memory traces? Studies on biochemical learning mutants. *Journal of Neurogenetics*, **4**: 65–73.

Bate, C. M. 1976. Pioneer neurones in an insect embryo. *Nature*, **260**: 54–56.

Berck, M. E., Khandelwal, A., Claus, L., Hernandez-Nunez, L., Si, G., Tabone, C. J., Li, F., Truman, J. W., Fetter, R. D., Louis, M., Samuel, A. D. and Cardona, A. 2016. The wiring diagram of a glomerular olfactory system. *eLife*, **5**: e14859.

Berger, M., Auweiler, K., Tegtmeier, M., Dorn, K., Khadrawe, T. E. and Scholz, H. 2023. Octopamine integrates the status of internal energy supply into the formation of food-related memories. *Preprint in bioRxiv*, https://doi.org/10.1101/2023.06.01.543187

Bhattacharya, A., Gu, G. -G. and Singh, S. 1999. Modulation of dihydropyridine-sensitive calcium channels in *Drosophila* by a cAMP-mediated pathway. *Journal of Neurobiology*, **39**: 491–500.

Bio-Rad Laboratories Inc. 2023. Image Analysis and Quantitation for Western Blotting. https://www.bio-rad.com/de-de/applications-technologies/image-analysis-quantitation-for-western-blotting?ID=PQEERM9V5F6X, access: 08/04/2023

Blendy, J. A. and Maldonado, R. 1998. Genetic analysis of drug addiction: the role of cAMP response element binding protein. *J Mol Med*, **76**: 104–110.

Blum, A. L., Li, W., Cressy, M. and Dubnau, J. 2009. Short- and Long-Term Memory in *Drosophila* Require cAMP Signaling in Distinct Neuron Types. *Current Biology*, **19**: 1341–1350.

Bolger, G., Michaeli, T., Martins, T., St John, T., Steiner, B., Rodgers, L., Riggs, M., Wigler, M. and Ferguson, K. 1993. A Family of Human Phosphodiesterases Homologous to the *dunce* Learning and Memory Gene Product of *Drosophila melanogaster* Are Potential Targets for Antidepressant Drugs. *Mol Cell Biol*, **13**: 6558–6571.

Bolger, G. B., Dunlop, A. J., Meng, D., Day, J. P., Klussmann, E., Baillie, G. S., Adams, D. R. and Houslay, M. D. 2015. Dimerization of cAMP phosphodiesterase-4 (PDE4) in living cells requires interfaces located in both the UCR1 and catalytic unit domains. *Cell Signal*, **27**: 756–769.

Bordeaux, J., Welsh, A. W., Agarwal, S., Killiam, E., Baquero, M. T., Hanna, J. A., Anagnostou, V. K. and Rimm, D. L. 2010. Antibody validation. *BioTechniques*, **48**: 197–209.

Bouzaiane, E., Trannoy, S., Scheunemann, L., Plaçais, P. -Y. and Preat, T. 2015. Two Independent Mushroom Body Output Circuits Retrieve the Six Discrete Components of *Drosophila* Aversive Memory. *Cell Reports*, **11**: 1280–1292.

Brand, A. 1995. GFP in *Drosophila*. *Trends in Genetics*, **11**: 324–325.

Brown, K. M., Day, J. P., Huston, E., Zimmermann, B., Hampel, K., Christian, F., Romano, D., Terhzaz, S., Lee, L. C. Y., Willis, M. J., Morton, D. B., Beavo, J. A., Shimizu-Albergine, M., Davies, S. A., Kolch, W., Houslay, M. D. and Baillie,

G. S. 2013. Phosphodiesterase-8A binds to and regulates Raf-1 kinase. *Proc Natl Acad Sci U S A*, **110**: E1533–E1542.

Brüning, V. 2022. Einfluss der subzellulären Lokalisation von Dunce-Isoformen auf das larvale Lernen *Drosophila melanogaster*. *Bachelor thesis,* University of Cologne

Burke, C. J., Huetteroth, W., Owald, D., Perisse, E., Krashes, M. J., Das, G., Gohl, D., Silies, M., Certel, S. and Waddell, S. 2012. Layered reward signalling through octopamine and dopamine in *Drosophila*. *Nature*, **492**: 433–437.

Byers, D., Davis, R. L. and Kiger, J. A. 1981. Defect in cyclic AMP phosphodiesterase due to the *dunce* mutation of learning in *Drosophila melanogaster*. *Nature*, **289**: 79–81.

Castellucci, V., Pinsker, H., Kupfermann, I. and Kandel, E. R. 1970. Neuronal Mechanisms of Habituation and Dishabituation of the Gill-Withdrawal Reflex in *Aplysia*. *Science*, **167**: 1745–1748.

Charbonneau, H., Beier, N., Walsh, K.A. and Beavo, J.A. 1986. Identification of a conserved domain among cyclic nucleotide phosphodiesterases from diverse species. *Proc Natl Acad Sci U S A*, **83**: 9308–9312.

Chen, C., Malone, T., Beckendorf, S. K. and Davis, R. L. 1987. At least two genes reside within a large intron of the *dunce* gene of *Drosophila*. *Nature*, **329**: 721–724.

Chen, C. -C., Wu, J. -K., Lin, H. -W., Pai, T. -P., Fu, T. -F., Wu, C. -L., Tully, T. and Chiang, A. -S. 2012. Visualizing long-term memory formation in two neurons of the *Drosophila* brain. *Science*, **335**: 678–685.

Chen, W., Yewdell, J. W., Levine, R. L. and Bennink, J. R. 1999. Modification of Cysteine Residues In Vitro and In Vivo Affects the Immunogenicity and Antigenicity of Major Histocompatibility Complex Class I–restricted Viral Determinants. *Journal of Experimental Medicine*, **189**: 1757–1764.

Cheung, U. S., Shayan, A. J., Boulianne, G. L. and Atwood, H. L. 1999. *Drosophila* Larval Neuromuscular Junction's Responses to Reduction of cAMP in the Nervous System. *Journal of Neurobiology*, **40**: 1–13.

Chu-Wang, I. -W. and Axtell, R. C. 1971. Fine structure of the dorsal organ of the house fly larva, *Musca domestica* L. *Z. Zellforsch.*, **117**: 17–34.

Chu-Wang, I. -W. and Axtell, R. C. 1972a. Fine structure of the terminal organ of the house fly larva, *Musca domestica* L. *Z.Zellforsch*, **127**: 287–305.

Chu-Wang, I. -W. and Axtell, R. C. 1972b. Fine structure of the ventral organ of the house fly larva, *Musca domestica* L. *Z.Zellforsch*, **130**: 489–495.

Cibik, O. 2007. Identifizierung TbH-positiver Neurone im adulten Gehirn von *Drosophila melanogaster*. *Diplom thesis*, University of Würzburg

Claridge-Chang, A., Roorda, R. D., Vrontou, E., Sjulson, L., Li, H., Hirsh, J. and Miesenböck, G. 2009. Writing Memories with Light-Addressable Reinforcement Circuitry. *Cell*, **139**: 405–415.

Cognigni, P., Felsenberg, J. and Waddell, S. 2018. Do the right thing: neural network mechanisms of memory formation, expression and update in *Drosophila*. *Current Opinion in Neurobiology*, **49**: 51–58.

Conti, A. C., Maas, J. W., Muglia, L. M., Dave, B. A., Vogt, S. K., Tran, T. T., Rayhel, E. J. and Muglia, L. J. 2007. Distinct regional and subcellular localization of adenylyl cyclases type 1 and 8 in mouse brain. *Neuroscience*, **146**: 713–729.

Conti, M., Richter, W., Mehats, C., Livera, G., Park, J. -Y. and Jin, C. 2002. Cyclic AMP-specific PDE4 Phosphodiesterases as Critical Components of Cyclic AMP Signaling *. *Journal of Biological Chemistry*, **278**: 5493–5496.

Corfas, G. and Dudai, Y. 1991. Morphology of a sensory neuron in *Drosophila* is abnormal in memory mutants and changes during aging. *Proceedings of the National Academy of Sciences*, **88**: 7252–7256.

Corrigall, W. A. and Coen, K. M. 1989. Nicotine maintains robust self-administration in rats on a limited-access schedule. *Psychopharmacology*, **99**: 473–478.

Creighton, J., Zhu, B., Alexeyev, M. and Stevens, T. 2008. Spectrin-anchored phosphodiesterase 4D4 restricts cAMP from disrupting microtubules and inducing endothelial cell gap formation. *Journal of Cell Science*, **121**: 110–119.

Daniels, R. W., Collins, C. A., Gelfand, M. V., Dant, J., Brooks, E. S., Krantz, D. E. and DiAntonio, A. 2004. Increased Expression of the *Drosophila* Vesicular Glutamate Transporter Leads to Excess Glutamate Release and a Compensatory Decrease in Quantal Content. *J. Neurosci.*, **24**: 10466–10474.

Daniels, R. W., Gelfand, M. V., Collins, C. A. and DiAntonio, A. 2008. Visualizing Glutamatergic Cell Bodies and Synapses in *Drosophila* Larval and Adult CNS. *Journal of Comparative Neurology*, **508**: 131–152.

Dauwalder, B. and Davis, R. L. 1995. Conditional Rescue of the *dunce* Learning/Memory and Female Fertility Defects with *Drosophila* or Rat Transgenes. *J Neurosci*, **15**: 3490–3499.

Davis, G. W., Schuster, C. M. and Goodman, C. S. 1996. Genetic Dissection of Structural and Functional Components of Synaptic Plasticity. III. CREB Is Necessary for Presynaptic Functional Plasticity. *Neuron*, **17**: 669–679.

Davis, R. L. 2023. Learning and memory using *Drosophila melanogaster*: a focus on advances made in the fifth decade of research. *Genetics*, iyad085.

Davis, R. L. and Kiger, J. A. 1981. *dunce* Mutants of *Drosophila melanogaster*: Mutants Defective in the Cyclic AMP Phosphodiesterase Enzyme System. *J Cell Biol*, **90**: 101–107.

Day, J. P., Dow, J. A. T., Houslay, M. D. and Davies, S. -A. 2005. Cyclic nucleotide phosphodiesterases in *Drosophila melanogaster*. *Biochem J*, **388**: 333–342.

DeLano, W. L. 2021. PyMOL Molecular Graphics System. *Software*, Schroedinger LLC

Delgado, R., Davis, R., Bono, M. R., Latorre, R. and Labarca, P. 1998. Outward Currents in *Drosophila* Larval Neurons: *dunce* Lacks a Maintained Outward Current Component Downregulated by cAMP. *J. Neurosci.*, **18**: 1399–1407.

Devaud, J. -M., Acebes, A. and Ferrús, A. 2001. Odor Exposure Causes Central Adaptation and Morphological Changes in Selected Olfactory Glomeruli in *Drosophila*. *J. Neurosci.*, **21**: 6274–6282.

Dodge, K. L., Khouangsathiene, S., Kapiloff, M. S., Mouton, R., Hill, E. V., Houslay, M. D., Langeberg, L. K. and Scott, J. D. 2001. mAKAP assembles a protein kinase A/PDE4 phosphodiesterase cAMP signaling module. *The EMBO Journal*, **20**: 1921–1930.

Dodge-Kafka, K. L., Soughayer, J., Pare, G. C., Carlisle Michel, J. J., Langeberg, L. K., Kapiloff, M. S. and Scott, J. D. 2005. The protein kinase A anchoring protein mAKAP coordinates two integrated cAMP effector pathways. *Nature*, **437**: 574–578.

Dudai, Y. 1983. Mutations affect storage and use of memory differentially in *Drosophila*. *Proc. Natl. Acad. Sci. U.S.A.*, **80**: 5445–5448.

Dudai, Y., Jan, Y. N., Byers, D., Quinn, W. G. and Benzer, S. 1976. *dunce*, a mutant of *Drosophila* deficient in learning. *Proc Natl Acad Sci U S A*, **73**: 1684–1688.

Duerr, J. S. and Quinn, W. G. 1982. Three *Drosophila* mutations that block associative learning also affect habituation and sensitization. *Proc Natl Acad Sci U S A*, **79**: 3646–3650.

Engel, J. E. and Wu, C. -F. 1996. Altered Habituation of an Identified Escape Circuit in Drosophila Memory Mutants. *J. Neurosci.*, **16**: 3486–3499.

Eschbach, C., Fushiki, A., Winding, M., Schneider-Mizell, C. M., Shao, M., Arruda, R., Eichler, K., Valdes-Aleman, J., Ohyama, T., Thum, A. S., Gerber, B., Fetter, R. D., Truman, J. W., Litwin-Kumar, A., Cardona, A. and Zlatic, M. 2020. Recurrent architecture for adaptive regulation of learning in the insect brain. *Nat Neurosci*, **23**: 544–555.

Eschment, M., Franz, H. R., Güllü, N., Hölscher, L. G., Huh, K. -E. and Widmann, A. 2020. Insulin signaling represents a gating mechanism between different memory phases in *Drosophila* larvae. *PLOS Genetics*, **16**: e1009064.

Expasy - Compute pI/Mw tool. 2023. https://web.expasy.org/compute_pi/, access 09/30/2023

Felsenberg, J., Barnstedt, O., Cognigni, P., Lin, S. and Waddell, S. 2017. Re-evaluation of learned information in *Drosophila*. *Nature*, **544**: 240–244.

Felsenberg, J., Jacob, P. F., Walker, T., Barnstedt, O., Edmondson-Stait, A. J., Pleijzier, M. W., Otto, N., Schlegel, P., Sharifi, N., Perisse, E., Smith, C. S., Lauritzen, J. S., Costa, M., Jefferis, G. S. X .E., Bock, D. D. and Waddell, S. 2018. Integration of Parallel Opposing Memories Underlies Memory Extinction. *Cell*, **175**: 709-722.e15.

Fenckova, M., Blok, L. E. R., Asztalos, L., Goodman, D. P., Cizek, P., Singgih, E. L., Glennon, J. C., IntHout, J., Zweier, C., Eichler, E. E., von Reyn, C. R., Bernier, R. A., Asztalos, Z. and Schenck, A. 2019. Habituation Learning Is a Widely Affected Mechanism in *Drosophila* Models of Intellectual Disability and Autism Spectrum Disorders. *Biological Psychiatry*, **86**: 294–305.

Fertig, B. A. and Baillie, G. S. 2018. PDE4-Mediated cAMP Signalling. *Journal of Cardiovascular Development and Disease*, **5**: 8.

Flood, J. F. and Morley, J. E. 1997. Learning and Memory in the SAMP8 Mouse. *Neuroscience & Biobehavioral Reviews*, **22**: 1–20.

FlyBase. 2023. FlyBase - A database of Drosophila Genes & Genomes https://flybase.org/, access 06/09/2023

Folkers, E., Waddell, S. and Quinn, W. G. 2006. The *Drosophila radish* gene encodes a protein required for anesthesia-resistant memory. *Proceedings of the National Academy of Sciences*, **103**: 17496–17500.

Forghani, R., Chandrasekaran, A., Papoian, G. and Giniger, E. 2023. A new view of axon growth and guidance grounded in the stochastic dynamics of actin networks. *Open Biology*, **13**: 220359.

Friggi-Grelin, F., Coulom, H., Meller, M., Gomez, D., Hirsh, J. and Birman, S. 2003. Targeted gene expression in *Drosophila* dopaminergic cells using regulatory sequences from tyrosine hydroxylase. *Journal of Neurobiology*, **54**: 618–627.

Furia, M., Digilio, F.A., Artiaco, D., Giordano, E. and Polito, L.C. 1990. A new gene nested within the *dunce* genetic unit of *Drosophila melanogaster*. *Nucl Acids Res*, **18**: 5837–5841.

Gailey, D. A., Hall, J. C. and Siegel, R. W. 1985. Reduced Reproductive Success for a Conditioning Mutant in Experimental Populations of *Drosophila Melanogaster*. *Genetics*, **111**: 795–804.

Ganguly, A. and Lee, D. 2013. Suppression of inhibitory GABAergic transmission by cAMP signaling pathway: alterations in learning and memory mutants. *European Journal of Neuroscience*, **37**: 1383–1393.

Gerber, B. and Hendel, T. 2006. Outcome expectations drive learned behaviour in larval *Drosophila*. *Proc Biol Sci*, **273**: 2965–2968.

Gerber, B., Tanimoto, H. and Heisenberg, M. 2004. An engram found? Evaluating the evidence from fruit flies. *Current Opinion in Neurobiology*, **14**: 737–744.

Gervasi, N., Tchénio, P. and Preat, T. 2010. PKA Dynamics in a *Drosophila* Learning Center: Coincidence Detection by Rutabaga Adenylyl Cyclase and Spatial Regulation by Dunce Phosphodiesterase. *Neuron*, **65**: 516–529.

Gompert, M. 2019. *Dunce*-Isoform spezifisches Lernen in der Larve von *Drosophila melanogaster*. *Bachelor thesis*, University of Cologne

Gong, Z. -F., Xia, S. -Z., Liu, L., Feng, C. -H. and Guo, A. -K. 1998. Operant visual learning and memory in *Drosophila* mutants *dunce*, *amnesiac* and *radish*. *Journal of Insect Physiology*, **44**: 1149–1158.

Gorczyca, M., Augart, C. and Budnik, V. 1993. Insulin-like Receptor and Insulin-like Peptide Are Localized at Neuromuscular Junctions in *Drosophila*. *J. Neurosci.*, **13**: 3692–3704.

Gundelfinger, E. D. and Hess, N. 1992. Nicotinic acetylcholine receptors of the central nervous system of *Drosophila*. *Biochimica et Biophysica Acta (BBA) - Molecular Cell Research*, **1137**: 299–308.

Hartenstein, V. 2011. Morphological Diversity and Development of Glia in *Drosophila*. *Glia*, **59**: 1237–1252.

Hayes, J. S. and Brunton, L. L. 1982. Functional compartments in cyclic nucleotide action. *J Cyclic Nucleotide Res*, **8**: 1–16.

Hayes, J. S., Brunton, L. L. and Mayer, S. E. 1980. Selective Activation of Particulate cAMP-dependent Protein Kinase by Isoproterenol and Prostaglandin E1. *Journal of Biological Chemistry*, **255**: 5113–5119.

Hazelrigg, T., Levis, R. and Rubin, G. M. 1984. Transformation of *white* Locus DNA in Drosophila: Dosage Compensation, *zeste* Interaction, and Position Effects. *Cell*, **36**: 469–481.

Heisenberg, M., Borst, A., Wagner, S. and Byers, D. 1985. *Drosophila* Mushroom Body Mutants are Deficient in Olfactory Learning. *Journal of Neurogenetics*, **2**: 1–30.

Hertweck, H. 1931. Anatomie und Variabilität des Nervensystems und der Sinnesorgane von *Drosophila melanogaster* (Meigen). *Z. wiss. Zool*, **139**: 559–663.

Hikosaka, O., Rand, M. K., Miyachi, S. and Miyashita, K. 1995. Learning of sequential movements in the monkey: process of learning and retention of memory. *Journal of Neurophysiology*, **74**: 1652–1661.

Hoang, B. and Chiba, A. 2001. Single-Cell Analysis of *Drosophila* Larval Neuromuscular Synapses. *Developmental Biology*, **229**: 55–70.

Honda, T., Lee, C. -Y., Honjo, K. and Furukubo-Tokunaga, K. 2016. Artificial Induction of Associative Olfactory Memory by Optogenetic and Thermogenetic Activation of Olfactory Sensory Neurons and Octopaminergic Neurons in *Drosophila* Larvae. *Frontiers in Behavioral Neuroscience*, **10**.

Hou, J., Kuromi, H., Fukasawa, Y., Ueno, K., Sakai, T. and Kidokoro, Y. 2004. Repetitive Exposures to Nicotine Induce a Hyper-Responsiveness via the cAMP/PKA/CREB Signal Pathway in *Drosophila*. *Journal of Neurobiology*, **60**: 249–261.

Houslay, K. F., Christian, F., MacLeod, R., Adams, D. R., Houslay, M. D. and Baillie, G. S. 2017. Identification of a multifunctional docking site on the catalytic unit of phosphodiesterase-4 (PDE4) that is utilised by multiple interaction partners. *Biochem J*, **474**: 597–609.

Houslay, M. D. 2001. PDE4 cAMP-specific Phosphodiesterases. In: *Progress in Nucleic Acid Research and Molecular Biology*, pp. 249–315.

Houslay, M. D. 2009. Underpinning compartmentalised cAMP signalling through targeted cAMP breakdown. *Trends in Biochemical Sciences*, **35**: 91–100.

Hu, Y., Sopko, R., Chung, V., Foos, M., Studer, R. A., Landry, S. D., Liu, D., Rabinow, L., Gnad, F., Beltrao, P. and Perrimon, N. 2019. iProteinDB: An Integrative Database of *Drosophila* Post-translational Modifications. *G3 Genes|Genomes|Genetics*, **9**: 1–11.

Hummel, T., Krukkert, K., Roos, J., Davis, G. and Klämbt, C. 2000. *Drosophila* Futsch/22C10 Is a MAP1B-like Protein Required for Dendritic and Axonal Development. *Neuron*, **26**: 357–370.

Hurd, D. D. and Saxton, W. M. 1996. Kinesin Mutations Cause Motor Neuron Disease Phenotypes by Disrupting Fast Axonal Transport in Drosophila. *Genetics*, **144**: 1075–1085.

Huser, A., Eschment, M., Güllü, N., Collins, K. A. N., Böpple, K., Pankevych, L., Rolsing, E. and Thum, A. S. 2017. Anatomy and behavioral function of serotonin receptors in *Drosophila melanogaster* larvae. *PLOS ONE*, **12**: e0181865.

Huser, A., Rohwedder, A., Apostolopoulou, A. A., Widmann, A., Pfitzenmaier, J. E., Maiolo, E. M., Selcho, M., Pauls, D., Essen, A. von, Gupta, T., Sprecher, S. G., Birman, S., Riemensperger, T., Stocker, R. F. and Thum, A. S. 2012. The Serotonergic Central Nervous System of the *Drosophila* Larva: Anatomy and Behavioral Function. *PLOS ONE*, **7**: e47518.

Isabel, G., Pascual, A. and Preat, T. 2004. Exclusive Consolidated Memory Phases in *Drosophila*. *Science*, **304**: 1024–1027.

Iwai, Y., Usui, T., Hirano, S., Steward, R., Takeichi, M. and Uemura, T. 1997. Axon Patterning Requires *D*N-cadherin, a Novel Neuronal Adhesion Receptor, in the Drosophila Embryonic CNS. *Neuron*, **19**: 77–89.

Jan, L. Y. and Jan, Y. N. 1976. Properties of the larval neuromuscular junction in *Drosophila melanogaster. The Journal of Physiology*, **262**: 189–214.

Jefferis, G.S.X.E. and Hummel, T. 2006. Wiring specificity in the olfactory system. *Seminars in Cell & Developmental Biology*, **17**: 50–65.

Jin, S. L., Swinnen, J. V. and Conti, M. 1992. Characterization of the Structure of a Low K_m, Polipram-sensitive cAMP Phosphodiesterase. Mapping of the catalytic domain. *Journal of Biological Chemistry*, **267**: 18929–18939.

Johansen, J., Halpern, M., Johansen, K. and Keshishian, H. 1989. Stereotypic Morphology of Glutamatergic Synapses on Identified Muscle Cells of *Drosophila* Larvae. *J Neurosci*, **9**: 710–725.

Jones, S. and Thornton, J. M. 1996. Principles of protein-protein interactions. *Proceedings of the National Academy of Sciences*, **93**: 13–20.

Jumper, J., Evans, R., Pritzel, A., Green, T., Figurnov, M., Ronneberger, O., Tunyasuvunakool, K., Bates, R., Žídek, A., Potapenko, A., Bridgland, A., Meyer, C., Kohl, S. A. A., Ballard, A. J., Cowie, A., Romera-Paredes, B., Nikolov, S., Jain, R., Adler, J., Back, T., Petersen, S., Reiman, D., Clancy, E., Zielinski, M., Steinegger, M., Pacholska, M., Berghammer, T., Bodenstein, S., Silver, D., Vinyals, O., Senior, A.W., Kavukcuoglu, K., Kohli, P. and Hassabis, D. 2021. Highly accurate protein structure prediction with AlphaFold. *Nature*, **596**: 583–589.

Kassambara, A. 2023a. ggpubr: "ggplot2" Based Publication Ready Plots. *R package*

Kassambara, A. 2023b. rstatix: Pipe-Friendly Framework for Basic Statistical Tests. *R package*

Keene, A. C., Krashes, M. J., Leung, B., Bernard, J. A. and Waddell, S. 2006. *Drosophila* Dorsal Paired Medial Neurons Provide a General Mechanism for Memory Consolidation. *Current Biology*, **16**: 1524–1530.

Keene, A. C., Mazzoni, E. O., Zhen, J., Younger, M. A., Yamaguchi, S., Blau, J., Desplan, C. and Sprecher, S. G. 2011. Distinct Visual Pathways Mediate *Drosophila* Larval Light Avoidance and Circadian Clock Entrainment. *J Neurosci*, **31**: 6527–6534.

Khoroshko, V. A., Pokholkova, G. V., Zykova, T. Yu., Osadchiy, I. S. and Zhimulev, I. F. 2019. Gene *dunce* Localization in the Polytene Chromosome of *Drosophila melanogaster* Long Span Batch of Adjacent Chromosomal Structures. *Dokl Biochem Biophys*, **484**: 55–58.

Khurana, S., Abubaker, M. B. and Siddiqi, O. 2009. Odour avoidance learning in the larva of *Drosophila melanogaster*. *J Biosci*, **34**: 621–631.

Khurana, S., Robinson, B. G., Wang, Z., Shropshire, W. C., Zhong, A. C., Garcia, L. E., Corpuz, J., Chow, J., Hatch, M. M., Precise, E. F., Cady, A., Godinez, R. M., Pulpanyawong, T., Nguyen, A. T., Li, W., Seiter, M., Jahanian, K., Sun, J. C., Shah, R., Rajani, S., Chen, W. Y., Ray, S., Ryazanova, N.V., Wakou, D., Prabhu, R.K. and Atkinson, N., S. 2012. Olfactory Conditioning in the Third Instar Larvae of *Drosophila melanogaster* Using Heat Shock Reinforcement. *Behav Genet*, **42**: 151–161.

Knapek, S., Sigrist, S. and Tanimoto, H. 2011. Bruchpilot, A Synaptic Active Zone Protein for Anesthesia-Resistant Memory. *J Neurosci*, **31**: 3453–3458.

Koh, Y. H., Popova, E., Thomas, U., Griffith, L. C. and Budnik, V. 1999. Regulation of DLG Localization at Synapses by CaMKII-Dependent Phosphorylation. *Cell*, **98**: 353–363.

Kohsaka, H., Okusawa, S., Itakura, Y., Fushiki, A. and Nose, A. 2012. Development of larval motor circuits in *Drosophila. Development, Growth & Differentiation*, **54**: 408–419.

Kreher, S. A., Kwon, J. Y. and Carlson, J. R. 2005. The Molecular Basis of Odor Coding in the *Drosophila* Larva. *Neuron*, **46**: 445–456.

Landgraf, M., Bossing, T., Technau, G. M. and Bate, M. 1997. The Origin, Location, and Projections of the Embryonic Abdominal Motorneurons of *Drosophila. J. Neurosci.*, **17**: 9642–9655.

Larkin, A., Karak, S., Priya, R., Das, A., Ayyub, C., Ito, K., Rodrigues, V. and Ramaswami, M. 2010. Central synaptic mechanisms underlie short-term olfactory habituation in *Drosophila* larvae. *Learn. Mem.*, **17**: 645–653.

Larsson, M. C., Domingos, A. I., Jones, W. D., Chiappe, M. E., Amrein, H. and Vosshall, L. B. 2004. Or83b Encodes a Broadly Expressed Odorant Receptor Essential for *Drosophila* Olfaction. *Neuron*, **43**: 703–714.

Lee, C. -R., Park, Y. -H., Kim, Y .-R., Peterkofsky, A. and Seok, Y. -J. 2013. Phosphorylation-Dependent Mobility Shift of Proteins on SDS-PAGE is Due to Decreased Binding of SDS. *Bulletin of the Korean Chemical Society*, **34**: 2063–2066.

Lee, D. 2015. Global and local missions of cAMP signaling in neural plasticity, learning, and memory. *Frontiers in Pharmacology*, **6**.

Lee, D. and O'Dowd, D. K. 2000. cAMP-Dependent Plasticity at Excitatory Cholinergic Synapses in *Drosophila* Neurons: Alterations in the Memory Mutant *Dunce. J. Neurosci.*, **20**: 2104–2111.

Lee, T., Lee, A. and Luo, L. 1999. Development of the *Drosophila* mushroom bodies: sequential generation of three distinct types of neurons from a neuroblast. *Development*, **126**: 4065–4076.

Lee, T. and Luo, L. 1999. Mosaic Analysis with a Repressible Cell Marker for Studies of Gene Function in Neuronal Morphogenesis. *Neuron*, **22**: 451–461.

Lesar, A., Tahir, J., Wolk, J. and Gershow, M. 2021. Switch-like and persistent memory formation in individual *Drosophila larvae. eLife*, **10**: e70317.

Levine, J. D., Casey, C. I., Kalderon, D. D. and Jackson, F. R. 1994. Altered Circadian Pacemaker Functions and Cyclic AMP Rhythms in the Drosophila Learning Mutant *dunce. Neuron*, **13**: 967–974.

Life Technologies Corporation. 2010. Superscript II Reverse Transcriptase. *Protocol*, MAN0001342

Liliental, J. and Chang, D. D. 1998. Rack1, a Receptor for Activated Protein Kinase C, Interacts with Integrin β Subunit *. *Journal of Biological Chemistry*, **273**: 2379–2383.

Liu, C., Plaçais, P. -Y., Yamagata, N., Pfeiffer, B. D., Aso, Y., Friedrich, A. B., Siwanowicz, I., Rubin, G. M., Preat, T. and Tanimoto, H. 2012. A subset of dopamine neurons signals reward for odour memory in *Drosophila*. *Nature*, **488**: 512–516.

Livingstone, M. S., Sziber, P. P. and Quinn, W. G. 1984. Loss of Calcium/Calmodulin Responsiveness in Adenylate Cyclase of *rutabaga*, a Drosophila Learning Mutant. *Cell*, **37**: 205–215.

Livingstone, M. S. and Tempel, B. L. 1983. Genetic dissection of monoamine neurotransmitter synthesis in *Drosophila*. *Nature*, **303**: 67–70.

Lynch, M. J., Baillie, G. S., Mohamed, A., Li, X., Maisonneuve, C., Klussmann, E., van Heeke, G. and Houslay, M. D. 2005. RNA Silencing Identifies PDE4D5 as the Functionally Relevant cAMP Phosphodiesterase Interacting with βArrestin to Control the Protein Kinase A/AKAP79-mediated Switching of the β2-Adrenergic Receptor to Activation of ERK in HEK293B2 Cells*. *Journal of Biological Chemistry*, **280**: 33178–33189.

Mackenzie, K.F., Topping, E.C., Bugaj-Gaweda, B., Deng, C., Cheung, Y.-F., Olsen, A.E., Stockard, C.R., High Mitchell, L., Baillie, G.S., Grizzle, W.E., De Vivo, M., Houslay, M.D., Wang, D. and Bolger, G.B. 2008. Human PDE4A8, a novel brain-expressed PDE4 cAMP-specific phosphodiesterase that has undergone rapid evolutionary change. *Biochem J*, **411**: 361–369.

MacKenzie, S. J., Baillie, G. S., McPhee, I., Bolger, G. B. and Houslay, M. D. 2000. ERK2 Mitogen-activated Protein Kinase Binding, Phosphorylation, and Regulation of the PDE4D cAMP-specific Phosphodiesterases: The involvement of COOH-terminal docing sites and NH$_2$-terminal UCR-regions. *Journal of Biological Chemistry*, **275**: 16609–16617.

MacKenzie, S. J., Baillie, G. S., McPhee, I., MacKenzie, C., Seamons, R., McSorley, T., Millen, J., Beard, M. B., van Heeke, G. and Houslay, M. D. 2002. Long PDE4 cAMP specific phosphodiesterases are activated by protein kinase A-mediated phosphorylation of a single serine residue in Upstream Conserved Region 1 (UCR1). *Br J Pharmacol*, **136**: 421–433.

Maiellaro, I. 2022. In Vivo cAMP Dynamics in *Drosophila* Larval Neurons. In: *cAMP Signaling: Methods and Protocols* (M. Zaccolo, ed, Springer, New York), pp. 181–194.

Maiellaro, I., Lohse, M. J., Kittel, R. J. and Calebiro, D. 2016. cAMP Signals in *Drosophila* Motor Neurons Are Confined to Single Synaptic Boutons. *Cell Rep*, **17**: 1238–1246.

Mancini, N., Hranova, S., Weber, J., Weiglein, A., Schleyer, M., Weber, D., Thum, A. S. and Gerber, B. 2019. Reversal learning in *Drosophila* larvae. *Learn. Mem.*, **26**: 424–435.

Maren, S. 2005. Synaptic Mechanisms of Associative Memory in the Amygdala. *Neuron*, **47**: 783–786.

Margulies, C., Tully, T. and Dubnau, J. 2005. Deconstructing Memory in *Drosophila*. *Current Biology*, **15**: R700–R713.

Martín, F., Charro, M. J. and Alcorta, E. 2001. Mutations affecting the cAMP transduction pathway modify olfaction in *Drosophila*. *J Comp Physiol A*, **187**: 359–370.

Martinez, J. M., Shen, A., Xu, B., Jovanovic, A., de Chabot, J., Zhang, J. and Xiang, Y. K. 2023. Arrestin-dependent nuclear export of phosphodiesterase 4D promotes GPCR-induced nuclear cAMP signaling required for learning and memory. *Science Signaling*, **16**: eade3380.

Melcher, C. and Pankratz, M. J. 2005. Candidate Gustatory Interneurons Modulating Feeding Behavior in the *Drosophila* Brain. *PLOS Biology*, **3**: e305.

Menon, K. P., Carrillo, R. A. and Zinn, K. 2013. Development and plasticity of the *Drosophila* larval neuromuscular junction. *WIREs Developmental Biology*, **2**: 647–670.

Michel, J. J. C. and Scott, J. D. 2002. AKAP Mediated Signal Transduction. *Annu. Rev. Pharmacol. Toxicol.*, **42**: 235–257.

Mika, D., Richter, W. and Conti, M. 2015. A CaMKII/PDE4D negative feedback regulates cAMP signaling. *Proceedings of the National Academy of Sciences*, **112**: 2023–2028.

Milner, B., Squire, L. R. and Kandel, E. R. 1998. Cognitive Neuroscience and the Study of Memory. *Neuron*, **20**: 445–468.

Mishra, D., Chen, Y. -C., Yarali, A., Oguz, T. and Gerber, B. 2013. Olfactory memories are intensity specific in larval *Drosophila*. *J Exp Biol*, **216**: 1552–1560.

Mohamed, A., Malekou, I., Sim, T., O'Kane, C. J., Maait, Y., Scullion, B. and Masuda-Nakagawa, L. M. 2023. Mushroom body output neurons MBON-a1/a2 define an odor intensity channel that regulates behavioral odor discrimination learning in larval *Drosophila*. *Frontiers in Physiology*, **14**.

Mohler, J. D. 1977. Developmental genetics of the *Drosophila* egg I. Identification of 59 sex-linked cistrons with maternal effects on embryonic development. *Genetics*, **85**: 259–272.

Monastirioti, M., Gorczyca, M., Rapus, J., Eckert, M., White, K. and Budnik, V. 1995. Octopamine Immunoreactivity in the Fruit Fly *Drosophila melanogaster*. *Journal of Comparative Neurology*, **356**: 275–287.

Monastirioti, M., Linn, C. E. Jr. and White, K. 1996. Characterization of *Drosophila Tyramine β-Hydroxylase* Gene and Isolation of Mutant Flies Lacking Octopamine. *J Neurosci*, **16**: 3900–3911.

Mongillo, M., McSorley, T., Evellin, S., Sood, A., Lissandron, V., Terrin, A., Huston, E., Hannawacker, A., Lohse, M. J., Pozzan, T., Houslay, M. D. and Zaccolo, M. 2004. Fluorescence Resonance Energy Transfer-Based Analysis of cAMP Dynamics in Live Neonatal Rat Cardiac Myocytes Reveals Distinct Functions of Compartmentalized Phosphodiesterases. *Circ Res*, **95**: 67–75.

Monte, P., Woodard, C., Ayer, R., Lilly, M., Sun, H. and Carlson, J. 1989. Characterization of the Larval Olfactory Response in *Drosophila* and Its Genetic Basis. *Behav Genet*, **19**: 267–283.

Morgan, T. H. 1911. The Origin of Five Mutations in Eye Color in *Drosophila* and Their Modes of Inheritance. *Science*, **33**: 534–537.

Mulle, C., Vidal, C., Benoit, P. and Changeux, J. P. 1991. Existence of Different Subtypes of Nicotinic Acetylcholine Receptors in the Rat Habenulo-interpeduncular System. *J. Neurosci.*, **11**: 2588–2597.

Müller, M. 2021. Charakterisierung von putativen Antikörpern gegen Dunce[PG] am larvalen Nervensystem der *Drosophila melanogaster*. *Bachelor thesis*, University of Cologne

Mysliveček, J. and Hassmannová, J. 1979. Ontogeny of Active Avoidance in the Rat: Learning and Memory. *Developmental Psychobiology*, **12**: 169–186.

Nelson, P. N. 2000. *Demystified...* Monoclonal antibodies. *Molecular Pathology*, **53**: 111–117.

Nicholson, L. and Keshishian, H. 2006. Neuromuscular Development. In: *Muscle Development in Drosophila* (H. Sink, ed, Springer, New York), pp. 113–124.

Nighorn, A., Healy, M. J. and Davis, R. L. 1991. The Cyclic AMP Phosphodiesterase Encoded by the Drosophila *dunce* Gene Is Concentrated in the Mushroom Body Neuropil. *Neuron*, **6**: 455–467.

Oki, N., Takahashi, S. -I., Hidaka, H. and Conti, M. 2000. Short Term Feedback Regulation of cAMP in FRTL-5 Thyroid Cells: Role of PDE4D3 phosphodiesterase activation. *Journal of Biological Chemistry*, **275**: 10831–10837.

Ong, S. T., Chalasani, M. L. S., Fazil, M. H. U. T., Prasannan, P., Kizhakeyil, A., Wright, G.D., Kelleher, D. and Verma, N. K. 2018. Centrosome- and Golgi-Localized Protein Kinase N-Associated Protein Serves As a Docking Platform for Protein Kinase A Signaling and Microtubule Nucleation in Migrating T-Cells. *Front Immunol*, **9**: 397.

Oppliger, F. Y., Guerin, P. M. and Vlimant, M. 2000. Neurophysiological and behavioural evidence for an olfactory function for the dorsal organ and a gustatory one for the terminal organ in *Drosophila melanogaster* larvae. *Journal of Insect Physiology*, **46**: 135–144.

Park, H., Lee, J. -A., Lee, C., Kim, M. -J., Chang, D. -J., Kim, H., Lee, S. -H., Lee, Y. -S. and Kaang, B. -K. 2005. An *Aplysia* Type 4 Phosphodiesterase Homolog

Localizes at the Presynaptic Terminals of *Aplysia* Neuron and Regulates Synaptic Facilitation. *J. Neurosci.*, **25**: 9037–9045.

Parnas, D., Haghighi, A. P., Fetter, R. D., Kim, S. W. and Goodman, C. S. 2001. Regulation of Postsynaptic Structure and Protein Localization by the Rho-Type Guanine Nucleotide Exchange Factor dPix. *Neuron*, **32**: 415–424.

Pauls, D., Pfitzenmaier, J. E. R., Krebs-Wheaton, R., Selcho, M., Stocker, R. F. and Thum, A. S. 2010. Electric Shock-Induced Associative Olfactory Learning in *Drosophila* Larvae. *Chemical Senses*, **35**: 335–346.

Pavlov, I. P. 1927. Conditioned reflexes: an investigation of the physiological activity of the cerebral cortex. *Oxford University Press.*

Pérez-Moreno, J. J. and O'Kane, C. J. 2019. *GAL4* Drivers Specific for Type Ib and Type Is Motor Neurons in *Drosophila*. *G3 Genes|Genomes|Genetics*, **9**: 453–462.

Perisse, E., Burke, C., Huetteroth, W. and Waddell, S. 2013. Shocking Revelations and Saccharin Sweetness in the Study of *Drosophila* Olfactory Memory. *Current Biology*, **23**: R752–R763.

Pfaffl, M. W. 2001. A new mathematical model for relative quantification in real-time RT–PCR. *Nucleic Acids Res*, **29**: e45.

Prasher, D. C., Eckenrode, V. K., Ward, W. W., Prendergast, F. G. and Cormier, M. J. 1992. Primary structure of the *Aequorea victoria* green-fluorescent protein. *Gene*, **111**: 229–233.

Préat, T. 1998. Decreased Odor Avoidance after Electric Shock in *Drosophila* Mutants Biases Learning and Memory Tests. *J. Neurosci.*, **18**: 8534–8538.

Python, F. and Stocker, R. F. 2002. Adult-Like Complexity of the Larval Antennal Lobe of *D. melanogaster* Despite Markedly Low Numbers of Odorant Receptor Neurons. *J Comp Neurol*, **445**: 374–387.

Qin, H., Cressy, M., Li, W., Coravos, J. S., Izzi, S. A. and Dubnau, J. 2012. Gamma Neurons Mediate Dopaminergic Input during Aversive Olfactory Memory Formation in *Drosophila*. *Current Biology*, **22**: 608–614.

Qiu, Y., Chen, C. -N., Malone, T., Richter, L., Beckendorf, S. K. and Davis, R. L. 1991. Characterization of the Memory Gene Dunce of *Drosophila melanogaster*. *Journal of Molecular Biology*, **222**: 553–565.

Qiu, Y. and Davis, R. L. 1993. Genetic dissection of the learning/memory gene *dunce* of *Drosophila melanogaster*. *Genes Dev.*, **7**: 1447–1458.

Quinn, W. G., Harris, W. A. and Benzer, S. 1974. Conditioned Behavior in *Drosophila melanogaster*. *Proceedings of the National Academy of Sciences*, **71**: 708–712.

R Core Team. 2021. R: A Language and Environment for Statistical Computing. *Software*

Ramaekers, A., Magnenat, E., Marin, E. C., Gendre, N., Jefferis, G. S. X. E., Luo, L. and Stocker, R. F. 2005. Glomerular Maps without Cellular Redundancy at Successive Levels of the *Drosophila* Larval Olfactory Circuit. *Current Biology*, **15**: 982–992.

Rees, C. T. and Spatz, H. -C. of. 1989. Habituation of the Landing Response of *Drosophila* Wild-Type and Mutants Defective in Olfactory Learning. *Journal of Neurogenetics*, **5**: 105–118.

Renger, J. J., Ueda, A., Atwood, H. L., Govind, C. K. and Wu, C. -F. 2000. Role of cAMP Cascade in Synaptic Stability and Plasticity: Ultrastructural and Physiological Analyses of Individual Synaptic Boutons in *Drosophila* Memory Mutants. *J. Neurosci.*, **20**: 3980–3992.

Rescorla, R. A. and Wagner, A. R. 1972. A Theory of Pavlovian Conditioning : Variations in the Effectiveness of Reinforcement and Nonreinforcement. *Classical conditioning, Current research and theory*, **2**: 64–69.

Richter, W. and Conti, M. 2002. Dimerization of the Type 4 cAMP-specific Phosphodiesterases Is Mediated by the Upstream Conserved Regions (UCRs). *Journal of Biological Chemistry*, **277**: 40212–40221.

Richter, W. and Conti, M. 2004. The Oligomerization State Determines Regulatory Properties and Inhibitor Sensitivity of Type 4 cAMP-specific Phosphodiesterases*. *Journal of Biological Chemistry*, **279**: 30338–30348.

Riemer, D., Stuurman, N., Berrios, M., Hunter, C., Fisher, P. A. and Weber, K. 1995. Expression of *Drosophila* lamin C is developmentally regulated: analogies with vertebrate A-type lamins. *Journal of Cell Science*, **108**: 3189–3198.

Robinow, S. and White, K. 1988. The Locus *elav* of *Drosophila melanogaster* is Expressed in Neurons at all Developmental Stages. *Developmental Biology*, **126**: 294–303.

Rørth, P. 1996. A modular misexpression screen in *Drosophila* detecting tissue-specific phenotypes. *Proc Natl Acad Sci U S A*, **93**: 12418–12422.

Ruppert, M., Franz, M., Saratsis, A., Velo Escarcena, L., Hendrich, O., Gooi, L. M., Schwenkert, I., Klebes, A. and Scholz, H. 2017. Hangover Links Nuclear RNA Signaling to cAMP Regulation via the Phosphodiesterase 4d Ortholog *dunce*. *Cell Reports*, **18**: 533–544.

Sánchez-Soriano, N. and Prokop, A. 2005. The Influence of Pioneer Neurons on a Growing Motor Nerve in *Drosophila* Requires the Neural Cell Adhesion Molecule Homolog FasciclinII. *J Neurosci*, **25**: 78–87.

Sarkar, D., Erlichman, J. and Rubin, C. S. 1984. Identification of a Calmodulin-binding Protein that Co-purifies with the Regulatory Subunit of Brain Protein Kinase II. *J Biol Chem*, **259**: 9840–9846.

Scherer, S., Stocker, R. F. and Gerber, B. 2003. Olfactory Learning in Individually Assayed *Drosophila* Larvae. *Learn Mem*, **10**: 217–225.

Scheunemann, L., Jost, E., Richlitzki, A., Day, J. P., Sebastian, S., Thum, A. S., Efetova, M., Davies, S. -A. and Schwärzel, M. 2012. Consolidated and Labile Odor Memory Are Separately Encoded within the *Drosophila* Brain. *J Neurosci*, **32**: 17163–17171.

Scheunemann, L., Plaçais, P. -Y., Dromard, Y., Schwärzel, M. and Preat, T. 2018. Dunce Phosphodiesterase Acts as a Checkpoint for Drosophila Long-Term Memory in a Pair of Serotonergic Neurons. *Neuron*, **98**: 350-365.e5.

Schimenti, K. J., Feuer, S. K., Griffin, L. B., Graham, N. R., Bovet, C. A., Hartford, S., Pendola, J., Lessard, C., Schimenti, J. C. and Ward, J. O. 2013. AKAP9 Is Essential for Spermatogenesis and Sertoli Cell Maturation in Mice. *Genetics*, **194**: 447–457.

Schindelin, J., Arganda-Carreras, I., Frise, E., Kaynig, V., Longair, M., Pietzsch, T., Preibisch, S., Rueden, C., Saalfeld, S., Schmid, B., Tinevez, J. -Y., White, D. J., Hartenstein, V., Eliceiri, K., Tomancak, P. and Cardona, A. 2012. Fiji: an open-source platform for biological-image analysis. *Nat Methods*, **9**: 676–682.

Schmid, A., Chiba, A. and Doe, C. Q. 1999. Clonal analysis of *Drosophila* embryonic neuroblasts: neural cell types, axon projections and muscle targets. *Development*, **126**: 4653–4689.

Schroll, C., Riemensperger, T., Bucher, D., Ehmer, J., Völler, T., Erbguth, K., Gerber, B., Hendel, T., Nagel, G., Buchner, E. and Fiala, A. 2006. Light-Induced Activation of Distinct Modulatory Neurons Triggers Appetitive or Aversive Learning in *Drosophila* Larvae. *Current Biology*, **16**: 1741–1747.

Schuster, C. M., Davis, G. W., Fetter, R. D. and Goodman, C. S. 1996a. Genetic Dissection of Structural and Functional Components of Synaptic Plasticity. I. Fasciclin II Controls Synaptic Stabilization and Growth. *Neuron*, **17**: 641–654.

Schuster, C. M., Davis, G. W., Fetter, R. D. and Goodman, C. S. 1996b. Genetic Dissection of Structural and Functional Components of Synaptic Plasticity. II. Fasciclin II Controls Presynaptic Structural Plasticity. *Neuron*, **17**: 655–667.

Schwaerzel, M., Monastirioti, M., Scholz, H., Friggi-Grelin, F., Birman, S. and Heisenberg, M. 2003. Dopamine and Octopamine Differentiate Between Aversive and Appetitive Olfactory Memories in *Drosophila*. *J Neurosci*, **23**: 10495–10502.

Selcho, M., Pauls, D., el Jundi, B., Stocker, R. F. and Thum, A. S. 2012. The Role of Octopamine and Tyramine in *Drosophila* Larval Locomotion. *Journal of Comparative Neurology*, **520**: 3764–3785.

Selcho, M., Pauls, D., Han, K. -A., Stocker, R. F. and Thum, A. S. 2009. The Role of Dopamine in *Drosophila* Larval Classical Olfactory Conditioning. *PLoS One*, **4**: e5897.

Shang, Y., Claridge-Chang, A., Sjulson, L., Pypaert, M. and Miesenböck, G. 2007. Excitatory Local Circuits and Their Implications for Olfactory Processing in the Fly Antennal Lobe. *Cell*, **128**: 601–612.

Si, G., Kanwal, J. K., Hu, Y., Tabone, C. J., Baron, J., Berck, M., Vignoud, G. and Samuel, A. D. T. 2019. Structured Odorant Response Patterns across a Complete Olfactory Receptor Neuron Population. *Neuron*, **101**: 950-962.e7.

Simpson, J. H. 2009. Chapter 3 Mapping and Manipulating Neural Circuits in the Fly Brain. In: *Advances in Genetics*, pp. 79–143.

Singh, R. N. and Singh, K. 1984. Fine structure of the sensory organs of *Drosophila melanogaster* meigen larva (Diptera : Drosophilidae). *International Journal of Insect Morphology and Embryology*, **13**: 255–273.

Skliris, G. P., Rowan, B. G., Al-Dhaheri, M., Williams, C., Troup, S., Begic, S., Parisien, M., Watson, P. H. and Murphy, L. C. 2009. Immunohistochemical validation of multiple phospho-specific epitopes for estrogen receptor α (ERα) in tissue microarrays of ERα positive human breast carcinomas. *Breast Cancer Res Treat*, **118**: 443–453.

Skube, S. B., Chaverri, J. M. and Goodson, H. V. 2010. Effect of GFP Tags on the Localization of EB1 and EB1 Fragments *In Vivo. Cytoskeleton*, **67**: 1–12.

Springer, M. and Nawrot, M. P. 2021. A Mechanistic Model for Reward Prediction and Extinction Learning in the Fruit Fly. *eNeuro*, **8**: ENEURO.0549-20.2021.

Stocker, R. F. 1994. The organization of the chemosensory system in *Drosophila melanogaster*: a rewiew. *Cell Tissue Res*, **275**: 3–26.

Sullivan, M., Rena, G., Begg, F., Gordon, L., Olsen, A. S. and Houslay, M. D. 1998. Identification and characterization of the human homologue of the short PDE4A cAMP-specific phosphodiesterase RD1 (PDE4A1) by analysis of the human HSPDE4A gene locus located at chromosome 19p13.2. *Biochemical Journal*, **333**: 693–703.

Sutherland, E. W. 1972. Studies on the Mechanism of Hormone Action. *Science*, **177**: 401–408.

Swan, A., Hijal, S., Hilfiker, A. and Suter, B. 2001. Identification of New X-Chromosomal Genes Required for *Drosophila* Oogenesis and Novel Roles for *fs(1)Yb*, *brainiac* and *dunce*. *Genome Res.*, **11**: 67–77.

Takagawa, K. and Salvaterra, P. 1996. Analysis of choline acetyltransferase protein in temperature sensitive mutant flies using newly generated monoclonal antibody. *Neuroscience Research*, **24**: 237–243.

Tanaka, N. K., Endo, K. and Ito, K. 2012. Organization of Antennal Lobe-Associated Neurons in Adult *Drosophila melanogaster* Brain. *J Comp Neurol*, **520**: 4067–4130.

Taskén, K. A., Collas, P., Kemmner, W. A., Witczak, O., Conti, M. and Taskén, K. 2001. Phosphodiesterase 4D and Protein Kinase A Type II Constitute a Signaling Unit in the Centrosomal Area. *Journal of Biological Chemistry*, **276**: 21999–22002.

Tempel, B. L., Bonini, N., Dawson, D. R. and Quinn, W. G. 1983. Reward learning in normal and mutant *Drosophila*. *Proceedings of the National Academy of Sciences of the United States of America*, **80**: 1482.

The UniProt Consortium. 2021. UniProt: the universal protein knowledgebase in 2021. *Nucleic Acids Research*, **49**: D480–D489.

ThermoFisher. 2016. TRIzol reagent. *Protocol*, MAN0001271

Thum, A. S., Leisibach, B., Gendre, N., Selcho, M. and Stocker, R. F. 2011. Diversity, Variability, and Suboesophageal Connectivity of Antennal Lobe Neurons in *D. melanogaster* Larvae. *Journal of Comparative Neurology*, **519**: 3415–3432.

Thum, A. S. and Gerber, B. 2019. Connectomics and function of a memory network: the mushroom body of larval *Drosophila*. *Current Opinion in Neurobiology*, **54**: 146–154.

Thum, A. S., Merhof, D., Münzig, S., Hartenstein, V., Truman, J. W., Bühler, K., Schulze, F., Swoboda, N., Toepfer, M. and Zillner, J. 2021. Larvalbrain. http://www.larvalbrain.org, access: 06/02/2023

Tissot, M., Gendre, N., Hawken, A., Störtkuhl, K. F. and Stocker, R. F. 1997. Larval Chemosensory Projections and Invasion of Adult Afferents in the Antennal Lobe of *Drosophila*. *Journal of Neurobiology*, **32**: 281–297.

Torroja, L., Luo, L. and White, K. 1996. APPL, the *Drosophila* Member of the APP-Family, Exhibits Differential Trafficking and Processing in CNS Neurons. *J Neurosci*, **16**: 4638–4650.

Truman, J. W., Taylor, B. J. and Awad, T. A. 1993. Formation of the adult nervous system. In: *The development of Drosophila melanogaster* (M. Bate and A. Martinez-Arias, editors).

Tully, T., Cambiazo, V. and Kruse, L. 1994. Memory through Metamorphosis in Normal and Mutant *Drosophila*. *J Neurosci*, **14**: 68–74.

Tully, T. and Gold, D. 1993. Differential Effects of *Dunce* Mutations on Associative Learning and Memory in *Drosophila*. *Journal of Neurogenetics*, **9**: 55–71.

Tully, T., Preat, T., Boynton, S. C. and Del Vecchio, M. 1994. Genetic Dissection of Consolidated Memory in Drosophila. *Cell*, **79**: 35–47.

Tully, T. and Quinn, W. G. 1985. Classical conditioning and retention in normal and mutant *Drosophila melanogaster*. *J. Comp. Physiol.*, **157**: 263–277.

Tumkaya, T., Ott, S. and Claridge-Chang, A. 2018. A systematic review of *Drosophila* short-term-memory genetics: Meta-analysis reveals robust reproducibility. *Neuroscience & Biobehavioral Reviews*, **95**: 361–382.

Turrel, O., Goguel, V. and Preat, T. 2018. Amnesiac Is Required in the Adult Mushroom Body for Memory Formation. *J Neurosci*, **38**: 9202–9214.

Turrel, O., Rabah, Y., Plaçais, P. -Y., Goguel, V. and Preat, T. 2020. *Drosophila* Middle-Term Memory: Amnesiac is Required for PKA Activation in the Mushroom Bodies, a Function Modulated by Neprilysin 1. *J Neurosci*, **40**: 4219–4229.

Ueda, A. and Wu, C. -F. 2012. Cyclic-AMP metabolism in synaptic growth, strength, and precision: Neural and behavioral phenotype-specific counterbalancing effects between *dnc* PDE and *rut* AC Mutations. *Journal of Neurogenetics*, **26**: 64–81.

Valsecchi, F., Ramos-Espiritu, L. S., Buck, J., Levin, L. R. and Manfredi, G. 2013. cAMP and Mitochondria. *Physiology (Bethesda)*, **28**: 199–209.

van Swinderen, B. 2007. Attention-Like Processes in *Drosophila* Require Short-Term Memory Genes. *Science*, **315**: 1590–1593.

Verbrüggen, M. 2021. Dnc^{PA} spezifische Funktion im Kurzzeitgedächtnis in der *Drosophila melanogaster* Larve. *Bachelor thesis*, University of Cologne

Vonhoff, F. and Keshishian, H. 2017. Cyclic Nucleotide Signaling is Required during Synaptic Refinement at the *Drosophila* Neuromuscular Junction. *Developmental Neurobiology*, **77**: 39–60.

Walkinshaw, E., Gai, Y., Farkas, C., Richter, D., Nicholas, E., Keleman, K. and Davis, R. L. 2015. Identification of Genes That Promote or Inhibit Olfactory Memory Formation in *Drosophila*. *Genetics*, **199**: 1173–1182.

Wang, Z., Li, Y., Hou, B., Pronobis, M. I., Wang, M., Wang, Y., Cheng, G., Weng, W., Wang, Y., Tang, Y., Xu, X., Pan, R., Lin, F., Wang, N., Chen, Z., Wang, S., Ma, L., Li, Y., Huang, D.,Jiang, L.Wang, Z., Zeng, W., Zhang, Y., Du, X., Lin, Y., Li, Z., Xia, Q., Geng, J., Dai, H., Yu, Y., Zhao, X., Yuan, Z., Yan, J., Nie, Q., Zhang, X., Wang, K., Chen, F., Zhang, Q., Zhu, Y, Zheng, S., Poss, K. D., Tao, S., Meng, X. 2020. An array of 60,000 antibodies for proteome-scale antibody generation and target discovery. *Science Advances*, **6**: eaax2271.

Wickham, H. 2016. *ggplot2*. (Springer, Cham)

Widmann, A., Artinger, M., Biesinger, L., Boepple, K., Peters, C., Schlechter, J., Selcho, M. and Thum, A. S. 2016. Genetic Dissection of Aversive Associative Olfactory Learning and Memory in *Drosophila* Larvae. *PLoS Genet*, **12**: e1006378.

Widmann, A., Eichler, K., Selcho, M., Thum, A. S. and Pauls, D. 2018. Odor-taste Learning in *Drosophila* Larvae. *Journal of Insect Physiology*, **106**: 47–54.

Widmer, Y. F., Fritsch, C., Jungo, M. M., Almeida, S., Egger, B. and Sprecher, S. G. 2018. Multiple neurons encode CrebB dependent appetitive long-term memory in the mushroom body circuit. *eLife*, **7**: e39196.

Wilson, R. I. and Laurent, G. 2005. Role of GABAergic Inhibition in Shaping Odor-Evoked Spatiotemporal Patterns in the *Drosophila* Antennal Lobe. *J. Neurosci.*, **25**: 9069–9079.

Wolfram|Alpha. 2023. Wolfram|Alpha: Making the world's knowledge computable. https://www.wolframalpha.com, access: 09/05/2023

Wu, Z., Gong, Z., Feng, C. and Guo, A. 2000. An emergent mechanism of selective visual attention in *Drosophila*. *Biol Cybern*, **82**: 61–68.

Xie, M., Blackman, B., Scheitrum, C., Mika, D., Blanchard, E., Lei, T., Conti, M. and Richter, W. 2014. The Upstream Conserved Regions (UCRs) Mediate Homo- and Hetero-oligomerization of Type 4 Cyclic Nucleotide Phosphodiesterases (PDE4s). *Biochem J*, **459**: 539–550.

Yarwood, S. J., Steele, M. R., Scotland, G., Houslay, M. D. and Bolger, G. B. 1999. The RACK1 Signaling Scaffold Protein Selectively Interacts with the cAMP-specific Phosphodiesterase PDE4D5 Isoform*. *Journal of Biological Chemistry*, **274**: 14909–14917.

Yin, J. C. P., Wallach, J. S., Del Vecchio, M., Wilder, E. L., Zhou, H., Quinn, W. G. and Tully, T. 1994. Induction of a Dominant Negative CREB Transgene Specifically Blocks Long-Term Memory in Drosophila. *Cell*, **79**: 49–58.

Yu, D., Ponomarev, A. and Davis, R. L. 2004. Altered Representation of the Spatial Code for Odors after Olfactory Classical Conditioning: Memory Trace Formation by Synaptic Recruitment. *Neuron*, **42**: 437–449.

Zaccolo, M. and Pozzan, T. 2002. Discrete Microdomains with High Concentration of cAMP in Stimulated Rat Neonatal Cardiac Myocytes. *Science*, **295**: 1711–1715.

Zars, T., Fischer, M., Schulz, R. and Heisenberg, M. 2000. Localization of a Short-Term Memory in *Drosophila*. *Science*, **288**: 672–675.

Zhang, J., Little, C. J., Tremmel, D. M., Yin, J. C. P. and Wesley, C. S. 2013. Notch-Inducible Hyperphosphorylated CREB and Its Ultradian Oscillation in Long-Term Memory Formation. *J. Neurosci.*, **33**: 12825–12834.

Zhao, C., Widmer, Y. F., Diegelmann, S., Petrovici, M. A., Sprecher, S. G. and Senn, W. 2021. Predictive olfactory learning in *Drosophila*. *Sci Rep*, **11**: 6795.

Zhao, K., Hong, H., Zhao, L., Huang, S., Gao, Y., Metwally, E., Jiang, Y., Sigrist, S. J. and Zhang, Y. Q. 2020. Postsynaptic cAMP signalling regulates the antagonistic balance of *Drosophila* glutamate receptor subtypes. *Development*, **147**: dev191874.

Zhong, Y., Budnik, V. and Wu, C. -F. 1992. Synaptic Plasticity in *Drosophila* Memory and Hyperexcitable Mutants: Role of cAMP Cascade. *J. Neurosci.*, **12**: 644–651.

Zhong, Y. and Wu, C. -F. 1991. Altered Synaptic Plasticity in *Drosophila* Memory Mutants with a Defective Cyclic AMP Cascade. *Science*, **251**: 198–201.

Zhong, Y. and Wu, C. -F. 2004. Neuronal Activity and Adenylyl Cyclase in Environment-Dependent Plasticity of Axonal Outgrowth in *Drosophila*. *J. Neurosci.*, **24**: 1439–1445.

Zito, K., Fetter, R. D., Goodman, C. S. and Isacoff, E. Y. 1997. Synaptic Clustering of Fasciclin II and Shaker: Essential Targeting Sequences and Role of Dlg. *Neuron*, **19**: 1007–1016.

Zito, K., Parnas, D., Fetter, R. D., Isacoff, E. Y. and Goodman, C. S. 1999. Watching a Synapse Grow: Noninvasive Confocal Imaging of Synaptic Growth in *Drosophila*. *Neuron*, **22**: 719–729.

8   Abbreviations

AKAP	A-kinase anchoring protein
AL	Antennal lobe
AM	Amyl acetate
APPL	Amyloid precursor protein homolog
ARM	Anaesthesia-resistant memory
BA	Benzaldehyde
bp	basepair
cAMP	Cyclic adenosine monophosphate
cGMP	Cyclic guanosine monophosphate
CaMKII	Ca^{2+}/calmodulin-dependent kinase II
CNS	Central nervous system
CREB	cAMP-response element-binding protein
CS	*CantonS*
DAPI	4′,6-diamidino-2-phenylindole
DLG	Discs large
Dnc	Dunce
dnc	*dunce*
EA	Ethyl acetate
FasII	Fasciclin II
FCS	Fetal bovine serum
FRET	Förster resonance energy transfer
GABA	γ-aminobutaric acid
GFP	Green fluorescent protein
hug	hugin
HRP	Horseradish peroxidase
LI	Learning index
LTM	Long-term memory
MB	Mushroom body
MBON	Mushroom body output neuron
MTM	Medium-term memory
n-Cath	n-Cathenin
NMJ	Neuromuscular junction

ORN	Olfactory receptor neuron
PAM	protocerebral anterior medial
PBS	Phosphate buffered saline
PCR	Polymerase chain reaction
PDE	Phosphodiesterase
PETAL™	Proteome epitope tag antibody library
PI	Preference index
PKA	Protein kinase A
PKC	Protein kinase C
PPL	protocerebral posterior lateral
qPCR	Quantitative polymerase chain reaction
SDS-PAGE	sodium dodecyl sulfonate-polyacrylamide gel electrophoresis
STM	Short-term memory
TBST	Tris-buffered saline with Tween
TH	Tyrosine hydroxylase
tss	Transcription start site
TβH	Tyramine β-hydroxylase
UCR	Upstream conserved region
US	Unconditioned stimulus
VNC	Ventral nerve cord

Curricilum vitae

Timo Hasselmann

Address	Weißhausstraße 36, 50939 Cologne, Germany thasselm@uni-koeln.de
Place and date of birth	15.09.1990, Bremen, Germany

Education

05/2019 - 03/2024	**PhD student in Neuroscience** University of Cologne ▪ Project: "Not a dunce after all? - Dunce isoforms show differential localisation and influence memory in *Drosophila melanogaster* larvae"
10/2014 - 01/2018	**Master of Science in Molecular Life Science** University of Lübeck ▪ Thesis: "Avian Malaria Prevalence in Blackcaps along the Central European Migratory Divide", MPRG Behavioural Genomics, Max Planck Institute for Evolutionary Biology, Plön
11/2016 - 01/2017	**Internship at the MEMEG** Lund University, Lund, Sweden
04/2016 - 06/2016	**Internship at the MPRG Behavioural Genomics** Max Planck Institute for Evolutionary Biology, Plön
10/2011 - 01/2015	**Bachelor of Science in Molecular Life Science** Lübeck University ▪ Thesis: "Molecular characterization of *Mycobacterium tuberculosis complex* strains from Ghana" Institute for Molecular and Experimental Mycobacteriology, Leibniz Institute, Borstel
2007 - 2010	**Abitur** Altes Gymnasium Bremen

Publications

Delmore, K.E., Van Doren, B.M., Conway, G.J., Curk, T., Garrido-Garduño, T., Germain, R.R., **Hasselmann, T**., Hiemer, D., van der Jeugd, H.P., Justen, H., Lugo Ramos, J.S., Maggini, I., Meyer, B.S., Phillips, R.J., Remisiewicz, M., Roberts, G.C.M., Sheldon, B.C., Vogl, W., Liedvogel, M., 2020. Individual variability and versatility in an eco-evolutionary model of avian migration. Proc. Biol. Sci. 287

Justen, H., **Hasselmann, T**., Illera, J.C., Delmore, K.E., Serrano, D., Flinks, H., Senzaki, M., Kawamura, K., Helm, B., Liedvogel, M., 2022. Population-specific association of Clock gene polymorphism with annual cycle timing in stonechats. Sci. Rep. 12

Conference abstracts

Hasselman, T., Gompert, M., Scholz, H. 2019: Dissecting the function of different Dunce isoforms at a cellular level. 30th Neurobiology Doctoral Students Workshop Würzburg

Hasselman, T., Gompert, M., Müller, M., Verbrüggen, M. Scholz, H. 2021: Characterization of different Dunce isoforms in *Drosophila melanogaster*. 18th European Drosophila neurobiology conference Neurofly2020 virtual / Spain

Hasselman, T., Gompert, M., Müller, M., Verbrüggen, M. Scholz, H. 2022: Characterization of different Dunce isoforms in *Drosophila melanogaster*. 31st Neurobiology Doctoral Students Workshop Cologne

Hasselman, T., Gompert, M., Verbrüggen, M., Müller, M., Brüning, V.,Scholz, H. 2023: Functional analysis of Dunce[PA] in learning and memory in *Drosophila melanogaster*. 15th Göttingen meeting of the German Neuroscience Society

Acknowledgements

Eidesstaatliche Erklärung

Hiermit versichere ich an Eides statt, dass ich die vorliegende Dissertation selbstständig und ohne die Benutzung anderer als der angegebenen Hilfsmittel und Literatur angefertigt habe. Alle Stellen, die wörtlich oder sinngemäß aus veröffentlichten und nicht veröffentlichten Werken dem Wortlaut oder dem Sinn nach entnommen wurden, sind als solche kenntlich gemacht. Ich versichere an Eides statt, dass diese Dissertation noch keiner anderen Fakultät oder Universität zur Prüfung vorgelegen hat; dass sie - abgesehen von oben angegebenen Teilpublikationen und eingebundenen Artikeln und Manuskripten - noch nicht veröffentlicht worden ist sowie, dass ich eine Veröffentlichung der Dissertation vor Abschluss der Promotion nicht ohne Genehmigung des Promotionsausschusses vornehmen werde. Die Bestimmungen dieser Ordnung sind mir bekannt. Darüber hinaus erkläre ich hiermit, dass ich die Ordnung zur Sicherung guter wissenschaftlicher Praxis und zum Umgang mit wissenschaftlichem Fehlverhalten der Universität zu Köln gelesen und sie bei der Durchführung der Dissertation zugrundeliegenden Arbeiten und der schriftlich verfassten Dissertation beachtet habe und verpflichte mich hiermit, die dort genannten Vorgaben bei allen wissenschaftlichen Tätigkeiten zu beachten und umzusetzen. Ich versichere, dass die eingereichte elektronische Fassung der eingereichten Druckfassung vollständig entspricht.

Köln, den 13. 12. 2023 , Timo Hasselmann

Timo Hasselmann